UNIVERSITÀ DEGLI STUDI DI MESSINA
Dipartimento di Scienze Chimiche, Biologiche, Farmaceutiche ed Ambientali

---

DOTTORATO DI RICERCA IN SCIENZE CHIMICHE
XXX CICLO

The supramolecular chemistry of water soluble calixarenes, cyclodextrins and pillararenes

Dott. Lucia Barbera

Supervisor:
Prof. Anna Notti

Coordinator:
Prof. S. Campagna

2014-2017

Index

Chapter 3:

Calix[5]arene-based Supra-amphiphiles

Chapter 4:

Self-sorting of supramolecular systems in water

Chapter 5:

Drug carriers based on a water soluble pillar[5]arene

Overview

The main focus of this PhD thesis is the synthesis of new water soluble macrocycles (calix[*n*]arenes, cyclodextrins and pillar[*n*]arenes) and the investigation of their supramolecular chemistry. After a brief introduction about the principles, perspectives, and recent developments in the field of water-soluble synthetic receptors (Chapter 1) the following sections describe the experimental results of my PhD project.

Chapter 2 reports the synthesis and the aggregation properties of new amphiphilic macrocycles based on anionic and neutral *p*-alkyl-calix[*n*]arenes and a mono-substituted cationic cyclodextrin by means of different techniques (1D and 2D ^{1}H NMR, DOSY, DLS, AFM, Cryo-Tem) together with different applications in the recognition and/or encapsulation of different substrates.

Chapter 3 describes the aggregation features of supramolecular amphiphilic systems (supra-amphiphiles) based on the water soluble *p*-*tert*-butylcalix[5]arene-penta-*O*-4-butylsulfonato and gemini α,ω-alkanediyldiammonium ions, demonstrating that the aggregation phenomena can be efficiently modulated by changing the length of the spacer in the gemini guest and/or the host-guest ratio. Furthermore, this

chapter demonstrated the great potential of calixarene-based supra-amphiphiles in the solubilisation of water insoluble drugs by using as a model the anticancer drug tamoxifen.

Chapter 4 provides a fascinating example of social (non integrative) self-sorting based on a four component system consisting of two water-soluble calix[5]arene derivatives differently substituted at the upper rim and two α,ω–alkanediyldiammonium ions of different lengths (H_3N^+-$(CH_2)_n$-NH_3^+, n = 8, 10). The obtained results demonstrated that among the ten possible complexes with mixed/different stoichiometry, only two capsular-complexes are formed.

Finally, Chapter 5 proposes a potential pillararene (**WP5**) based drug-transport system where **WP5** and the antibiotic drugs amikacin and levofloxacin interact with each other forming stable inclusion complexes in aqueous solution. Furthermore, **WP5** was employed for the preparation of layer-by-layer (LbL) thin solid films on glass surfaces loaded with the above mentioned antibiotics, with the ultimate goal of fabricating antibacterial multilayered coatings for controlled drug release.

Chapter 1

Introduction

1.1. Supramolecular Chemistry: a brief overview

Supramolecular chemistry has obtained tremendous attention in all branches of science (chemistry, biology, material science) since 1987, when Lehn, Cram, and Pedersen won the Chemistry Nobel Prize on account of their discoveries in the host-guest systems.[1] Different noncovalent interactions, such as hydrogen-bonding, van der Waals force, π–π stacking, electrostatic and hydrophobic/hydrophilic etc., can be involved to obtain supramolecular assemblies.[2] During the past decades supramolecular chemistry has been widely explored in various areas, including catalysis, functional materials, electronic devices, sensors, molecular machines and nanomedicine,[3] as finally demonstrated by the award of the 2016 Nobel Prize in Chemistry to Jean-Pierre Sauvage, Sir J. Fraser Stoddart and Bernard L. Feringa for the "Design and synthesis of molecular machines".[4]

In 1983 Jean-Pierre Sauvage succeeded in linking two ring-shaped molecules together in form of a chain, called catenanes.[5] The two interlocked rings were able to move relative to each other when gaining energy, which is a basic requirement for any machine to be able to perform a task. Then, in 1991, Fraser Stoddart developed a rotaxane, a molecular ring around a thin molecular axle, and

proved that the ring was able to move along the axle.[6] Later in 1999, Bernard Feringa was the first person to develop a molecular motor, and also designed a nano-car with dimensions 1000 times thinner than a single hair strand (Figure 1.1.1).[7]

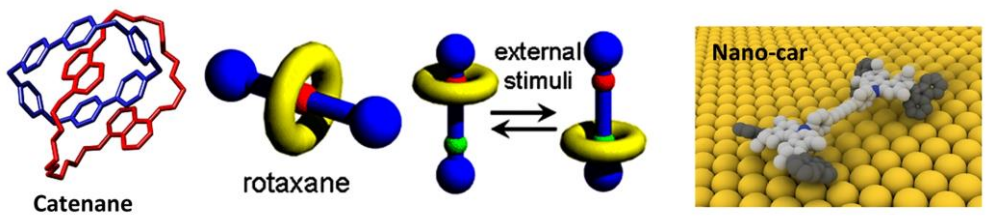

Figure 1.1.1. From catenanes to nano-cars.

Non-covalent interactions present several advantages when compared to covalent ones. First, the noncovalent strategies are easier than multi-step synthesis and are often low-cost and environmentally friendly. Furthermore, supramolecular systems can be synthesized by taking advantage of the spontaneous self-assembly process of suitable building blocks in solution at ambient conditions.[8] Upon external stimuli, supramolecular materials can rearrange their structure or morphology toward more stable states driven by the decrease of the Gibbs free energy. Therefore, this behaviour can be used to design stimuli-responsive functional materials based on supramolecular architectures. Finally, the possibility of manipulating molecules as scaffolds for building supramolecular architectures (*i.e.* the "bottom-up" approach) allow us to control accurately both the size and the morphology of the

resulting new system. Moreover, the fabrication of supramolecular materials with a size ranging in the nanometer domain has become a hot research topic, particularly, in the field of nanomedicine.

Because of the aforementioned advantages, together with an acceptable biocompatibility or low toxicity of certain molecules and materials, supramolecular systems have been widely exploited in the biological field. Many authors reported polymeric supramolecular systems developed for drug delivery, which include polymeric micelles, vesicles, and polymeric hydrogels.[9,10]

Among various noncovalent interactions, host-guest interactions have been extensively investigated. The host molecule usually contains a large cavity volume to accommodate guest molecules on the basis of shape and size complementarity. The high selectivity between the host and guest molecules provides strong dynamic interactions in molecular self-assemblies and offers vast possibilities in the construction of novel supramolecular biomaterials with high degree of structural complexity and programmable functions.[11]

During the past few decades, a series of macrocyclic molecules and their derivatives have been developed, including calix[*n*]arenes (CAs), crown ethers, cyclodextrins (CDs), cyclophanes, cucurbit[*n*]urils, pillar[*n*]arenes, and so on. These macrocyclic molecules have gained increasing popularity, especially for their applications in biomedical field. One major reason is that they are basically friendly to the biological environment and exhibit good biocompatibility.[12] Another reason is that the host-guest complex

formation is a facile way to design stimuli-responsive supramolecular systems.

1.1.1. Historical background of macrocyclic compounds

Historically, the synthesis or discovery of new macrocyclic molecules was in many cases by chance.

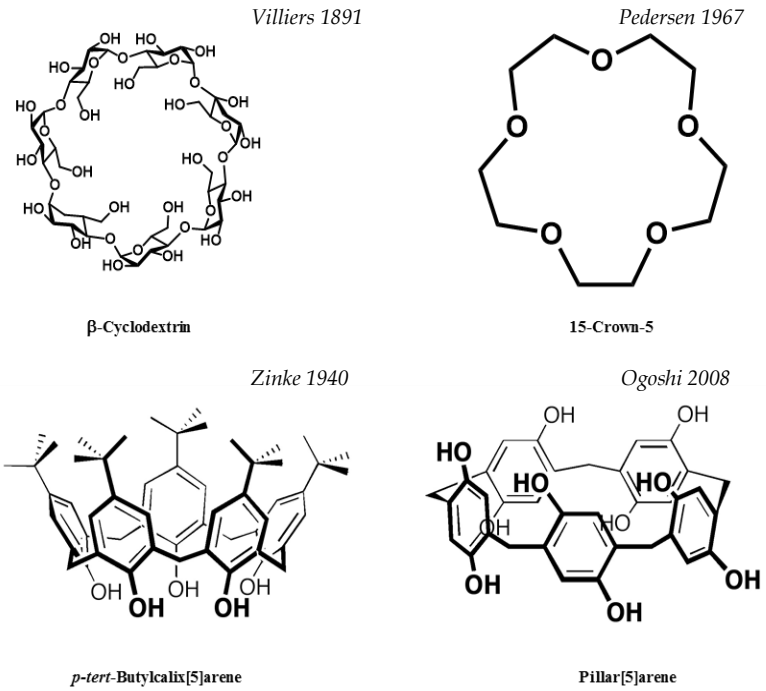

Figure 1.1.1.1. Chemical structure of cyclodextrins, crown ethers, calixarenes and pillararenes.

Cyclodextrins were discovered in 1891, when the French scientist Villiers[13] described the isolation of 3 g of a crystalline substance

from bacterial digest of 1000 g of starch; cyclodextrin derivatives were later characterized in the first half of the last century but only came available as highly purified excipients during the past forty years.[14] As shown in Figure 1.1.1.1, CDs are cyclic oligosaccharides consisting of glucopyranose units attached by α-1,4-linkages. The most common and commercially available CDs named α–, β–, and γ–CD consist of six, seven or eight glucopyranose units respectively, and their cavity size increases by increasing the number of repeating units (4.9 Å – 9.5 Å). Since their discovery, extensive work has been conducted exploring the molecular recognition and encapsulation of substrates by CDs and their derivatives for a wide variety of scientific and commercial applications.[15] Because of their chirality, CDs have attracted considerable interest in the field of chiral separation[16] and can be used as a chiral scaffold to afford moderate to high diastereomeric excesses for several diastereo-differentiating photoreactions.[17]

Crown ethers were first serendipitously synthesized by Pedersen[18] in 1967. He observed that the etherification between bi-functional catechol and 1,2-bis(2-chloroethoxy)ethane afforded dibenzo-18-crown-6 as a minor product. Focusing on these minor products, Pedersen developed a general synthetic protocol for differently sized crown ethers by using metal cation templates, which can be selectively accommodated inside the macrocycle.[18,19] Despite the selective recognition of ions is a fundamental function in living systems, ion-recognition by synthetic compounds had not been reported until the discovery of crown ethers. Therefore, this

discovery was a starting point not only in the fields of molecular recognition and supramolecular chemistry, but also in the field of biomimetic chemistry.

Back in 1872, Adolph von Baeyer[20] reacted phenols with formaldehyde under strongly acidic conditions, producing a hard resin-like product which he was unable to characterise at that time. Nearly three decades later, Leo Baekeland[21] re-examined this process and, as a result, produced phenol/formaldehyde-based resins or heavily cross-linked polymers, which he commercialised under the name "Bakelite". During the 1940s and 1950s, Zinke and co-workers[22] modified the reaction conditions, heating various *para*-substituted phenols with aldehydes in strongly basic solutions to yield cyclic tetramers instead of polymeric resins. These cyclic tetramers did not become popular until David Gutsche[23]—who coined the term "calixarenes"—reported an optimised synthesis[24] in the late 1970s, leading to their convenient preparation in larger quantities. Calix[*n*]arenes (CAs) are composed of phenolic units linked by methylene bridges at their 2- and 6-positions (*meta* positions). Gutsche *et al.* discovered that calix[*n*]arenes (n = 4–9) were selectively obtained by tuning the reaction conditions. Among CAs, the structures of the odd-numbered members (n = 5, 7, 9) and of the large calix[*n*]arene homologous, formed in low yields, were fully elucidated only after the discovery of the even-numbered calix[*n*]arenes.[25] The host–guest/supramolecular chemistry[26] of CAs has been investigated since the 1970s revealing their ability to interact with anionic, cationic and neutral guests.[27]

During last two decade, the research on CAs has been focused on the development of anion receptors,[28] fluorescent sensors,[29] colorimetric chiral recognition,[30] multivalent ligands,[31] supramolecular nanostructures,[32] polymers,[33] and functional nanomaterials.[34]

Finally, the more recent discovery of pillar[*n*]arenes was also by chance. Ogoshi and co-workers[35] investigated in 2008 the reaction of 1,4-dimethoxybenzene with paraformaldehyde to synthesise new phenolic resins and, surprisingly, the obtained product was not a polymer with a wide distribution but rather a highly symmetrical cyclic molecule. The chemical structure of this new species is very similar to that of a calix[*n*]arenes. However, one of the main differences is the position of the methylene bridges. More in details, the units of any calix[*n*]arenes are bound through methylene bridges at the *meta* position (2,6-positions) of phenolic units while those of pillar[*n*]arenes show the same connection but at the *para* position (2,5-positions). The different positions of the methylene bridges dramatically affect the properties of such structures. Ogoshi was inspired by the Parthenon at Athens in Greece in defining the motif of this macrocycle, therefore he decided to name the new cyclic pentamer pillar[5]arene. Synthesis and yields of pillar[*n*]arenes are superior to those of other typical host molecules.[36] Owing to the cylindrical structure of pillar[*n*]arenes, guest molecules can access the cavity from both rims. As a relatively new class of synthetic macrocycles, pillar[*n*]arenes have become a focus of particular attention since

they can provide different sizes of rigid π-electronrich cavities to interact strongly with various electron-deficient species, including pyridinium, imidazolium, and alkylammonium cations as well as some neutral molecules.[37] The diverse and facile functionalisation of pillar[*n*]arenes can provide various modified versatile derivatives with anticipated chemical or physical properties for a wide range of applications in supramolecular chemistry,[38] materials science,[39] and biology.[40]

1.2. The Supramolecular host-guest Chemistry in water

Water is a unique molecule that provides an environment for life and regulates many processes occurring in nature. Water is more and more exploited as reaction medium, because it is an inexpensive "green" solvent and its usage has minimal ecological impact. Furthermore, its unique properties provide an enhancement of both the rate and selectivity of many reactions.[41] The concepts of molecular recognition and self-organization in synthetic supramolecular architectures rely on inspiration from natural systems. Natural receptors such as enzymes and antibodies show strong and selective host–guest complexation through multiple weak, non-covalent interactions between the functional groups on the binding partners. Concomitantly, the design, synthesis, and study of supramolecular assemblies in water are intriguing goals.[42] First, the host needs to be soluble in water. This severely limits the type of building blocks which can be used for its

construction. Second, special interactions and approaches have to be chosen to overcome the competitive influence of water. Another important feature of large water-soluble receptors is the encapsulation of several guests. This facility allows molecular interactions to be studied within a confined space and to carry out chemical reactions in aqueous media. The main driving force for self-assembly in water of most supramolecular architectures, either biological or synthetic, is the hydrophobic effect. Additionally, strengthening and directing polar interactions such as hydrogen bonding, ion–ion, and ion–dipole interactions can take place. It is important to note that self-assembly processes in aqueous solutions depend on the concentration and the type of salts present in solution.[43] For example, salt effects are considerable for self-assembly systems based on ion–ion interactions, but of much lesser influence on self-assembly processes mainly driven by hydrophobic interactions. As a result, most of the supramolecular systems applied to biological targets feature a strong hydrophobic assembly component, combined with structuring polar interactions.

Recently various micelles, vesicles, and supramolecular nanoparticles have been developed for the construction of supramolecular nanocarriers. The combination of supramolecular chemistry with biology thus offers a wealth of new possibilities to study and influence biological processes.

1.2.1. Cyclodextrins

A lot of research has demonstrated the significant role of CDs in supramolecular chemistry, especially for the preparation of CD based supramolecular assemblies for biological applications.[44] Cyclodextrins exhibit good water solubility, good biocompatibility, and non-toxicity towards biological systems.[45] For instance, many pioneer researchers, like Bender,[46] Breslow,[47] Tabushi,[48] and Saenger,[49] demonstrated the use of CDs as enzyme models. From then on, numerous studies showed that, after associating catalytically active groups with CDs, the resultant functionalized CDs can be used as artificial enzyme models to catalyse many biomimetic reactions.[50] Furthermore, by forming the host-guest complexes between drugs and CDs or CD derivatives, the water solubility of hydrophobic drugs can be greatly increased, thereby enhancing the drug availability in biological systems. This is the direct application of CDs for drug delivery.[51] Wang *et al.* developed a nanovector for gene delivery by integrating a pH-responsive cyclodextrin material and low molecular weight polyethylenimine (Figure 1.2.1.1).[52] However, for better pharmaceutical uses, chemical modifications on CDs were carried out to further improve their solubility and drug encapsulation/realising ability, while minimizing the toxicity of the CDs. In this aspect, a variety of functional groups were inserted onto CDs. Cationic CDs were synthesized by introducing amino groups onto the primary side of

the CDs,[53] whereas anionic CDs were produced by attaching carboxylmethyl groups or sulfonic groups.[54]

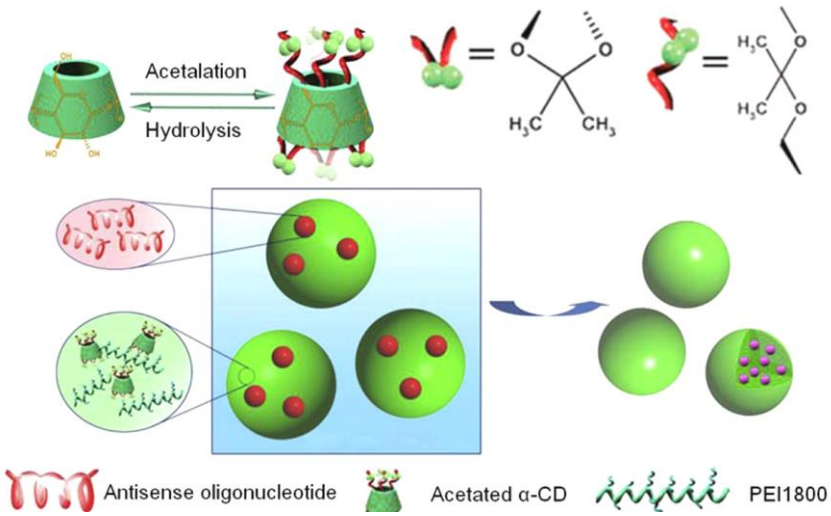

Figure 1.2.1.1. Synthesis of acetated-α-CD by kinetically controlled acetalation and fabrication of hybrid nanoparticles. (Adapted from ref. 52).

The inclusion complexation abilities of natural CDs and simply modified CDs are usually limited, which is inevitably unfavourable for the bioavailability and bioactivity of CDs. To avoid this disadvantage, scientists focused on the construction of CD-based supramolecular assemblies, a class of CD aggregates of nanometer size. Jiang and co-authors discussed the construction strategy of supramolecular self-assemblies based on CDs, which includes the formation of micelles by CD modified polymers, layer-by-layer hollow microcapsules, reversible micelles and vesicles, as well as polymer hydrogels formed by host-guest recognition.[55] Zhou *et al.* conjugated hydrophilic hyperbranched polyglycerol (**HPG**) onto β-

CD (**CD-HPG**), and hydrophobic alkyl chain (**C18**) was coupled with Adamantane (**Ad-C18**). Through the host-guest complexation between β-CD and **Ad**, supramolecular amphiphiles were constructed, which could further self-assemble into core-shell structured vesicles (Figure 1.2.1.2).[56]

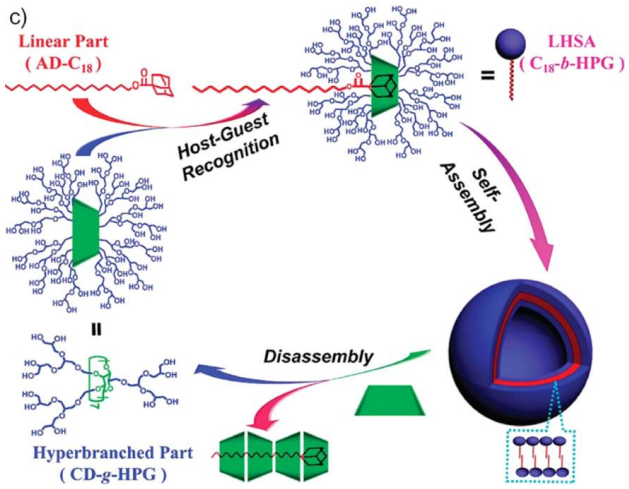

Figure 1.2.1.2. Preparation, self-assembly, and disassembly of the vesicle by a linear hyperbranched supramolecular amphiphile. (Adapted from ref. 56).

1.2.2. Calix[n]arenes

During recent years CAs-based supramolecular systems have shown promising applications in biomedical field.[57] As compared to CDs, a reduced number of studies have been reported for the biomedical applications of CAs,[58] mainly because of their high hydrophobicity and poor water solubility. To avoid this problem, researchers have designed hydrophilic and water-soluble CAs. Sulfonation at the upper rim provided a common strategy to

prepare water soluble CAs.[59] In addition, the conjugation of carboxylic acid groups onto the lower rim[60] and the functionalization of both rims with polar groups were also carried out for the same purpose.[61] By using click chemistry, cationic, anionic, and non-ionic CAs derivatives with a good water solubility were efficiently synthesized.[62] For instance, poly(pyridinium)-functionalized CAs were obtained for biosensing applications (Figure 1.2.2.1a).[63] Consoli *et al*. modified both the lower and the upper rims of CAs to obtain a folic acid-calix[4]arene conjugate that is able to encapsulate the hydrophobic drug model indomethacin, and enhance its solubility in water (Figure 1.2.2.1b).[64]

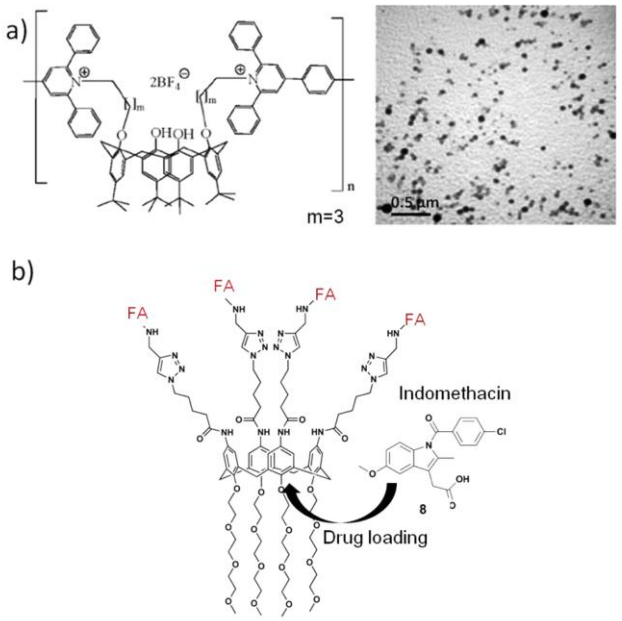

Figure 1.2.2.1. (a) Chemical structure of poly(pyridinium) salt containing calix[4]arene unit (left) and its interaction with DNA studied by TEM (right). (Adapted from ref. 63). (b) Folic acid conjugated-Calix[4]arene for drug delivery by forming the host−guest inclusion with indomethacin. (Adapted from ref. 64).

In terms of biocompatibility, the water-soluble *p*-sulfonatocalix[*n*]arenes exhibit low toxicity, and the in vivo dosage can reach up to 100 mg kg^{-1} without a toxic effect in mice.[65]

In 2012 Liu e co-workers developed an enzyme-responsive supramolecular vesicle by employing biocompatible *p*-sulfonatocalix[4]arene (**SC4A**) to deliver the drug tacrine, specifically for the treatment of Alzheimer's disease.[66] The binary vesicle formed by the host-guest complexation between **SC4A** and myristoylcholine exhibited highly specific and efficient responsiveness to cholinesterase enzyme that could break the hydrophilic-hydrophobic balance, leading to the disassembly of the binary vesicle and thus the release of loaded drugs. Such kind of binary vesicles could be achieved using other host molecules (Figure 1.2.2.2.).

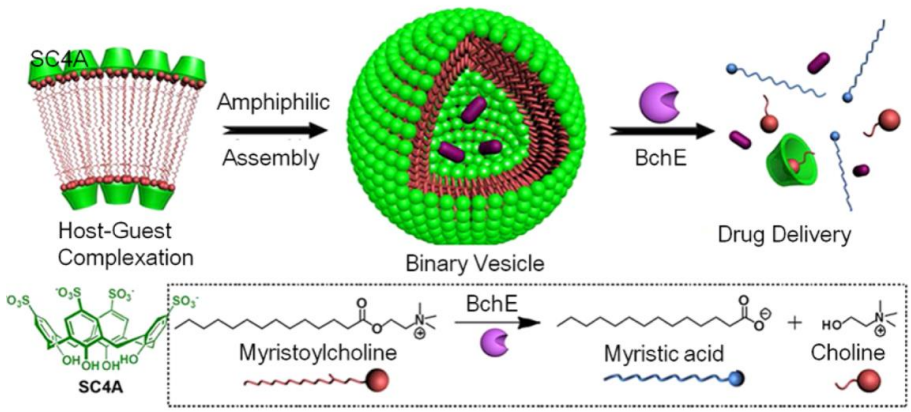

Figure 1.2.2.2. Amphiphilic assembly of myristoylcholine in the presence of **SC4A** for responsive drug release. (Adapted from ref. 66).

Thus far, water soluble CAs have found wide applications in the solubilization of hydrophobic drugs, biomimic of ion channels, biochemical recognition, drug/gene delivery, and enzyme-like activity. In addition to their host-guest chemistry, some CAs have also shown interesting inhibition activities toward virus,[67] bacterial,[68] fungus,[69] and some cancers.[70]

1.2.3. Pillar[n]arenes

Pillar[*n*]arene assemblies based on host-guest interactions have shown great potential in biology, especially in recognition of biomolecules, cell imaging, drug delivery, and biomedicine.[40a]

The parent pillar[*n*]arenes are totally insoluble in water, for this reason many strategies have been proposed to improve water solubility by introducing water-soluble functional groups such as phosphates, carboxylates, oligoethers, polyethers, amines, and ammoniums. Ogoshi *et al*. reported the synthesis of the first water soluble pillar[5]arene derivative, known as carboxylato-pillar[5]arene (**WP5**), along with its ability to form strong 1:1 inclusion complex with paraquat in aqueous medium.[71] Yang *et al*.[72] recently designed tryptophan-pillar[5]arene, which resulted highly water-soluble. Hou and co-workers[73] reported a cation transport system based on pillar[5]arene capable of voltage-driven reversible insertion in a lipid bilayer (Figure 1.2.3.1).

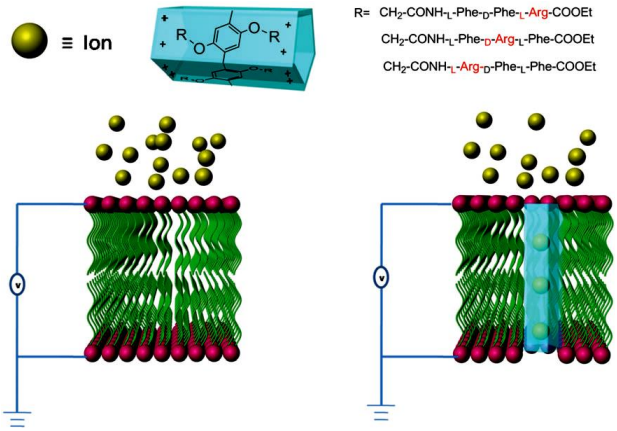

Figure 1.2.3.1. Schematic representation of the artificial voltage-gated ion channel prepared by the incorporation of positively charged Arg units to pillar[5]arene side chains. Cation transport through the ion channel is regulated by voltage-dependent reversible insertion of the artificial ion channel in the lipid bilayer. (Adapted from ref. 73).

Recently, Schalley *et al.*[74] presented a versatile, simplified hydrophobic guest transport system based on the water soluble pillararene **WP5** (Figure 1.2.3.2). The supramolecular interaction between **WP5** derivative and the drug Norharmane (**NHM**) exhibited an improvement of the water solubility of the bioactive molecule and, compared with the individual **NHM**, the **NHM**/ **WP5** supramolecular transport showed a significant reduction of the drug's cell toxicity.

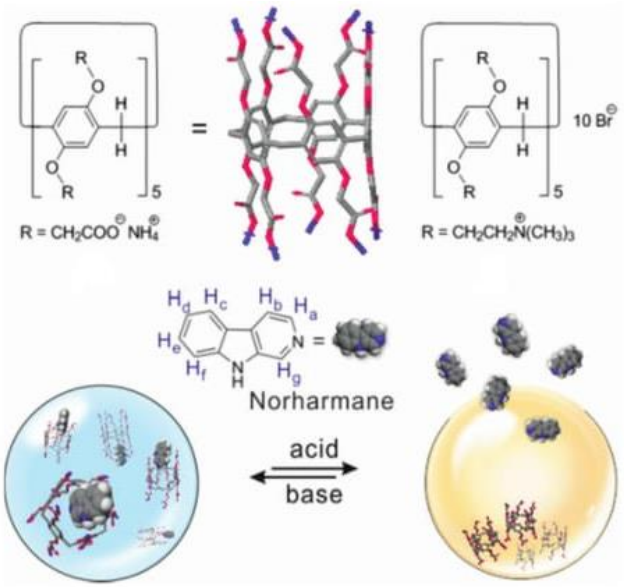

Figure 1.2.3.2. Schematic description of the supramolecular hydrophobic guest transport system based on pillar[5]arene (WP5). (Adapted from ref. 74).

In 2013, Wang and co-workers managed to construct a novel type of supramolecular vesicles with a thin thickness of about 7 nm, where the self-assembly process was driven by the host-guest inclusion between a water soluble pillar[6]arene (**WP6**) and hydrophobic ferrocene derivative N-1-decylferrocenylmethylamine (**G**), in aqueous environment (Figure 1.2.3.3.).[75] Then the anticancer drug mitoxantrone (**MTZ**) was encapsulated in the vesicles. The rapid **MTZ** release under acidic pH indicates the potential application of this vesicle carrier for controlled drug release inside the cancer cells. The drug delivery system was tested against SMMC-7721 cancer cell and NIH3T3 normal cell, respectively. Very recently, Wang and co-workers reported another multiple stimuli-

responsive supramolecular vesicle by using **WP6**; in this system the anticancer drug Doxorubicin (**Dox**) was loaded and then released in a controllable manner.[76]

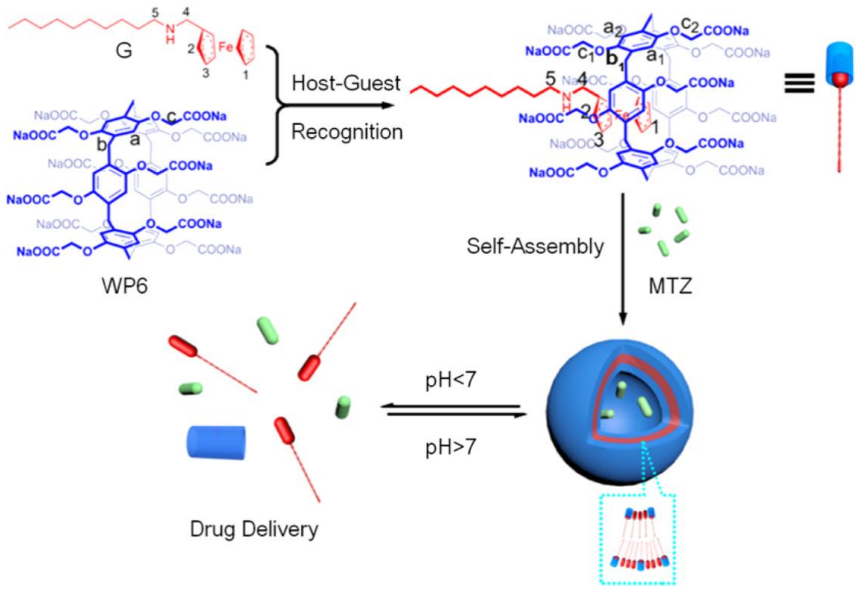

Figure 1.2.3. Formation of a supramolecular vesicle and its pH-responsive drug release. (Adapted from ref. 75).

Pei and co-workers[77] synthesized a Ferrocenium-capped amphiphilic-pillar[5]arene (**FCAP**) able to self-assemble into cationic vesicles with high loading efficiency for polyanionic siRNA. When exposed to a reducing agent (glutathione), the disassembly of the cationic vesicles was achieved, and up to 92% of the model drug **Dox** was released to cancer cells.

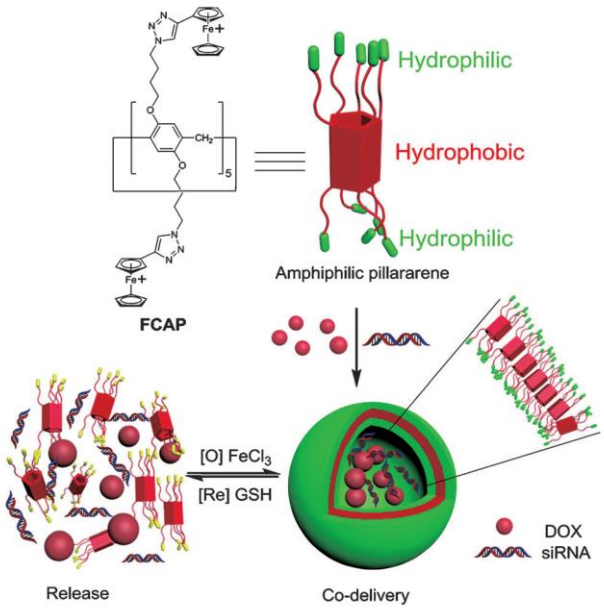

Figure 1.2.3.4. formation of cationic vesicles, and their redox-responsive drug/siRNA release. (Adapted from ref. 77).

Considering the advancements on pillar[*n*]arenes over such as a short time span and their ever-expanding applications, pillar[*n*]arenes will undoubtedly emerge as indispensable cyclophanes in biological applications.

References

[1] (a) Lehn J.M., *Angew. Chem., Int. Ed. Engl.,* **1988**, 27, 89; (b) Cram, D.J., *Angew. Chem., Int. Ed. Engl.,* **1988**, 27, 1009; (c) Pedersen, C.J., *Angew. Chem., Int. Ed. Engl.,* **1988**, 27, 1021.

[2] (a) Sijbesma R.P., Beijer F.H., Brunsveld L., Folmer B.J.B., Hirschberg J.H.K.K., Lange R.F.M., Lowe J.K.L., Meijer E.W., *Science*, **1997**, 278, 1601; (b) Park T., Zimmerman S.C., Nakashima S., *J. Am. Chem. Soc.*, **2005**, 127, 6520; (c) Ryu J.H., Hong D.J., Lee M., *Chem. Commun*., **2008**, 1043; (d) Hartgerink J.D., Beniash E., Stupp S.I., *Science*, **2001**, 294, 1684; (e) Zhang W., Jin W., Fukushima T., Saeki A., Seki S., Aida T., *Science*, **2011**, 334, 340.

[3] (a) Ariga K., Kunitake T., *Supramolecular Chemistry-Fundamentals and Applications,* **2006**; (b) Wang F., Zhang J., Ding X., Dong S., Liu M., Zheng B., Li S., Wu L., Yu Y., Gibson H.W., Huang F., *Angew. Chem., Int. Ed*., **2010**, 49,1090; (c) Zhang Z., Luo Y., Chen J., Dong S., Yu Y., Ma Z., Huang F., *Angew. Chem., Int. Ed*., **2011**, 50, 1397; (d) Wang F., Han C., He C., Zhou Q., Zhang J., Wang C., Li N., Huang F., *J. Am. Chem. Soc.*, **2008**, 130, 11254.

[4] (a) Feringa B.L., *Angew. Chem., Int. Ed.,* **2017**, 56, 11060; (b) Stoddart J.F., *Angew. Chem., Int. Ed.,* **2017**, 56, 11094; (c) Sauvage, J.P., *Angew. Chem., Int. Ed.,* **2017**, 56, 11080.

[5] Dietrich-Buchecker C.O., Sauvage J.P., Kintzinger J.P., *Tet. Lett.,* **1983**, 24, 5095.

[6] Anelli P.L., Spencer N., Stoddart J.F., *J. Am. Chem. Soc.,* **1991**, 113 5131.

[7] Koumura N., Zijlstra R.W.J., Delden R.A., Harada N., Feringa B.L., *Nature*, **1999**, 401, 152.

[8] Liu K., Kang Y., Wang Z., Zhang X., *Adv. Mater.,* **2013**, 25, 5530.

[9] Yoon H.J., Jang W.D., *J. Mater. Chem.*, **2010**, 20, 211.

[10] Zhao Y., Sakai F., Su L., Liu Y., Wei K., Chen G., Jiang M., *Adv. Mater.*, **2013**, 25, 5215.

[11] (a) Harada A., Takashima Y., Nakahata M., *Acc. Chem. Res.,* **2014**, 47, 2128; (b) Yang Y.W., Sun Y.L., Song N., *Acc. Chem. Res.,* **2014**, 47, 1950.

[12] (a) Challa R., Ahuja A., Ali J., Khar R.K., *AAPS Pharm. Sci. Tech.*, **2005**, 6, 329; (b) Stella V., Rajewski R., *Pharm. Res.*, **1997**, 14, 556; (c) Uzunova V.D., Cullinane C., Brix K., Nau W.M., Day A.I., *Org. Biomol. Chem.*, **2010**, 8, 2037; (d) Wang L., Li L.L., Fan Y.S., Wang H., *Adv. Mater.*, **2013**, 25, 3888.

[13] Villiers A., *Compt. Rend. Acad. Sci.* ,**1891**, 112, 536.

[14] Loftsson T., Duchêne D., International Journal of Pharmaceutics 2007, 329, 1.

[15] (a) Breslow R., Dong S.D., *Chem. Rev.,* **1998**, 98, 1997; (b) Cramer F., *Cyclodextrins and their Industrial Uses, ed. D. Duchêne, Editions de Santé, Paris,* **1987**; (c) Szejtli J., *Chem. Rev.,* **1998**, 98, 1743; (d) Crini G., *Chem. Rev.,* **2014**, 114, 10940.

[16] (a) Zhou J., Tan J., Tang W., *Trends in Analytical Chemistry*, **2015**, 65, 22; (b) Shpigun O.A., Ananieva I.A., Budanova N.Y., Shapovalova E.N., *Russ. Chem. Rev.*, **2003**, 72, 1035.

[17] (a) Nakamura A., Inoue Y., *J. Am. Chem. Soc.,* **2003**, 125, 966; (b) Nakamura A., Inoue Y., *J. Am. Chem. Soc.,* **2005**, 127, 5338; (c) Rekharsky M.V., Inoue Y., *J. Am. Chem. Soc.,* **2002**, 124, 813; (d) Yang C., Mori T., Origane Y., Ko Y.K., Selvapalam N., Kim K., Inoue Y., *J. Am. Chem. Soc.,* **2008**, 130, 8574.

[18] Pedersen C.J., *J. Am. Chem. Soc.,* **1967**, 89, 7017.

[19] Gokel G.W., Leevy W.M, Weber M.E., *Chem. Rev.,* **2004**, 104, 2723.

[20] Baeyer A., *Ber. Dtsch. Chem. Ges.,* **1872**, 5, 280.

[21] Baekeland L.H., *US Pat., US942699*, **1909**.

[22] Zinke A., Kretz R., Leggewie E., Hössinger K., Hoffmann G., Weber P., Ostwalden V., Wiesenberger E., Sobotka M., Kretz R., *Monatsh. Chem. Verw. Teile Anderer Wiss.,* **1952**, 83, 1213.

[23] Gutsche C.D., *Acc. Chem. Res.,* **1983**, 16, 161.

[24] (a) Gutsche C.D., Muthukrishnan R., *J. Org. Chem.,* **1978**, 43, 4905; (b) Gutsche C.D., Dhawan B., No K.H., Muthukrishnan R., *J. Am. Chem. Soc.,* **1981**, 103, 3782.

[25] (a) Ninagawa A., Matsuda H., *Makromol. Chem., Rapid Commun.,* **1982**, 3, 65; (b) Stewart D.R., Gutsche C.D., *J. Am. Chem. Soc.,* **1999**, 121, 4136.

[26] Michinori T., Seiji S., *Bull. Chem. Soc. Jpn.,* **1995**, 68, 1088.

[27] Neri P., Sessler J.L., Wang M.X., *Calixarenes and Beyond, Springer,* **2016**.

[28] P. Lhoták, in Anion Sensing, *ed. I. Stibor, Springer Berlin Heidelberg, Berlin, Heidelberg,* **2005**, 65.

[29] Kim J.S., Quang D.T., *Chem. Rev.,* **2007**, 107, 3780.

[30] Kubo Y., Maeda S.Y., Tokita S., Kubo M., *Nature,* **1996**, 382, 522.

[31] Baldini L., Casnati A., Sansone F., Ungaro R., *Chem. Soc. Rev.,* **2007**, 36, 254.

[32] Prins L.J., Timmerman P., Reinhoudt D.N., *Pure Appl. Chem.,* **1998**, 70, 1459.

[33] (a) Guo D.S., Liu Y., *Chem. Soc. Rev.,* **2012**, 41, 5907; (b) Sun R., Xue C., Ma X., Gao M., Tian H., Li Q., *J. Am. Chem. Soc.,* **2013**, 135, 5990.

[34] Wei A., *Chem. Commun.,* **2006**, 1581.

[35] Ogoshi T., Kanai S., Fujinami S., Yamagishi T., Nakamoto Y., *J. Am. Chem. Soc.,* **2008**, 130, 5022.

[36] Ogoshi T., Pillararenes (Monographs in Supramolecular Chemistry), Royal Society of Chemistry, 2015

[37] (a) Zhang Z., Luo Y., Chen J., Dong S., Yu Y., Ma Z., Huang F., *Angew. Chem., Int. Ed.,* **2011**, 50, 1397; (b) Strutt N.L., Forgan R.S., Spruell J.M., Botros Y.Y., Stoddart J.F., *J. Am. Chem. Soc.,* **2011**, 133, 5668.

[38] Zhang H., Strutt N.L., Stoll R.S., Li H., Zhu Z., Stoddart J.F., *Chem. Commun.,* **2011**, 47, 11420.

[39] (a) Tan L.L., Li H., Tao Y., Zhang S.X., Wang B., Yang Y.W., *Adv. Mater.,* **2014**, 26, 7027; (b) Wang W., Chen L.J., Wang X.Q., Sun B., Li X., Zhang Y., Shi J., Yu Y., Zhang L., Liu M., Yang H.B., *Proc. Natl. Acad. Sci. U. S. A.,* **2015**, 112, 5597.

[40] (a) Sathiyajith C., Shaikh R.R., Han Q., Zhang Y., Meguellati K., Yang Y.W., *Chem. Commun.,* **2017**, 53, 677; (b) Si W., Xin P., Li Z.T., Hou J.L., *Acc. Chem. Res.,* **2015**, 48, 1612; (c) Si C.W., Zhang L.,. Tang G., Li Z.T., Hou J.L., *J. Am. Chem. Soc.,* **2013**, 135, 2152.

[41] (a) Blandamer M.J., Engberts J.B.F.N., Gleeson P.T., Reis J.C.R., *Chem. Soc. Rev.*, **2005**, 34, 440; (b) Li C.J., *Chem. Rev.,* **2005**, 105, 3095; (c) Otto S., Engberts J.B.F.N., *Org. Biomol. Chem.,* **2003**, 1, 2809; (d) Lindstrom U.M., *Chem. Rev.*, **2002**, 102, 2751; (e) Akiya N., Savage P.E., *Chem. Rev.,* **2002**, 102, 2725; (f) Engberts J.B.F.N., Blandamer M.J., *Chem. Commun.*, **2001**, 1701.

[42] (a) Schrader T., Hamilton A.D., *Functional Synthetic Receptors Wiley-VCH, Weinheim,* **2005**; (b) Ariga K., Kunitake T., *Supramolecular Chemistry – Fundamentalsand Applications*, *Springer, Berlin,* **2005**. (c) Kubik S., Reyheller C., Stuwe S., *J. Inclusion Phenom. Macrocyclic Chem.*, **2005**, 52, 137.

[43] Schneider H.J., Kramer R., Simova S., Schneider U., *J. Am. Chem. Soc.*, **1988**, 110, 6442.

[44] Zang J., Ma P.X., *Advanced Drug Delivery Reviews,* **2013**, 65, 1215.

[45] Irie T., Uekama K., *J. Pharm. Sci.*, **1997**, 86, 147.

[46] D'Souza V.T., Bender M.L., *Acc. Chem. Res.*, **1987**, 20, 146.

[47] Breslow R., *Science*, **1982**, 218, 532.

[48] Tabushi I., *Acc. Chem. Res.*,**1982**, 15, 66.

[49] Saenger W., *Angew. Chem., Int. Ed. Engl.*, **1980**, 19, 344.

[50] Murakami Y., Kikuchi J.I., Hisaeda Y., Hayashida O., *Chem. Rev.*, **1996**, 96, 721.

[51] Brewster M.E., Loftsson T., *Adv. Drug Delivery Rev.*, **2007**, 59, 645.

[52] Chen H., Liu X., Dou Y., He B., Liu L., Wei Z., Li J., Wang C., Mao C., Zhang J., Wang G., *Biomaterials*, **2013**, 34, 4159.

[53] (a) Donohue R., Mazzaglia A., Ravoo B.J., Darcy R., *Chem. Commun.*, **2002**, 2864; (b) Zhao Y.L., Li Z., Kabehie S., Botros Y.Y., Stoddart J.F., Zink J.I., *J. Am. Chem. Soc.*, **2010**, 132, 13016.

[54] (a) Dubes A., Bouchu D., Lamartine R., Parrot-Lopez H., *Tetrahedron Lett.*, **2001**, 42, 9147; (b) Sukegawa T., Furuike T., Niikura K., Yamagishi A., Monde K., Nishimura S.I., *Chem. Commun.*, 2**002**, 430.

[55] Chen G., Jiang M., *Chem. Soc. Rev.,* **2011**, 40, 2254.

[56] Tao W., Liu Y., Jiang B., Yu S., Huang W., Zhou Y., Yan D., *J. Am. Chem. Soc.*, **2011**, 134, 762.

[57] Nimse S.B., Kim T., *Chem. Soc. Rev.*, **2013**, 42, 366.

[58] Guo D.S., Liu Y., *Acc. Chem. Res.*, **2014**, 47, 1925.

[59] Perret F., Lazar A.N., Coleman A.W., *Chem. Commun.*, **2006,** 23, 2425.

[60] Arduini A., Pochini A., Raverberi S., Ungaro R., *J. Chem. Soc. Chem. Commun.*, **1984**, 981.

[61] Shahgaldian P., Coleman A.W., Kalchenko V.I., *Tetrahedron Lett.*, **2001**, 42, 577.

[62] Ryu E.H., Zhao Y., *Org. Lett.*, **2005**, 7, 1035.

[63] Lu Y., Xiao C., Yu Z., Zeng X., Ren Y., Li C., *J. Mater. Chem.*, **2009**, 19, 8796.

[64] Consoli G.M.L., Granata G., Geraci C., *Org. Biomol. Chem.*, **2011**, 9, 6491.

[65] Coleman A.W., Jebors S., Cecillon S., Perret P., Garin D., Marti-Battle D., Moulin M., *New J. Chem.*, **2008**, 32, 780.

[66] Guo D.S., Wang K., Wang Y.X., Liu Y., *J. Am. Chem. Soc.*, **2012**, 134, 10244.

[67] Hwang K.M., Liu S.Y., Qi Y.M., *Method of Treating Viral Infections with Aryl Macrocyclic Compounds,* Google Patents, **1994**.

[68] (a) Casnati A., Fabbi M., Pelizzi N., Pochini A., Sansone F., Unguro R., Di Modugno E., Tarzia G., *Bioorg. Med. Chem. Lett.*, **1996**, 6, 2699; (b) Colston M.J., Hailes H.C., Stavropoulos E., Herve A.C., Herve G., Goodworth K.J., Hill A.M., Jenner P., Hart P.D., Tascon R.E., *Infect. Immun.*, 2**004**, 72, 6318.

[69] Hart P.D., Armstrong J.A., Brodaty E., *Infect. Immun.*, **1996**, 64, 1491.

[70] Menger F.M., Bian J., Sizova E., Martinson D.E., Seredyuk V.A., *Org. Lett.*, **2003**, 6, 261.

[71] Ogoshi T., Hashizume M., Yamagishi T.A., Nakamoto Y., *Chem. Commun.*, **2010**, 46, 3708.

[72] Yang K., Chang Y., Wen J., Lu Y., Pei Y., Cao S., Wang F., Pei Z., *Chem. Mater.*, **2016**, 28, 1990.

[73] Si W., Li Z.T., Hou J.L., *Angew. Chem., Int. Ed.*, **2014**, 53, 4578.

[74] Qi Z., Achazi K., Haag R., Dong S., Schalley C.A., *Chem. Commun.*, **2015**, 51, 10326.

[75] Duan Q., Cao Y., Li Y., Hu X., Xiao T., Lin C., Pan Y., Wang L., *J. Am. Chem. Soc.*, **2013**, 135, 10542.

[76] Cao Y., Zou X., Xiong S., Li Y., Shen Y., Hu X., Wang L., *Chin. J. Chem.*, **2015**, 33, 329.

[77] Chang Y., Yang K., Wei P., Huang S., Pei Y., Zhao W., Pei Z., *Angew. Chem., Int. Ed.*, **2014**, 53, 13126.

Chapter 2

Macrocyclic amphiphiles

2.1. Introduction

In the field of self-assembly systems, amphiphiles are a class of interesting molecules containing both hydrophilic and hydrophobic portions connected by covalent bonds.

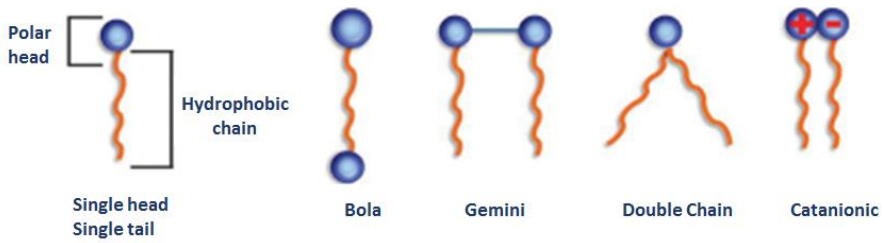

Figure 2.1.1. Conventional amphiphiles.

When dissolved in aqueous media, the hydrophilic component of an amphiphile tends to interact with the aqueous phase while its hydrophobic part prefers staying in the nonpolar solvent or residing in the air.[1] Thus they are able to self-assemble in water into various well-defined structures, ranging from simple micelles and vesicles to highly organized nanofibers, nanohelices, nanotubes, nanorods and nanosheets. Furthermore, after an external stimuli, such as temperature, concentration, pH and ionic strength,[2] they are also able to reorganize their structure.

Amphiphiles play a significant role in nature at many different levels, from peptides, proteins and genes (*e.g.* DNA, RNA) to viruses and cell membrane.[3] Inspired by nature, researchers engineered and produced artificial self-assembly structures which have been widely applied in many fields including nanodevices, drug/gene delivery and cell imaging.[4] Over the past decades, among all kinds of synthetic amphiphiles, macrocyclic amphiphiles obtained from macrocyclic scaffolds have captured much attention due to their unique superiority in the self-assembly process. Compared with traditional linear amphiphiles, macrocyclic amphiphiles can be designed to promote their self-assembly into various well-defined architectures by locating hydrophilic and hydrophobic chains on the respective sides of the macrocyclic frameworks.

This chapter will describe the experimental results on the synthesis and aggregation properties of new amphiphilic macrocycles based on anionic and neutral calixarenes and a cationic cyclodextrin, together with different applications in the recognition and/or encapsulation of different substrates.

2.2. Macrocyclic amphiphiles based on calixarenes

Calix[*n*]arenes are macrocyclic oligomers composed of *n* phenolic units linked by methylene groups at the meta-positions, forming a unique basket shape.[5] Due to their unique structure and facile functionalization of both upper and lower rims, calix[*n*]arenes have been widely used to construct macrocyclic amphiphiles. The most obvious feature that distinguishes these amphiphiles from conventional linear surfactants is

the presence of a cavity that can be used to include guest molecules. In fact, calixarene-based surfactants were defined by Shinkai as "surfactants with a host–guest recognition site".[6]

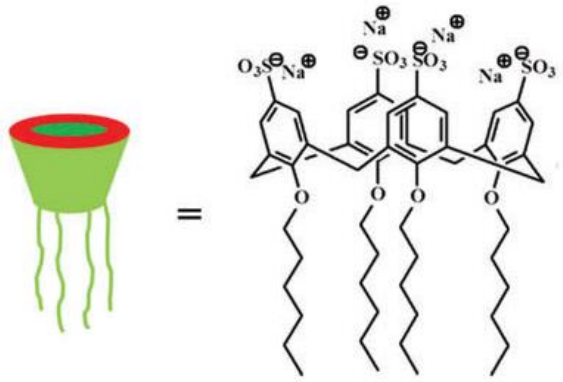

Figure 2.2.1. Cartoon and chemical structure of an amphiphilic calix[4]arene.

The parent calixarenes show effectively zero solubility in aqueous solution, and undoubtedly this property is the one which delayed the biopharmaceutical application of calixarene derivatives as compared to cyclodextrins and crown ethers. Various methods have been developed since the 1980s to obtain water-soluble calixarenes through functionalization at three possible sites: at the phenolic functions, para to the phenolic groups, and by modification of the methylene bridges. Ungaro and co-workers reported the first example of such a compound in 1984, with carboxylic acid groups coupled to the lower rim of a calix[4]arene.[7] More recently, functions such as phosphates, ammonium groups or sulfonates functions have been used. Regen *et al.*, in 1989, prepared vesicles by injecting a tetrahydrofuran solution of an unmodified calix[6]arene into water.[8] From then on, various kinds of amphiphilic calix[*n*]arenes were synthesised to investigate their self-

assembly behaviors. In 2001, Shahgaldian *et al*. demonstrated that further modification of the acyl-calix[4]arenes could be used to generate calixarene analogues of the natural phospholipids.[9]

Among the several calixarene-based surfactants described in the literature, *p*-sulfonatocalix[*n*]arenes bearing alkyl groups at the lower rim are probably the most studied.[10] Conversely, apart from Shinkai's pioneering work,[11] very few examples of lower rim *O*-alkylsulfonato derivatives have been thoroughly investigated.[12] Upon micelle formation, unlike their *p*-sulfonato analogues, *O*-alkylsulfonato-calixarenes direct their hydrophobic cavities towards the inner core of the micelle, exposing their charged moieties to bulk water. As a result, they are expected to display different recognition, solubilisation and aggregation properties than their upper rim analogues.

Among neutral calixarene-based surfactants, a series of large-ring PEGylatedcalix[6,7,8]arene analogues have been synthesised and are able to modify the growth of *M. tuberculosis* in infected cells.[13] In 2011, Zhu *et al*.[14] took advantage of the host-guest interaction between a PEGylated calix[4]arene and the hydrophobic chlorin e6 to form supramolecular polymeric micelles, which exhibited more efficient photodynamic therapy efficacy than the free chlorin e6 (Figure 2.2.2).

Raston *et al*. established new micellular delivery systems based on phospholipid calix[4]arenes with potent antioxidant activity.[15]

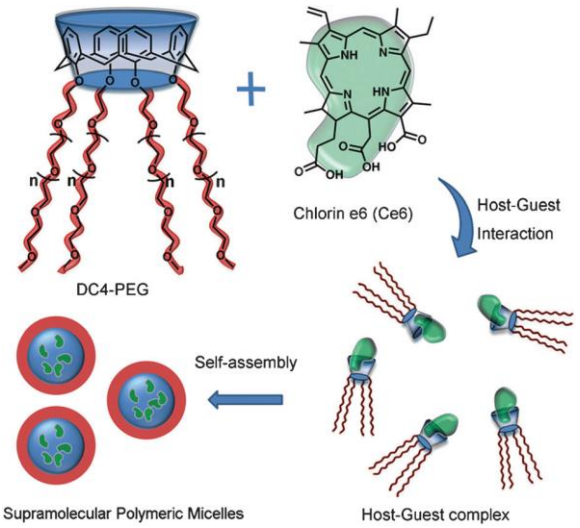

Figure 2.2.2. Representation of supramolecular polymeric micelles based on host–guest interaction. (Adapted from ref. 14).

2.2.1. Our contribution to anionic calixarene-based surfactants: results and discussion

During 2013 my research group reported on the synthesis of a new water-soluble *p-tert*-butylcalix[5]arene **1**, bearing *O*-4-butylsulfonato groups at the lower rim, and its aggregation properties in water.[16]

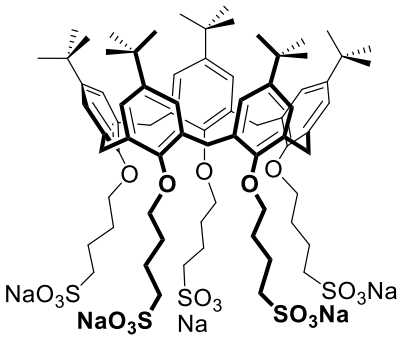

1

Figure 2.2.1.1. Calixarene **1**.

According to the method previously reported for calixarene **1,** two new amphiphilic calixarenes bearing *O*-4-butylsulfonato pendant groups at the lower rim (*p-tert*-calix[4]arene **2** and *p*-methyl-calix[5]arene **3**; Scheme 2.2.1.1) were synthesized and their aggregation properties investigated.

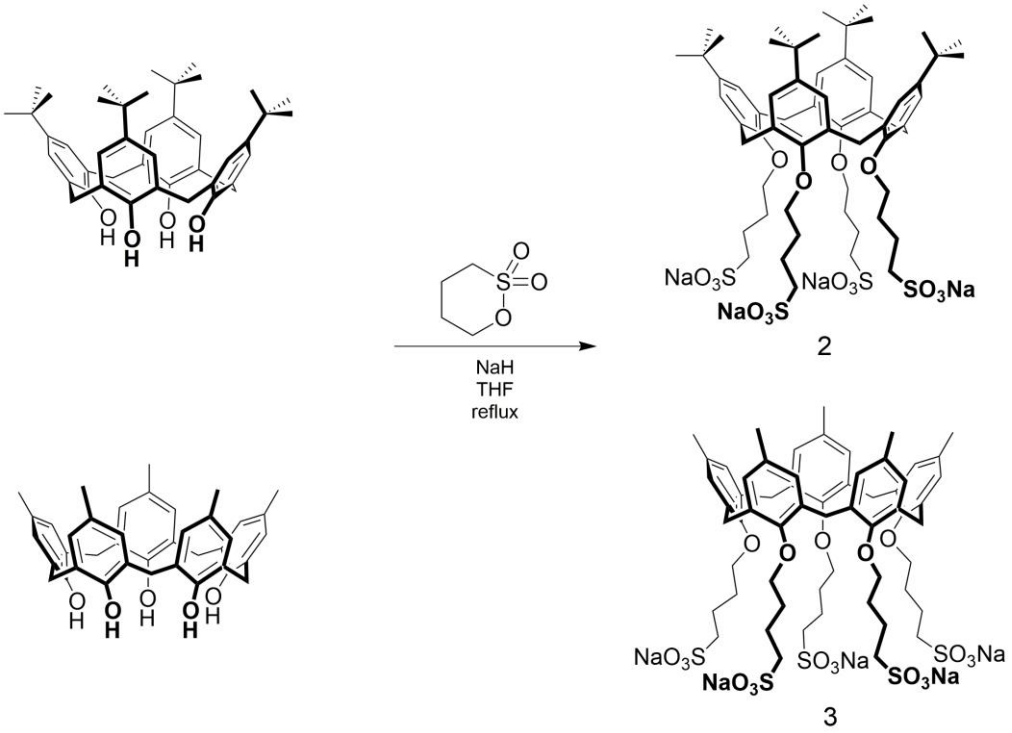

Scheme 2.2.1.1. Synthesis of *p-tert*-butylcalix[4]arene **2** and *p*-methyl-calix[5]arene **3**.

Amphiphilic calixarene **2** and **3** were obtained (in 64% and 56% yields, respectively) from *p-tert*-butylcalix[4]arene and *p*-methylcalix[5]arene, by reaction with 1,4-butanesultone (3 equiv. x OH) and NaH (3 equiv. x OH) in refluxing anhydrous THF for 48 hours. The white powder obtained after addition of MeOH was collected, washed with EtOH, redissolved in water and finally precipitated by the salting-out method using a solution of sodium acetate. As expected, both derivates **2** and **3**

showed an amphiphilic nature. The detailed amphiphilic features of derivatives **2** and **3** will be reported in the next section and in Chapter 4 respectively.

2.2.2. Self-assembly of amphiphilic anionic calix[4]arene **2** *and drug solubilisation.*‡

Here I will describe a deep insight on the aggregation properties of the amphiphilic *p-tert*-butylcalix[4]arene tetra-*O*-butylsulfonate (**2**) by means of complementary techniques, 1D and 2D NMR, Dynamic light scattering (DLS) and atomic force microscopy (AFM). Furthermore the ability of the micellar aggregates of calixarene **2** to increase the solubility of poorly water soluble drugs was also studied.

The amphiphilic nature of derivative **2** was immediately tested through preliminary NMR experiments. The ^{1}H NMR spectrum of **2**, recorded at a low concentration ([**2**] = 0.2 mM, D_2O), displays a set of sharp resonances typical of calixarene species adopting a cone conformation (Figure 2.2.2.1a).[17] In particular the presence of singlets at δ 6.87 and δ 0.97 ppm (relative to the aromatic and *tert*-butyl hydrogens, respectively) together with one single AX system (δ 4.31 and 3.13 ppm, J = 12.5 Hz) for the axial and equatorial hydrogens of the bridging methylenes, experiencing different magnetic anisotropy generated by aryl residues, confirm the cone conformation of derivative **2**. Upon increasing the concentration to 1.4 mM (Figure 2.2.2.1b), the resonances broaden, indicating that an aggregation process is taking place, and thus

‡ *The experimental results reported in this section have been already published: Barbera L. et al., Org. Biomol. Chem.,* ***2015****, 13, 6468.*

confirming the surfactant nature of **2**. A comparison of traces (a) and (d) in Figure 2.2.2.1 revealed that the resonances relative to the aromatic and the *tert*-butyl hydrogens underwent an upfield shift upon concentration. This can be explained considering that in the micelle, calixarene molecules are forced to stay closer and, as a consequence, some resonances resulted affected by the anisotropic shielding of the aromatic rings of surrounding calixarenes.

A closer inspection of the aromatic region in traces (b) and (c) revealed a second broad signal for the aromatic protons at δ 6.78 ppm (see arrows in Figures 2.2.2.1b and 2.2.2.1c), whose intensity increases until it becomes the predominant species in solution (for [**2**] ≥ 4.0 mM, Figure 2.2.2.1d) and can be assigned to the formation of micellar aggregates. The concomitant presence of two close but distinct sets of aromatic signals indicates a slow exchange on the NMR time-scale between the two species (monomer and micelle). This phenomenon is quite unusual in conventional surfactants but has been already reported for some amphiphilic calixarenes.[18]

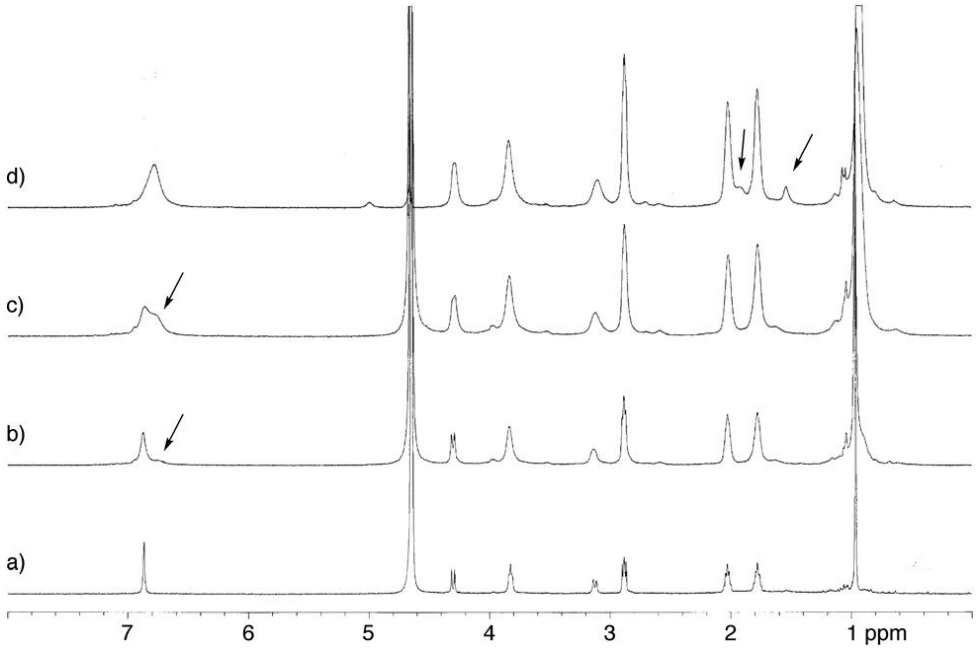

Figure 2.2.2.1. ^{1}H NMR (500 MHz, 298 K, D_2O) spectra of calix[4]arene **2** at different concentrations: (a) 0.2 mM, (b) 1.4 mM, (c) 2.3 mM and (d) 4 mM.

The critical micellar concentration (cmc) for **2** in D_2O was determined by diffusion-ordered NMR (DOSY)[19] studies, using calixarene solutions in the 10.0–0.10 mM concentration range. In table 2.2.2.1 are reported the Diffusion Coefficients ($D_{2,obs}$) for selected resonances (SCH_2) which were found isochronous in the concentration range investigated and therefore represent the weighted average Diffusion Coefficients for monomers and micelles present in solutions. As can be observed, the values of $D_{2,obs}$ decreases (from 2.52×10^{-10} to 0.80×10^{-10} m^2/s) by increasing the concentration of derivative **2**. This result is consistent with the formation of bigger, and therefore slower diffusing species (micelle). A cmc of 1.15 mM was estimated from the intersection point of the two lines best fitting the experimental data points obtained by plotting the self-diffusion coefficient ($D_{2,obs}$) *vs*. the inverse of the concentration of

calixarene **2** (Figure 2.2.2.2). Another research group determined for the same calixarene a cmc of 1.76 mM by surface tension analysis.[20]

[**2**] (mM)	$D_{2,obs} \times 10^{-10}$ (m^2/s)
10	0.80 ± 0.03
7.5	0.88 ± 0.03
5	0.98 ± 0.01
4	1.14 ± 0.03
3	1.33 ± 0.08
2.8	1.38 ± 0.01
2.6	1.43 ± 0.03
2.5	1.48 ± 0.01
2.4	1.49 ± 0.01
2.3	1.54 ± 0.02
2.2	1.58 ± 0.02
2.1	1.62 ± 0.03
2.0	1.70 ± 0.03
1.9	1.76 ± 0.01
1.8	1.82 ± 0.02
1.7	1.88 ± 0.04
1.6	1.94 ± 0.04
1.5	2.01 ± 0.03
1.4	2.08 ± 0.02
1.3	2.16 ± 0.01
1.2	2.20 ± 0.02
1.1	2.28 ± 0.03
1.0	2.35 ± 0.02
0.9	2.39 ± 0.03
0.6	2.47 ± 0.02
0.4	2.48 ± 0.01
0.2	2.52 ± 0.01
0.1	2.52 ± 0.02

Table 2.2.2.1. Diffusion coefficients ($D_{2,obs}$) of the species present at 298 K in D_2O solutions of calixarene **2** at different concentrations. Data were calculated from DOSY experiments, using the SCH_2 resonance (δ = 2.89 ppm) as the probe signal.

A closer inspection of the concentration ranges slightly below and above the cmc (see the insert in Figure 2.2.2.2) showed the presence of two distinct break points (at 0.83 mM and 1.41 mM, respectively), reasonably ascribable to two distinct aggregation phenomena of **2**. The former (0.83 mM) likely refers to the initial formation of small oligomers (premicelles)[21] seen – on the NMR time-scale – in a fast-exchange regime with the monomers. The latter (1.41 mM), on the other hand, most probably indicates the onset of micellar aggregation (Figure 2.2.2.1b).

As the concentration of **2** increases further (above 3.0 mM), new peaks appear in the ^{1}H NMR spectrum (see arrows in Figure 2.2.2.1d) and, accordingly, new aggregates form as a result of an additional structural transition (micelle–micelle or micelle–vesicle). These newly-formed aggregates could not be studied by NMR because of the poor solubility of **2** at concentration above 10 mM.

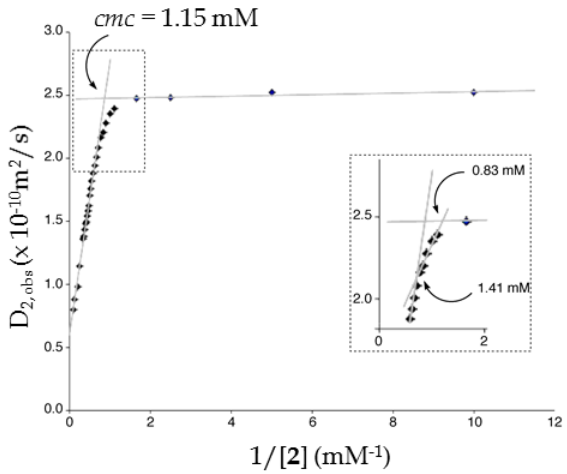

Figure 2.2.2.2. Plot of the self-diffusion coefficients ($D_{2,obs}$) *vs.* the inverse of the concentration of calixarene **2** in D_2O at 298 K.

The hydrodynamic radii (R_h) of the monomer (7.9 Å) and the micelle (24.9 Å) were conveniently obtained from the $D_{2,obs}$ values determined below ([**2**] = 0.1 mM) and above ([**2**] = 10.0 mM) the cmc, using the Stokes–Einstein equation ($D_{obs} = k_BT/6\pi\eta R_h$) which correlates Diffusion Coefficient and hydrodynamic radii assuming a spherical shape of the objects under investigation.

Additional evidence corroborating micelle formation was obtained from 2D NOESY studies (Figure 2.2.2.3.). The spectrum of a 5.0 mM solution of **2** shows NOE cross-peaks for all the calixarene resonances. Interestingly, there are cross-peaks indicating the proximity of the upper-rim *tert*-butyl hydrogen atoms and the lower-rim butanesulfonate residues of adjacent calixarene molecules. The absence of cross-peaks in the spectrum of **2** in the monomeric form (0.5 mM) demonstrates the intermolecular origin of the NOEs mentioned earlier (*i.e.*, [**2**] = 5.0 mM), suggesting that in the micellar aggregate the calixarene units are probably arranged in a staggered fashion (Figure 2.2.2.4).[22]

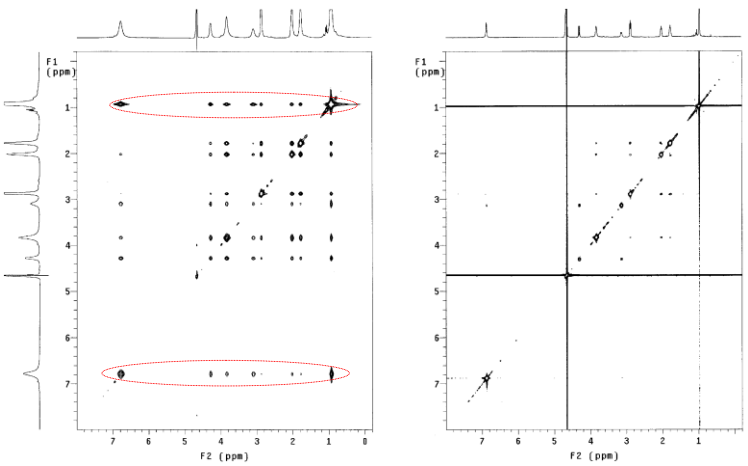

Figure 2.2.2.3. 2D NOESY spectra of: (a) [**2**] = 5.0 mM, (b) [**2**] = 0.5 mM.

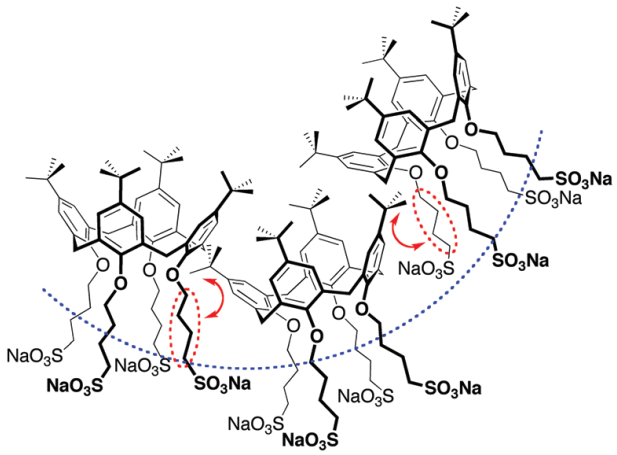

Figure 2.2.2.4. Schematic representation of staggered calixarene molecules within a micelle. Arrows indicate relevant NOE cross-peaks.

As already observed for the homologous calix[5]arene,[23] NMR quantitative analysis of D_2O solutions of calixarene **2** below the cmc, carried out using the quantitative qNMR software *Varian Vnmrj 3.2*, showed an apparent discrepancy between the nominal and the detectable concentrations of monomers in solution (for example, for [**2**] = 0.2 mM, a concentration of [**2**] = 0.1 mM was calculated), indicating that NMR "invisible" aggregates of **2** were present even at low concentrations. This finding is in line with previous observations on the tendency of amphiphilic calixarene-type surfactants to aggregate below the cmc in large infinite structures ("open model"[24]). In order to confirm the presence of such big aggregates, dynamic light scattering (DLS) experiments were performed on solutions of calixarene **2** below the estimated cmc value. The DLS experiments (Figure 2.2.2.5) revealed the presence of two populations of very large aggregates, with hydrodynamic radii of approximately 100 and 300 nm. The number fraction of the 300 nm aggregates was found to be about 0.03.[25]

When 0.5 and 5.0 mM aqueous solutions of **2** were pre-filtered through a 0.45 μm Millipore membrane, the 100 nm aggregates became even more predominant, with the number fraction of the larger aggregates (300 nm) decreasing to about 0.01 and becoming almost negligible in the two solutions, respectively (Figure 2.2.2.5b). Remarkably, no smaller micellar aggregates (*i.e.*, in the 2 nm range) were visible by DLS either before or after filtration. The obtained results demonstrated that a combined use of DOSY – for the smaller aggregates – and DLS – for the larger ones, "transparent" to NMR[26]– is necessary to get a full picture of the aggregation behaviour of amphiphilic molecules such as **2**.[27]

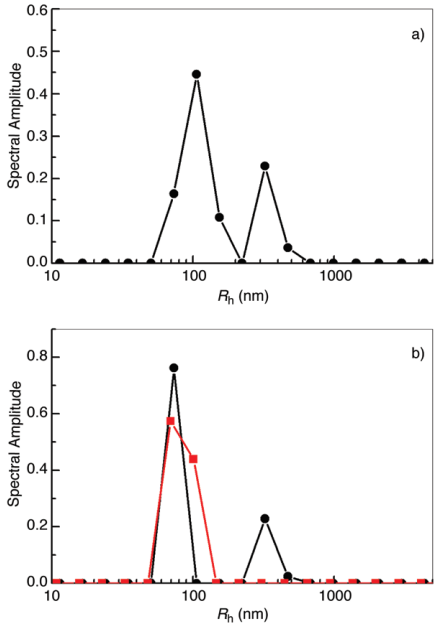

Figure 2.2.2.5. Size distributions of the calixarene **2** aggregates in aqueous solution: (a) [**2**] = 0.5 mM; (b) [**2**] = 0.5 and 5.0 mM (black and red trace, respectively) after filtration through a 0.45 μm Millipore filter.

Further information on the morphology of the aggregates were finally provided by atomic force microscopy (AFM) measurements. As showed

in figure 2.2.2.6, derivative **2** tends to form complex structures, most of them having an average diameter of 100–200 nm, though many smaller particles (ca. 50 nm) are also visible (Figure 2.2.2.6.).

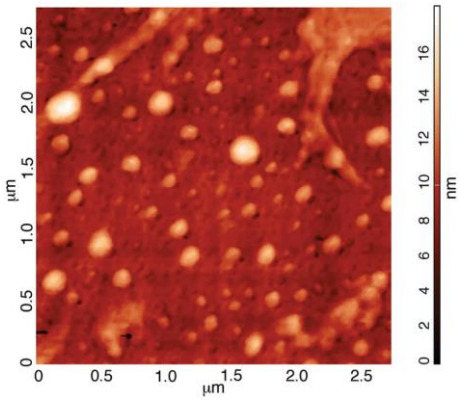

Figure 2.2.2.6. AFM topography image of calixarene **2**.

All these data indicate that calixarene **2** self-assembles in premicelles and very large aggregates below the cmc, as schematically depicted in Figure 2.2.2.7.

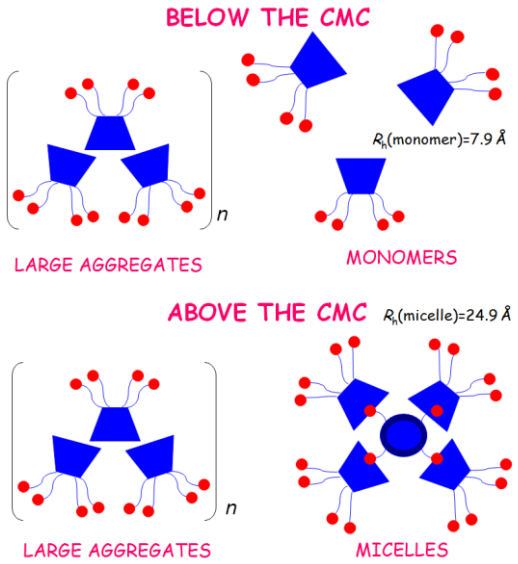

Figure 2.2.2.7. Cartoons of the aggregation process.

Micellar systems find medical and pharmacological applications as drug delivery systems, especially thanks to their ability to solubilise in aqueous media poor-water soluble drugs. Moreover their reduced size, loading and releasing abilities, governed by their cmc, make micelle-based drug delivery systems more advantageous than other systems such as water soluble polymers or liposomes.

In order to test the potential of amphiphilic calix[4]arene **2** to act as a molecular carrier upon micelle formation, we decided to investigate its ability to increase the water solubility of the nonsteroidal anti-inflammatory hydrophobic drugs naproxen (**4**) and flurbiprofen (**5**).

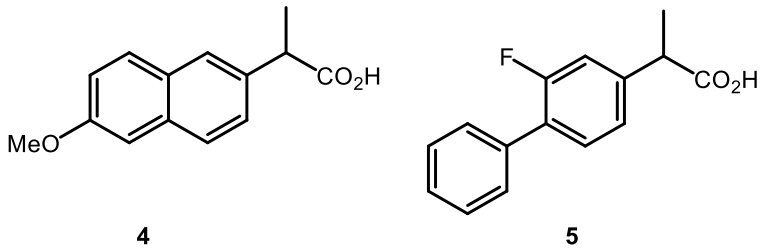

4 **5**

Figure 2.2.2.8. Structures of naproxen (**4**) and flurbiprofen (**5**).

In these experiments, a fixed amount of solid **4** or **5** (5 μmol) was added to 1 mL of the surfactant solution above the cmc ([**2**]= 5 mM, D_2O) previously filtered through a 0.1 μm Millipore filter, and the samples were stirred at room temperature overnight. The solutions were then centrifugated to remove undissolved solid. The ^1H NMR spectra of naproxen and flurbiprofen in D_2O prior to and after segregation within the 5.0 mM micellar solution of **2** are shown in Figure 2.2.2.9. In both cases under examination, all the resonances of **4** and **5** underwent significant complexation-induced shifts, as a result of an interaction

between the drug and the micellar environment provided by **2**. In order to rule out the formation of inclusion complexes between **2** (as a monomer) and the two drug molecules, parallel extraction experiments, were performed below the cmc (Figure 2.2.2.10.).

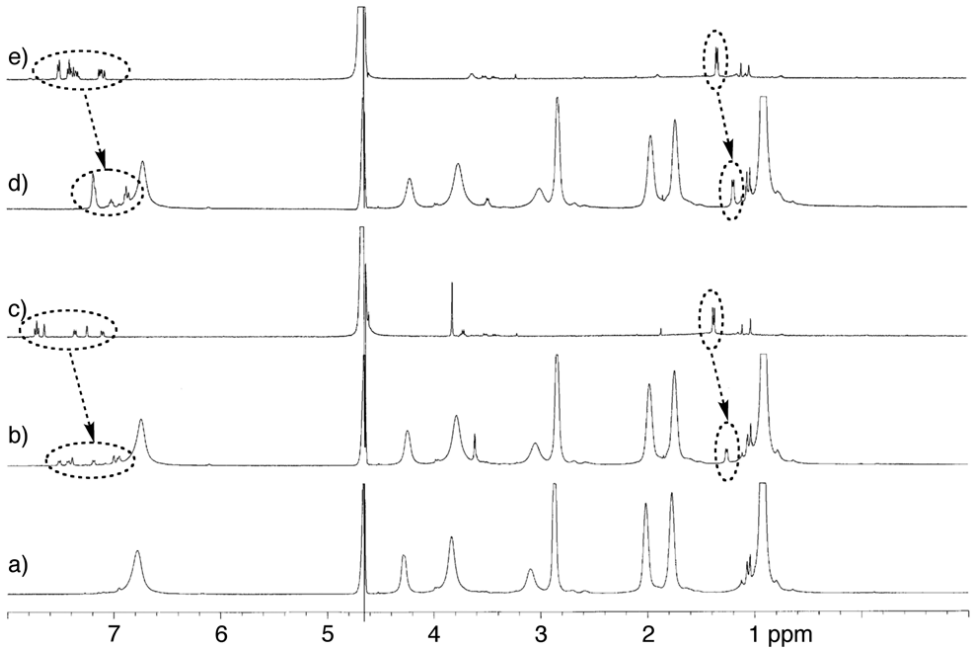

Figure 2.2.2.9. ^{1}H NMR (500 MHz, 298 K, D2O) spectra of: (a) [**2**] = 5.0 mM; (b) **4** after extraction with a 5.0 mM solution of **2**; (c) [**4**] = 0.14 mM; (d) **5** after extraction with a 5.0 mM solution of **2** and (e) [**5**] = 0.13 mM.

As shown in Figure 2.2.2.10 for drug **5**, adding increasing amount of **2** (in the 0.25 – 0.75 mM range, that is below the cmc) to a 0.13 mM solution of flurbiprofen (**5**) did not produce any detectable complexation-induced shifts of the drugs' resonances. These data confirm that the drug molecule was not encapsulated inside the calixarene cavity, but rather located in the lipophilic palisade of the micellar aggregate.

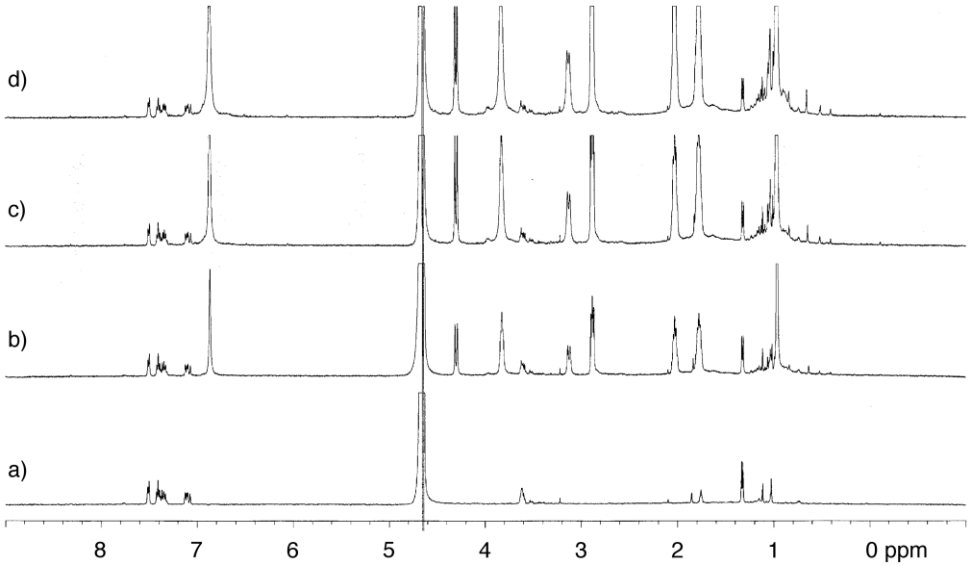

Figure 2.2.2.10. Flurbiprofen (**5**) extraction experiments with **2** below the cmc: a) [**5**] = 0.13 mM; b) [**2**] = 0.25 mM, [**5**] = 0.13mM; c) [**2**] = 0.5 mM, [**5**] = 0.13 mM; d) [**2**] = 0.75 mM, [**5**] = 0.13 mM.

To confirm this hypothesis 2D NOESY NMR experiments were used to shed light on the location and orientation of the drugs within the micelles.

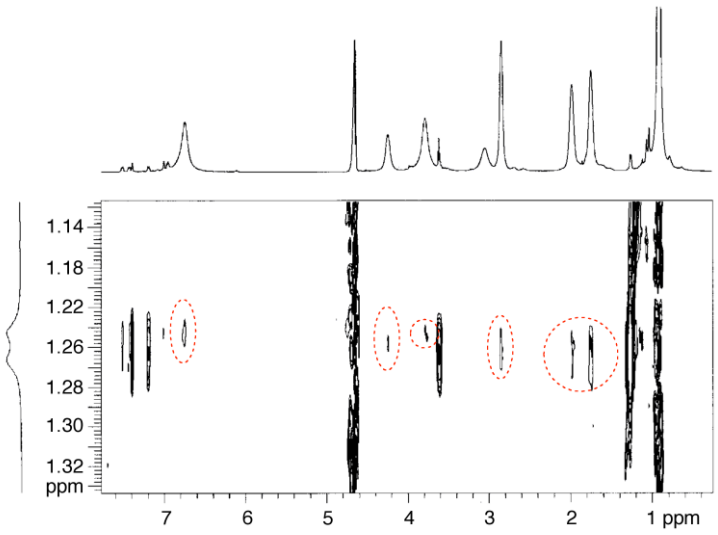

Figure 2.2.2.11. Section of the 2D NOESY spectrum (500 MHz, 298 K) of a D_2O solution of **2** and **4**.

In the case of **4**, the α-CH_3 group shows NOE interactions with the hydrogen atoms of both the aromatic and the aliphatic moieties of **2** (Figure 2.2.2.11.)

In the case of Flurbiprofen (**5**) stronger correlation peaks of the aromatic signal at δ 7.19 ppm with all the calixarene resonances (red circles in Figure 2.2.2.12.), demonstrated the presence of NOE contacts. Cross-peaks are consistent with the aromatic unit of **5** and the lower-rim aliphatic moieties of **2** being in close proximity. All these findings suggest that both naproxen and flurbiprofen molecules most likely reside within the micellar palisade of **2**, oriented in such a way that the aromatic ring of the drug points towards the interior of the micelle, where they can experience favourable π–π interactions with the calixarene outer faces, while the carboxylic acid moiety points in the opposite direction, towards the bulk.

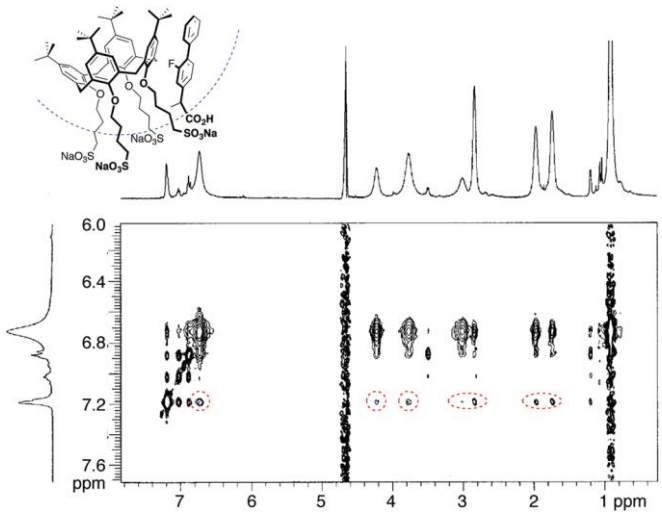

Figure 2.2.2.12. Section of the 2D NOESY spectrum (500 MHz, 298 K) of a D_2O solution of **2** and **5**.

Our next objective was to estimate the degree of solubilisation of the two drugs by the calixarene micellar solutions. To this purpose, three different solutions of **2** with concentrations above the cmc (2.5, 5.0 and 10.0 mM) were employed for solid–liquid extraction experiments with a fixed aliquot of drug samples (5 μmoles). After 24 h stirring at room temperature, the resulting suspensions were centrifuged to remove the undissolved **4** or **5**, as well as any large calixarene/drug aggregates formed, and then the concentrations of the calixarene and naproxen/flurbiprofen present in the supernatant were determined by a quantitative NMR protocol.

Data in Figure 2.2.2.13 show the amount of naproxen and flurbiprofen solubilised as a function of the surfactant concentration. The linear correlation observed is a clear evidence that the water solubility of these drugs[28] significantly improves with increasing calixarene concentration. Molar solubilisation capacities of 0.20 and 0.51, for naproxen and flurbiprofen respectively, were derived from the slope of the linear regression. To the best of our knowledge, these results compare well with those reported for other anionic surfactants.[29]

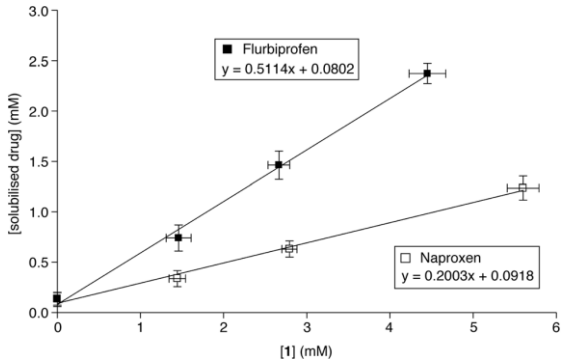

Figure 2.2.2.13. Plots of drug vs. calixarene concentrations determined by quantitative NMR.

It is a matter of fact that the extent of segregation of molecules bearing acid moieties inside anionic micelles depends on the pKa of the target molecule, that is, the lower the pKa of the target molecule, the stronger the repulsion between the acidic guest (in the deprotonated form) and the anionic head-groups of the micelles is expected to be, thus decreasing the solubilisation efficiency.[30] On the other hand, it is known that the pKa of lipophilic carboxyl acids may increase in the hydrophobic medium of micelles with respect to aqueous solution.[31] Naproxen and flurbiprofen (p*Ka ca.* 4.2–4.8)[32] are not fully ionized in an aqueous solution of calixarene **2** (pH 5.4) and, as a result, the undissociated form can easily be incorporated inside the anionic micelles.

Being aware that quantitative NMR measurements cannot indicate the molar fraction of drug molecules segregated inside very large aggregates (R_h = 100–300 nm) – as these are "NMR invisible"– the total concentration of naproxen dissolved in an aqueous 5.0 mM micellar solution of **2** was also investigated by UV spectroscopy. To this end, to avoid the potential overlapping of calixarene and naproxen absorbance bands during the analysis in aqueous solution, naproxen was extracted in $CHCl_3$ and its concentration was spectrophotometrically determined, in the absence of **2**, before and after filtration of the aqueous solutions through 0.1 μm Millipore filters.

	UV (prior filtration)	UV (after filtration)	NMR
Dissolved Naproxen			
mM	0.85 ± 0.03	0.63 ± 0.03	0.63 ± 0.05
mg/mL	0.196 ± 0.007	0.145 ± 0.07	0.145 ± 0.011

Table 2.2.2.2. UV and NMR determination of naproxen (**4**) solubility in a 5.0 mM micellar solution of **2**.

Data obtained (Table 2.2.2.2.) for the filtered solutions ([**4**] = 0.63 ± 0.03 mM) are in excellent agreement with the NMR measurements, whereas slightly higher values were found for the unfiltered ones ([**4**] = 0.85 ± 0.03 mM), thus indicating that the bigger aggregates of **2** are also able to encapsulate the drugs under investigation (Figure 2.2.2.14).

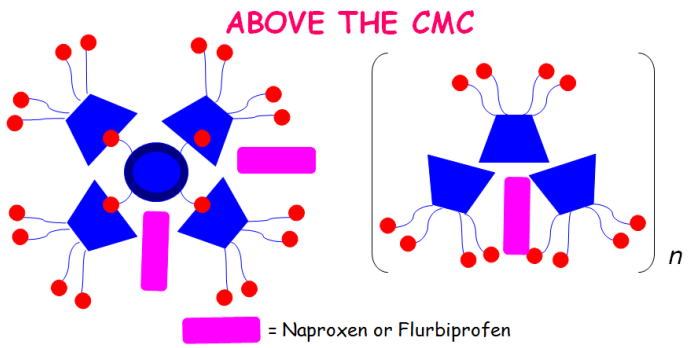

Figure 2.2.2.14. Cartoons of the drugs encapsulation inside the aggregates.

The affinity of drugs **4** and **5** for the micellar environment of calixarene **2** was also demonstrated by means of DOSY measurements. Data in Table 2.2.2.3 show that the diffusion coefficients of naproxen and flurbiprofen decrease from 5.47–5.66 × 10^{-10} m^2/s (for the free species) to values closer to those of the calixarene micellar aggregates. These results clearly

demonstrate that the translational mobility of **4** and **5** is considerably reduced as a result of their binding to the micelles.

Moreover, the diffusion coefficients of calixarene **2** in drug-encapsulated micelles ($D_{2,drug}$ Table 2.2.2.3) are even smaller than those measured for **2** on its own (D_2). These latter values were calculated in D_2O solutions of calixarene **2** at concentrations equivalent to those measured (by quantitative NMR) in the supernatant of the solid-liquid extraction experiments mentioned earlier (*i.e.,* [**2**] = 2.5 and 2.8 mM in the cases of **4** and **5** respectively). The decrease of $D_{2,drug}$ values indicates that upon drug encapsulation, micellar aggregates of calixarene **2** grow in size.

	D_{drug}	$D_{drug,2}$	$D_{2,drug}$
4	5.47 ± 0.08	1.58 ± 0.04	0.98 ± 0.02 (D_2 = 1.38 ± 0.01 at 2.5 mM)
5	5.66 ± 0.07	1.29 ± 0.02	1.01 ± 0.02 (D_2 = 1.48±0.01 at 2.8 mM)

Table 2.2.2.3. Diffusion coefficients ($\times 10^{-10}$ m^2/s) of drugs **4** and **5** on their own (D_{drug}), after extraction with a 5.0 mM solution of **2** ($D_{drug,2}$), and **2** after binding the drug ($D_{2,drug}$).

These findings were further confirmed through AFM images showing, especially in the case of the flurbiprofen (Figure 2.2.2.15), a different micellar morphology.

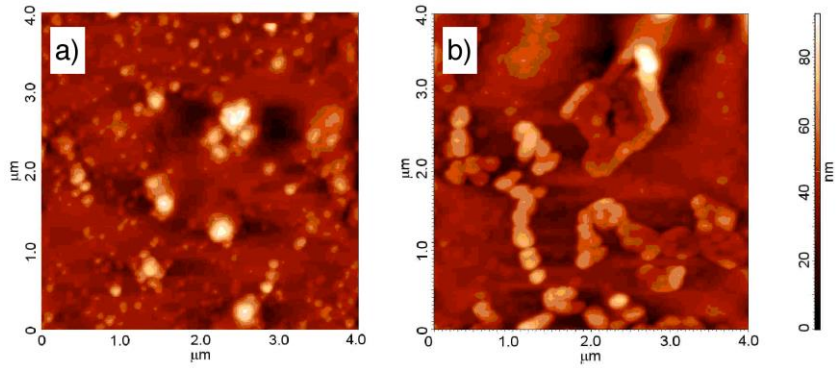

Figure 2.2.2.15. AFM images of a) **2** + **4**; b) **2** + **5**.

2.2.3. PEGylated-Calix[5]arenes: results and discussion

Due to its biocompatibility, polyethylene glycol (PEG), is widely used to functionalize bioactive molecules for drug delivery and nanotechnology applications.[33] Because of the several applications of PEGylated substrates, considering the biological activity of large-ring PEGylated calixarenes,[13] the potentials of any calix[4]arene derivatives as drug-delivery systems,[14] and inspired by the recent report on the supramolecular PEGylation of the insulin protein by a PEGylated cucurbit[7]uril,[34] during my PhD project, I synthesised new water soluble neutral PEGylated-calix[5]arenes via the modification of the lower rim.

Calix[5]arenes **6** and **7** were synthesised in one step (Scheme 2.2.3.1), respectively by reacting *p-tert*-butyl-calix[5]arene or *p*-methyl-calix[5]arene with $MeOPEG_{550}$-OTs (3 equiv. x OH) and K_2CO_3 (3.5 equiv. x OH) in refluxing anhydrous CH_3CN. Purification through multiple chromatographic separations (CH_2Cl_2/MeOH 98:2 – 9:1) gave pure **6** and **7** in 40% and 44% respectively.

This new family of macrocycles displays a great solubility in both organic solvents and in water.

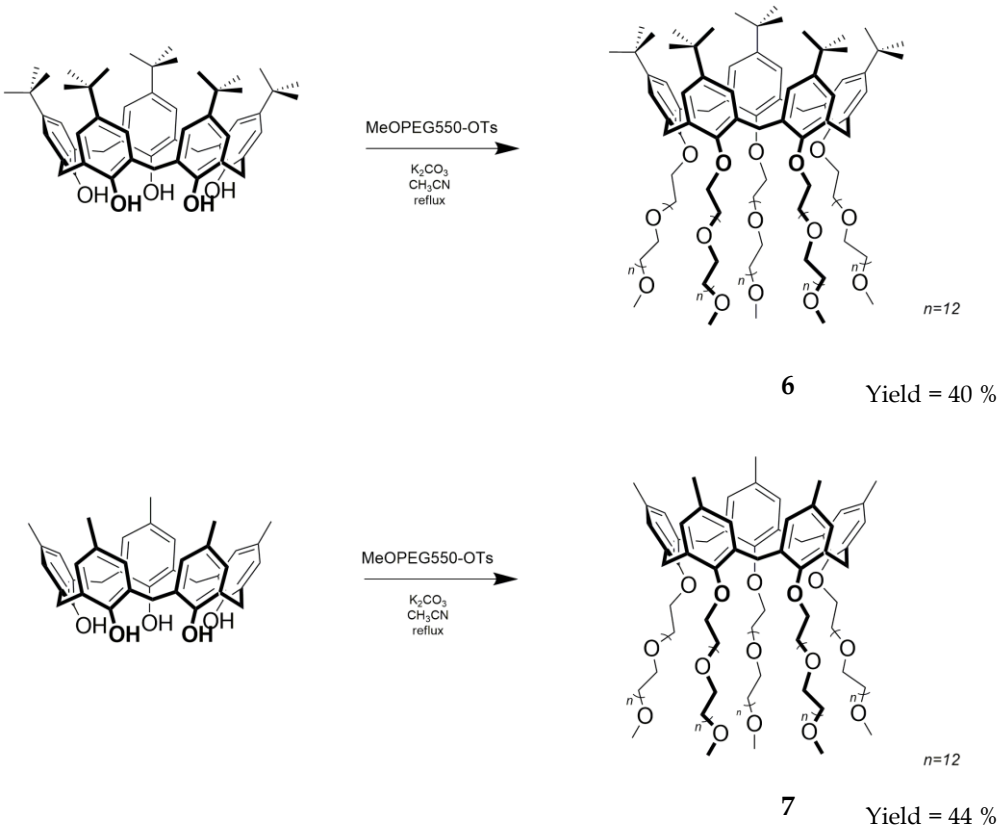

Scheme 2.2.3.1 Synthesis of calix[5]arenes **6** and **7.**

The synthesised PEGylated-calix[5]arenes were characterized by means of NMR spectroscopic techniques in both organic and aqueous solvents. ^{1}H NMR spectra of calix[5]arenes **6** and **7** in organic solvent ($CDCl_3$) show the typical resonances of *p*-alkyl-calix[5]arenes adopting a C_{5v} cone conformation (Figures 2.2.3.1a and 2.2.3.2a), that is one singlet for the

aromatic hydrogen atoms, one AX system for the bridging methylenes and one singlet for *p*-*tert*-butyl or *p*-methyl groups.

In line with its amphiphilic nature, when dissolved in D_2O, calixarene **6** showed broad signals (trace 2.2.3.1b) indicating that an aggregation process is taking place in this solvent. Notwithstanding the broadening of signals, the broad singlets for aromatic and *tert*-butyl hydrogens atoms revealed that the calixarene framework maintained a regular cone conformation. Unexpectedly the ^1H NMR analysis of a D_2O solution of calixarene **7** (trace 2.2.3.2b) showed a very complex broad spectrum not compatible with a regular cone conformation.

It is known that calixarene derivates may display, depending on the substituents at both the upper and lower rim, conformational interconversions to the non-cone structures. In the case of calix[5]arene derivates the so called "upper-rim-through-the-annulus" rotation is allowed only when hydrogen is present in the *para*-position, while groups bulkier than a propyl residue completely inhibit the "lower-rim-to-the-annulus" interconversion.[35] On this basis, the interconversion of cone **7** to less regular conformers could be ruled out and the complexity of the NMR spectrum was ascribed to a very distorted, and hence not symmetrical cone conformation (trace 2.2.3.2b). Upon increasing the temperature (T >338 K) the distorted conformation of calixarene **7** evolved into a predominant regular cone conformation (Figures 2.2.3.3a-e).

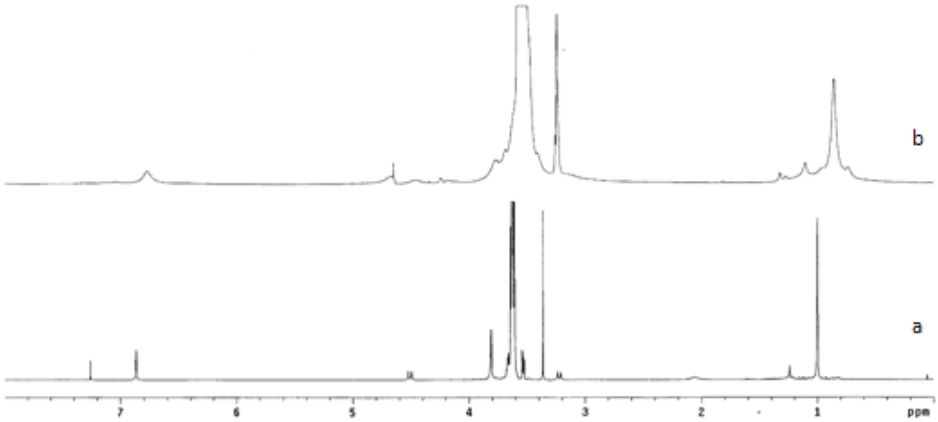

Figure 2.2.3.1 ^{1}H NMR (500 MHz, 298 K) spectra of: (a) [**6**] = 5.0 mM, $CDCl_3$. [**6**] = 5.0 mM, D_2O.

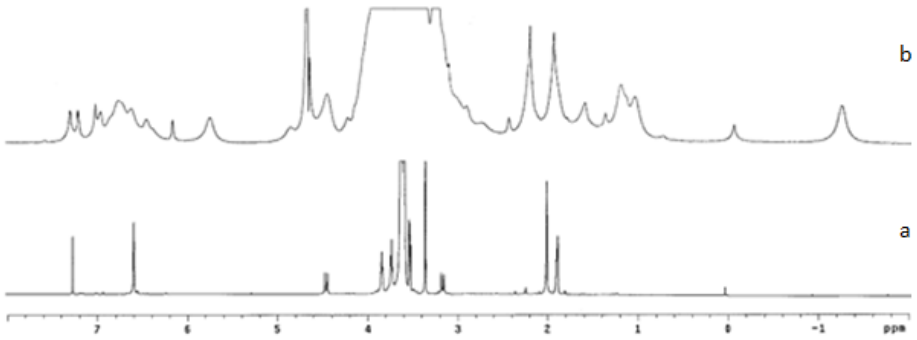

Figure 2.2.3.2 ^{1}H NMR (500 MHz, 298 K) spectra of: (a) [**7**] = 8 mM, $CDCl_3$, 298 K; (b) [**7**] = 8 mM, D_2O.

The presence of five distinct resonances for the methyl groups are more evident at lower temperature (T = 278 K, trace a Figure 2.2.3.3) in the region δ 2 – -2 ppm. In particular the high field resonance at ~δ –1.2 ppm indicates that derivative **7** probably adopts an overall *cone-in* conformation with one methyl group leaning toward the interior of the cavity and therefore being affected by the anisotropic shielding of the calixarene cavity.

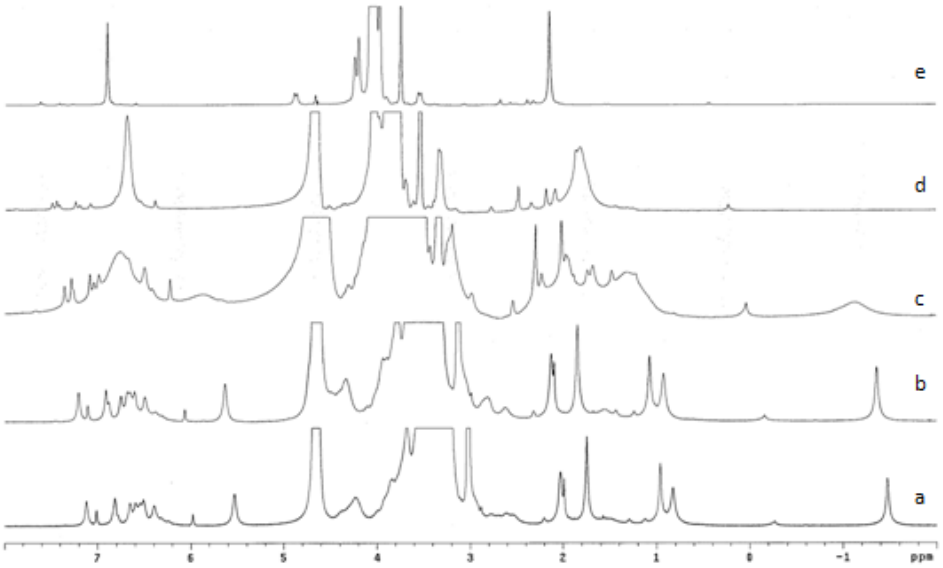

Figure 2.2.3.3 ^{1}H NMR (500 MHz, D_2O) spectra of: (a) [**7**] = 8 mM, 278 K; (b) [**7**] = 8 mM, 288 K; (c) [**7**] = 8 mM, 308 K; (d) [**7**] = 8 mM, D_2O, 328 K; (e) [**7**] = 8 mM, D_2O, 353 K.

NMR spectroscopy revealed to be unsuitable to determine the very low cmc value for these new surfactants, these values being conveniently determined by the Rose Bengal micellization method.[36] Dyes such as Merocyanine, Eosin, Rhodamine, Rose Bengal and Sudan are known to show a shift in their absorption maximum wavelength (λ_{max}) when included in the apolar environment of micelles.

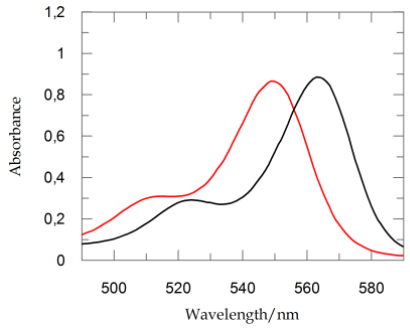

Figure 2.2.3.4 Absorption spectra of Rose Bengal in water (red line) and in an apolar medium (black line).

In particular, Rose Bengal in water shows a λ_{max} at 546 nm, while in an apolar environment λ_{max} shifts to 563-565 nm (Figure 2.2.3.4).In order to determine the aggregation features of derivates **6** and **7,** a series of 10 μM solutions of Rose Bengal containing different amounts of calixarenes **6** or **7** (in the range 0 – 1 mM) were prepared and stirred overnight. The cmc was estimated by plotting the absorbance at λ = 563 nm *vs.* the concentrations of **6** and **7**. Graphics in figures 2.2.3.5b,d show three different regions with increasing the calixarene concentrations: a first linear trend compatible with the presence in solution of monomeric species, a clear change in the slope suggesting the formation of aggregates, an almost flattened region indicating that the aggregation process was completed (most of the dye shifted to the micelles). The experimental data obtained by the two lines best fitting the points gave a value of 0.5 μM (1.73 mg/L) and 4.5 μM (14.67 mg/L) respectively for calix[5]arene **6** and **7** (Figure 2.2.3.5a,c). These low values are about two orders of magnitude smaller than those usually obtained for traditional surfactants with similar characteristics[37] (*e.g.* Triton X-100, cmc = 0.2—0.9 mM) but are comparable with data already reported for PEGylated-cyclodextrins.[38]

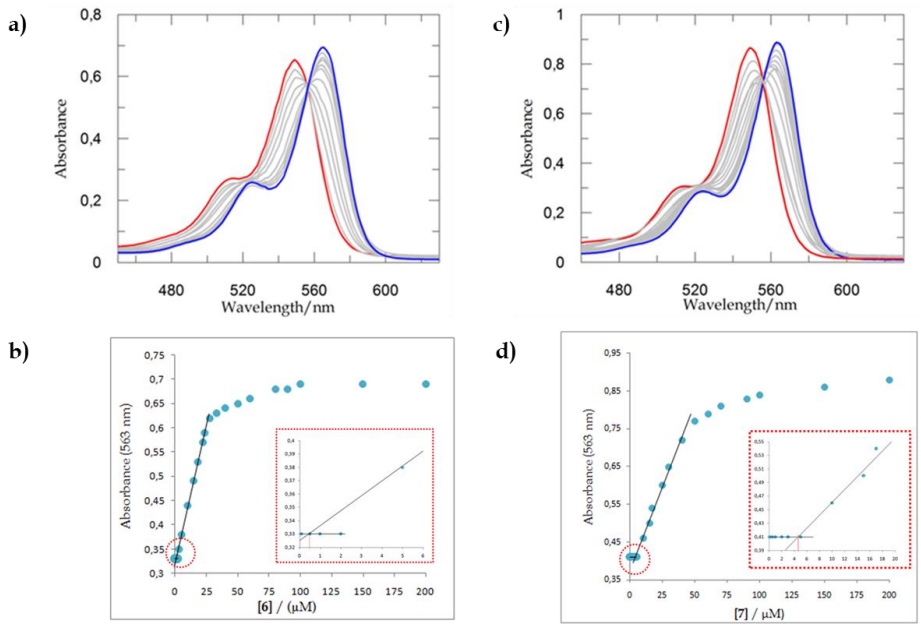

Figure 2.2.3.5. a) Absorption spectra of Rose Bengal 10 μM at different concentrations of calixarene **6**, starting from 0 (red line) to 250 μM (blu line); b)Plot of dye absorbance at 563 nm against concentration of calixarene **6;** c) Absorption spectra of Rose Bengal 10 μM at different concentrations of calixarene **7**, starting from 0 (red line) to 1 mM (blu line); d) Plot of dye absorbance at 563 nm against concentration of calixarene **7.**

Moreover, preliminary experimental data demonstrated that by heating (T= 338K) a solution of PEGylated-calix[5]arene/Rose Bengal (above the cmc), the Rose Bengal maximum wavelength shifted back from 563 nm to 553 nm, indicating that the drug was released from the micellar environment after an increasing of the temperature. Rose Bengal is currently used in ophthalmology for the diagnosis of dry eyes[39] and as photosensitizer for the photodynamic therapy of tumors. However, the low lipid solubility of Rose Bengal has limited its capacity to cross biological barriers such as the cell membranes, and thus limits its clinical application.[40] Low-cmc PEGylated-systems therefore represent interesting candidates for improving the drug lipophilicity by encapsulation inside the micellar environment and for favouring its

delivery after an external stimuli (*e.g.* heating). The presence of the macrocyclic cavity as a further "host-guest recognition site" makes these derivatives fascinating tools for the non-covalent PEGylation of biological substrates. At the moment studies are in progress to determine the morphological features of the PEGylated calixarenes and their potential as supramolecular PEGylation agents for bioactive substrates through host-guest interactions.

2.3. Macrocyclic amphiphiles based on cyclodextrins

Cyclodextrins are cyclic oligosaccharides composed of six, seven, or eight D-glucose units (α–, β–, or γ– CDs, respectively) connected by α-1,4-glucosidic linkages, respectively.[41] CDs assume a toroidal shape with the primary hydroxyl groups on the narrow side and the secondary hydroxyl groups on the wide side. The exterior of the cavity is highly polar due to the presence of hydroxy groups, while the interior is nonpolar, making them suitable and fascinating hosts for supramolecular chemistry.[42] Thanks to their unique structural features and the easy modification on both sides, CDs are also good candidates for constructing macrocyclic amphiphiles.

In early studies, several groups reported on amphiphilic cyclodextrin derivatives that form monolayers at the air–water interface,[43] micelles in water[44] and nanoparticles of pharmaceutical interest.[45] Actually, thanks to their strong binding affinity for hydrophobic drugs, CDs constitute potential carriers for transport through biological barriers.[46] In particular, it is thought that amphiphilic β-CD derivatives interact with biological membranes due to their lipophilic character and many

modified cyclodextrins have been synthesized for that purpose.[47] Concurrently, studies have also shown that cationic entities may be anchored to membranes due to the electronic attraction force between the positive charge of these species and the negative charge of the lipid bilayers of the membrane.[48]

During my PhD, I spent a six-months period in the research group of Professor L. García Río, working on amphiphilic cyclodextrins. In order to take benefits from both cationic and lipophilic properties, we have focused our attention on modified CDs containing a long-chain alkylammonium moiety. Mono- and per-substituted cationic β-CDs with alkylammonium chains of different lengths have been object of studies over the past decades.[49] In particular it has been argued about the possibility of the self-inclusion of the lipophilic alkyl chain of mono-substituted derivatives inside the CD's apolar cavity, and on the morphology of the aggregated systems. Contrary to what generally observed, Hapiot and coworkers[49a] concluded that in *N*-alkyl-*N*,*N*-dimethylammonium-β-cyclodextrins the self-inclusion process decreased their amphiphilic character preventing the micellar aggregation to occur. To gain a deeper inside into the aggregation properties of *N*-alkyl-*N*,*N*-dimethylammonium-β-CDs, the cationic β-CDC_{14} **8** was synthesized.[49a]

The next section describes the self-assembly of the cationic water-soluble amphiphilic β-CDC_{14} **8** by means of different experimental techniques (conductivity, surface tension, turbidity, cryo-tem, DLS). Finally the location (cavity and/or bilayers) of different fluorescent probes was revealed by means of parallel experiments carried out on the native β–CD **9**.

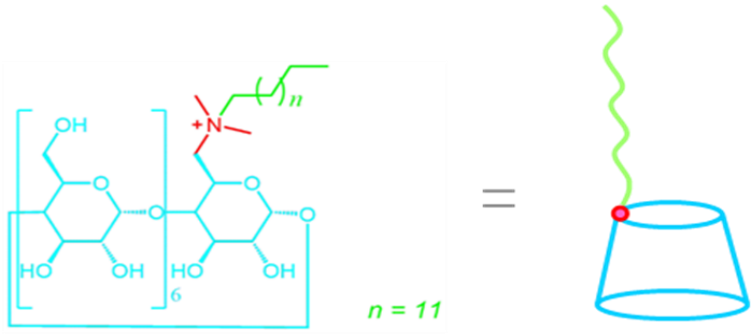

8

Figure 2.3.1. A schematic representation of β-CDC_{14} **8**.

2.3.1. Results and discussion

Mono-substituted cationic cyclodextrin **8** was synthesized according to the procedure reported in literature.[49a]

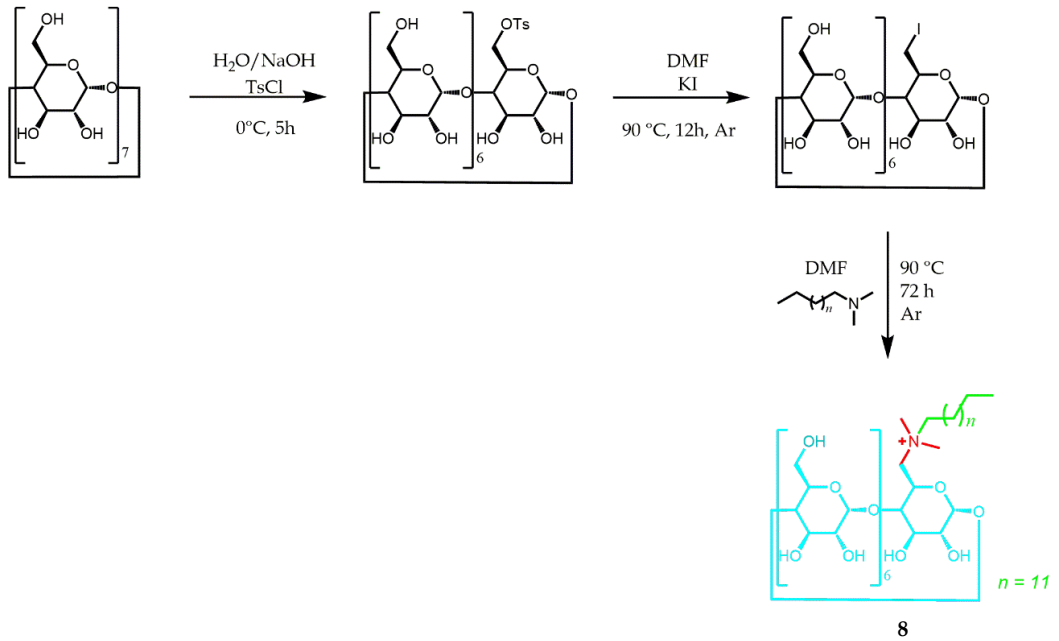

8

Scheme 2.3.1.1. Synthesis of β-CDC_{14} **8**.

Starting from the native β–CD, mono-tosylated[50] and monoiodide[51] β-CDs were successively obtained (Scheme 2.3.1.1). The mono-iodide β-CDI was then reacted with the tertiary N,N-dimethyl-N-tetradecylamine affording the expected N-alkyl-N,N-dimethylammonium cyclodextrin β-CDC_{14} (**8**) in a 74% yield. The ^{1}H NMR spectrum of derivative **8**, as already reported by Hapiot *et al.*,[49a] shows that the two methyl groups bound on the nitrogen atom resulted chemically not equivalent (see arrows in Figure 2.3.1.1) as a consequence of the self-inclusion phenomenon of the alkyl chain inside the CD cavity.

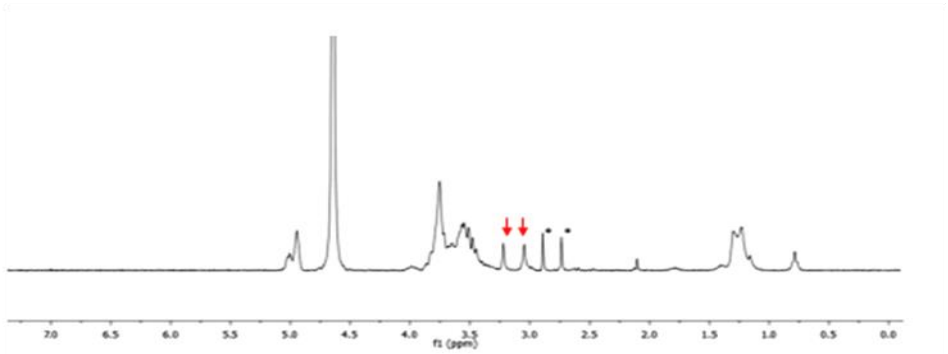

Figure 2.3.1.1. ^{1}H NMR (300 MHz, 298 K) spectrum of cyclodextrin **8** ([**8**] = 2 mM; D_2O). Asterisks indicates DMF from reaction.

More recently, Chevalier *et al.*[49b] demonstrated that only the four terminal residues are involved in the intramolecular inclusion complex with the β-CD head of similar long-chain alkylammonium β-CDs, while the other part of the alkyl chain is in contact to water and contributes to the amphiphilic characteristics. Our experimental data are also in favour of an amphiphilic nature of long-chain cyclodextrins. In details, systematic measurements of surface tension, electrical conductivity and turbidity were carried out in order to explore any possible aggregation

processes and determine the critical aggregation concentration (cac). The experimental results gave values in the range 0.99 – 1.1 mM (Table 2.3.1.1) and not relevant changes were observed on varying the temperature and the ionic force of the medium (see turbidity experiments Figure 2.3.1.3).

	Surface Tension	**Turbidity**	**Conductivity**
cac (M)	1.0×10^{-3}	0.99×10^{-3}	1.1×10^{-3}

Table 2.3.1.1. The cac values of cyclodextrin **8** determined by different experimental techniques.

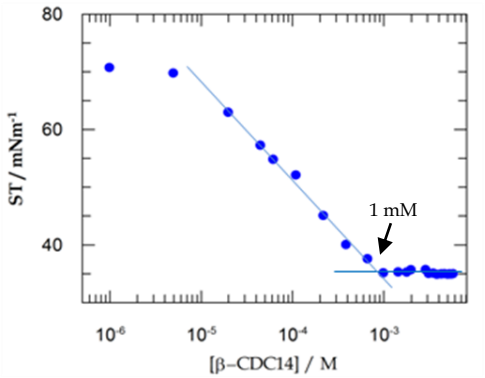

Figure 2.3.1.2. Plot of the surface tension values (ST) *vs.* the concentration of β-CDC_{14} **8** in H_2O at 298 K.

Focusing on the conductivity experiments (Figure 2.3.1.4), a close inspection of the diagram obtained by plotting the conductivity experimental data *vs* the concentration of **8**, shows the presence of two distinct break points at the intersections of the line best fitting the experimental points: according with the other techniques the cac was derived from the clear break point at 1.1 mM; the inflection point in the

region below the cac (at 12 μM) is probably ascribable to an initial aggregation process.

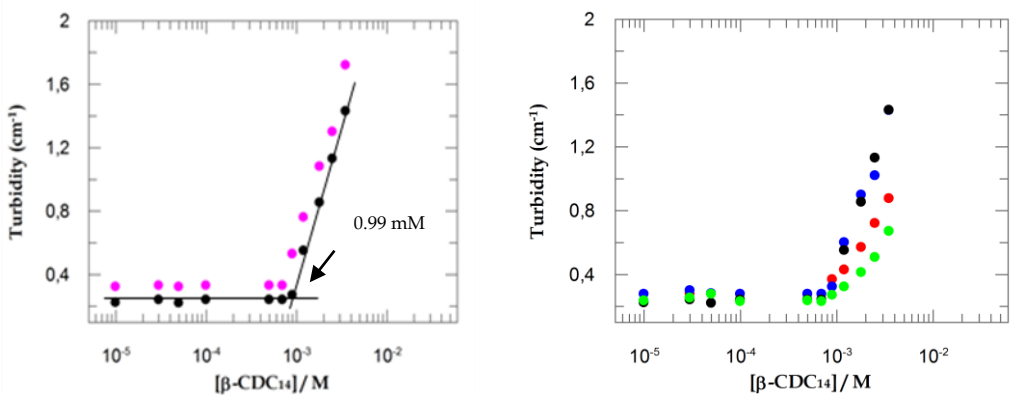

Figure 2.3.1.3. (left) Plot of the Turbidity *vs.* the concentration of β-CDC_{14}: (black) in H_2O at 298 K; (purple) in NaCl 3 M at 298K. (right) Plot of the Turbidity values *vs.* the concentration of β-CDC_{14} in H_2O: green at 288 K, black at 298 K, blue at 308K, red at 318K.

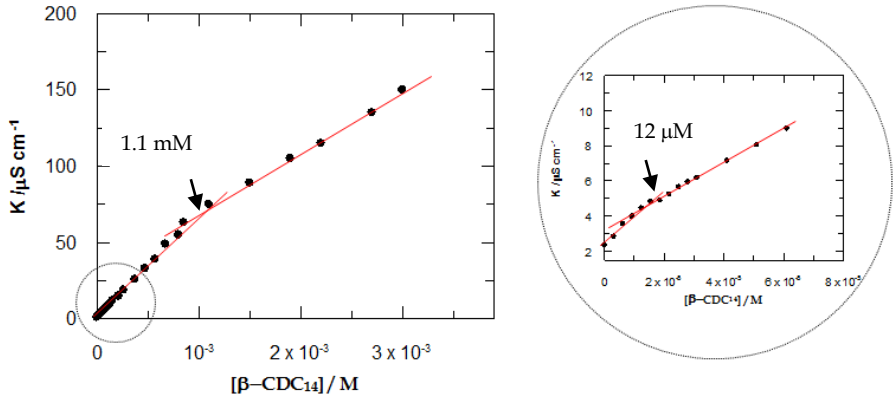

Figure 2.3.1.4. Electrical conductivity *K vs.* the concentration of cyclodextrin **8** in aqueous solutions at 298K.

The morphology of β-CDC_{14} aggregates was obtained by means of Cryo-tem experiments from a 3 mM aqueous solution. As showed in Figure

2.3.1.5 cyclodextrin **8** tends to form very large vesicles with a diameter in the 0.5-2 μm range.

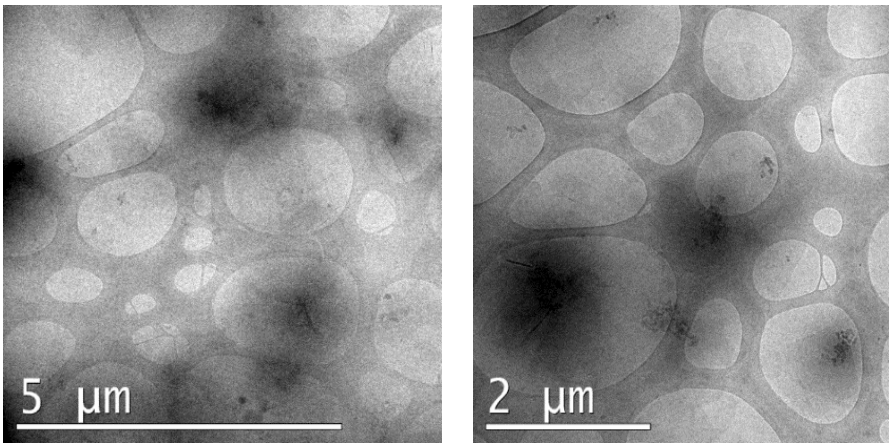

Figure 2.3.1.5. Cryo-tem images.

In line with these observations, dynamic light scattering (DLS) experiments performed on a 10 mM solution of β–CDC_{14} (Figure 2.3.1.6) revealed the presence of a population of aggregates with a diameter of 400-900 nm. When the same solution was pre-filtered through a 0.45 μm Millipore membrane the presence of two different populations were observed, a predominant one with a diameter in the range 1-6 nm (red curve in the insert), and another of 100-400 nm (Figure 2.2.1.6b).

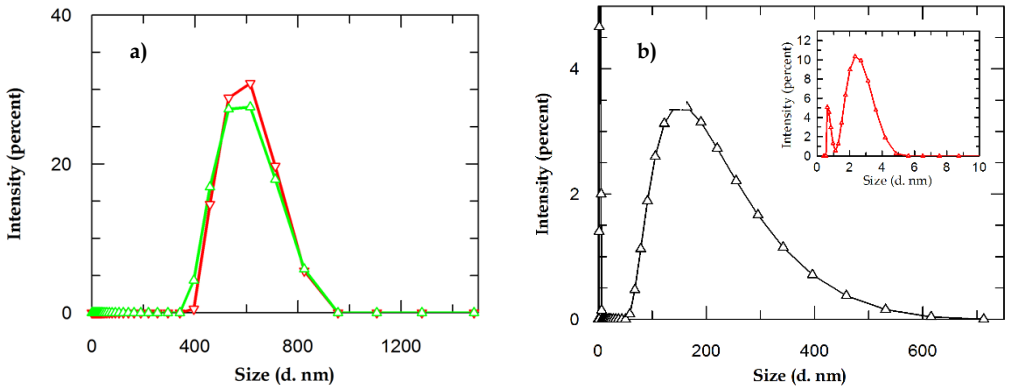

Figure 2.3.1.6. Size distributions of the cyclodextrin aggregates in aqueous solution: (a) [**8**] = 10 mM (red line 298 K; green line 338 K); (b) [**8**] = 10 mM (298 K) after filtration through a 0.45 μm Millipore filter.

Considering all the experimental results, we suggest that after the initial formation of small aggregates (probably micelles or smaller aggregate) at ~10^{-5} M, the aggregation process evolves into the formation of large bilyered vesicles as evidenced by Cryo-tem measurments (Figure 2.2.1.7.).

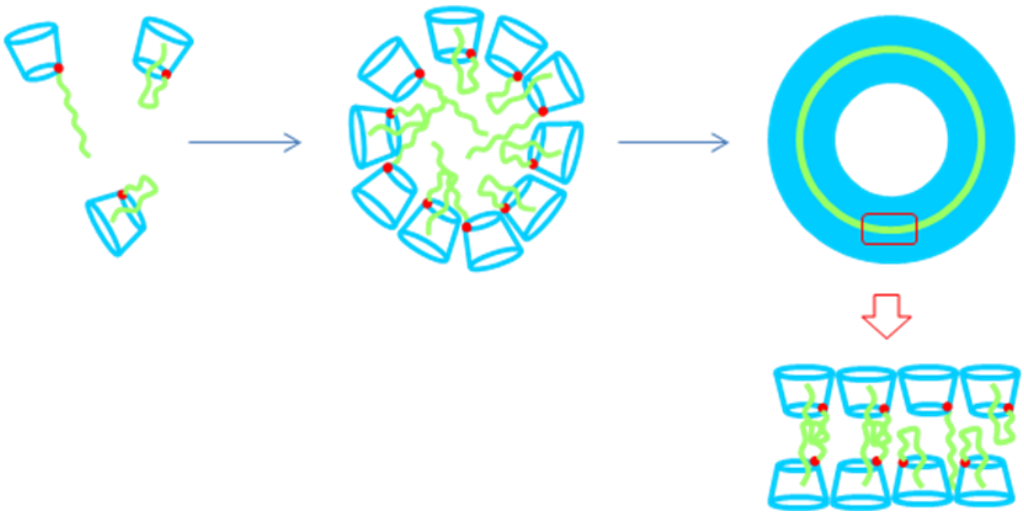

Figure 2.2.1.7. Cartoons of the aggregation process.

As observed for calixarene amphiphiles, also cyclodextrin-based aggregates offer two different guest recognition sites: the apolar cavity and the lipophilic bilayer of vesicles. In order to determine the binding site of different fluorescent probes inside the vesicles, a series of preliminary fluorescence experiments were performed both with the native β–CD and the modified β–CDC_{14} by using Pyrene (**10**) and 8-Anilino-1-naphthalenesulfonic acid (ANS, **11**).

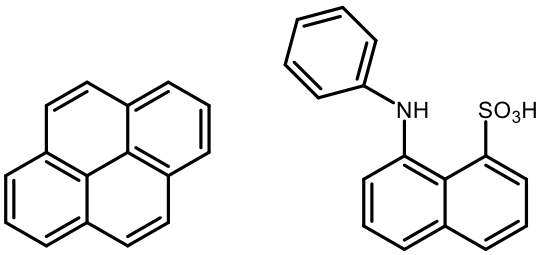

10 **11**

Figure 2.3.1.8. Chemical structures of Pyrene (**10)** and ANS (**11)**.

It is known that fluorescence spectra of pyrene undergo considerable modification due to changes in the solubility, mobility and microenvironment of the probe.[52] To test the aggregation ability of β-CDC_{14}, fluorescence emission spectra of pyrene were recorded at increasing concentration of β-CDC_{14}, and results compared with a parallel experiment with native β-CD. The titration curve, obtained by plotting the ratio (I_1/I_3) of the intensities of pyrene fluorescent peaks *vs* β-CD concentrations is shown in Figure 2.3.1.9a. It is known that in aqueous media pyrene is included in the apolar cavity of β-CD yielding to a β-CD/pyrene 1:1 and 2:1 complexes.[53]

The trend observed for the two β-CDs below the previously determined cac value (~1 mM) is in line with a predominant interaction with the cyclodextrins' cavities. On increasing the concentration above 1 mM, it can be observed that the I_1/I_3 ratio of Pyrene in β–CDC_{14} solutions (I_1/I_3 = 0.94) decreases at a lesser extent than in the β–CD solutions (I_1/I_3 = 0.80). These data may indicate that below the *cac* Pyrene is involved in the formation of a 1:2 stoichiometry complex;[52] as far as aggregation occurs, pyrene molecules are moving from the cyclodextrin's cavity to the lipophilic environment of the aggregates. Because water is able to penetrate inside the core of a micelle or the bilayer of a vesicle,[54] when located in these environment Pyrene senses a more polar surrounding than in the capsular space provided by the two cyclodextrins' cavities.

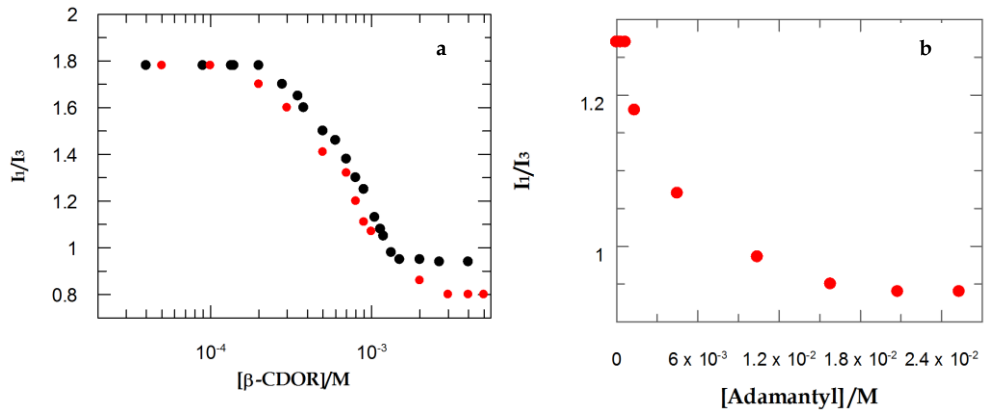

Figure 2.3.1.9. a) Dependence of the Pyrene I_1/I_3 emission intensity ratio with increasing concentrations of β-CDC_{14} (black curve) and β-CD (red curve). b) Dependence of the pyrene I_1/I_3 emission intensity ratio of *β*-CDC_{14} solution ([**8**] = 8 10^{-4} M) upon addition of increasing amounts of N,N,N-trimethyl-1-adamantyl-iodide.

To confirm our hypothesis, increasing amount of *N,N,N*-trimethyl-1-adamantyl ammonium iodide (**12**) were added to a 8 × 10^{-4} M solution of β-CDC_{14}, that is below the cac. It's reported that adamantyl derivatives

form 1:1 inclusion complexes with β-CDs with high values of the association equilibrium constant, typically between 10^4 – 10^5 M^{-1}.[55]

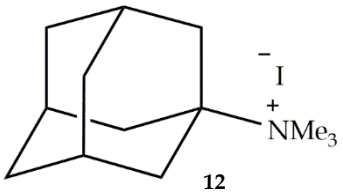

12

Figure 2.3.1.10. *N,N,N*-trimethyl-1-adamantyl ammonium iodide (**12**).

Because it is known that aggregation phenomena are affected by the ionic force, first of all we checked that the cac did not change as a consequence of the addition of salt **12**. To this aim, conductivity experiments were performed in a β-CDC_{14}/**12** 1 : 5 ratio; the experimental results did not show any change of the cac value (Figure 2.3.1.11).

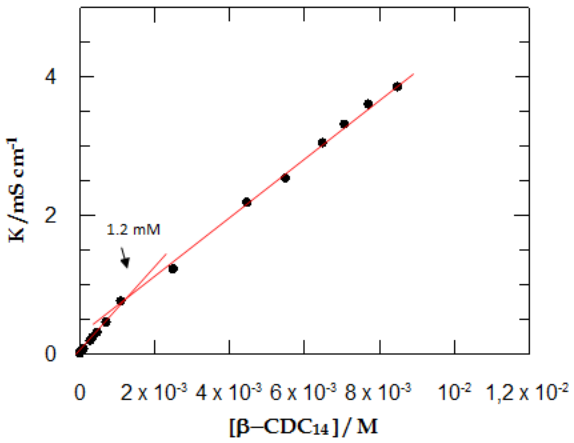

Figure 2.3.1.11. Electrical conductivity *K vs.* the concentration of cyclodextrin **8** (β-CDC_{14}/**12** 1 : 5 ratio) in aqueous solutions at 298K.

As it can be seen in Figure 2.3.1.9b, an increased concentration of **12** determined a decrease of the I_1/I_3 ratio (up to 0.94). This demonstrates that, as a consequence of the greater affinity of β-CDs towards the adamantyl residue, pyrene molecules move from the cavity towards an apolar environment and not to the aqueous solution. This result confirms the formation, below the cac value, of smaller aggregates with lipophilic domains as already evidenced by the conductivity experiments. All the results obtained using pyrene as a fluorescent probe confirmed that at lower concentration of surfactant the interaction of Pyrene with the cavity is favoured while above the cac or after an external stimulus (*e.g.* upon addition of a competitive guest), Pyrene prefers to shift into the lipophilic environment of the aggregates.

The seven-unit glucose host molecules are also known to form 1:1 and 2:1 complex with ANS in aqueous solution.[56]

In agreement with previous works, the fluorescence spectra of ANS in water with excitation at 350 nm show the existence of a low intensity short wavelength band at 530 nm. Addition of β-CDs results in a dramatic increasing of the fluorescence intensity accompanied by a gradual blue shift in the emission maximum (λ_{em}) of ANS. Such changes are indicative of the penetration of ANS into the hydrophobic cavities resulting in the formation of ANS–β-CDs complexes.

Here, the fluorescence titration of ANS with β–CDC_{14} showed a larger increase of the fluorescence intensity and of the correspondent blue shift when compared with the native β–CD under the same experimental conditions (Figures 2.3.1.12 and 2.3.1.13).

Furthermore, such changes are observed at lower concentrations if compared with the native β–CD. Such data could indicate a stronger interaction with the cavity or the interaction of the guest with a different site.

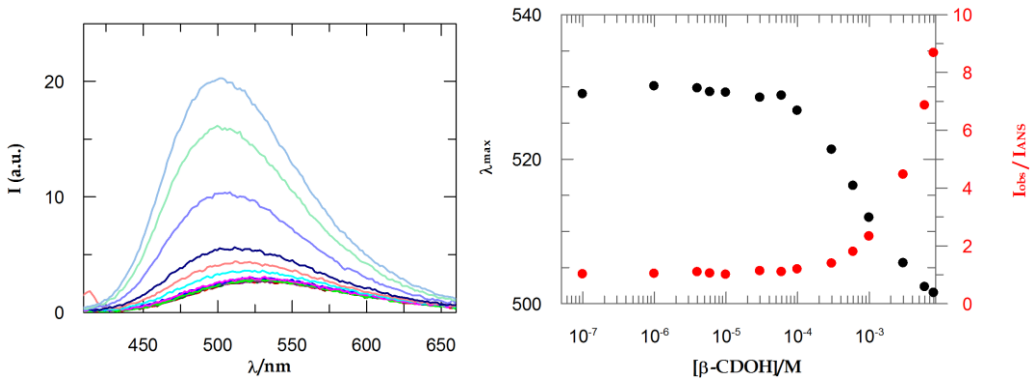

Figure 2.3.1.12. (Left) Fluorescence spectra of ANS (2 x 10^{-5} M) upon addition of increasing concentrations of β-CD in aqueous solution, ranging from 0 (bottom) to 8 x 10^{-3} M (top spectrum). (Right) Plot of emission maximum position (λ_{max}) and normalised fluorescence intensity at 505.07 nm (I_{obs}/I_{ANS}).

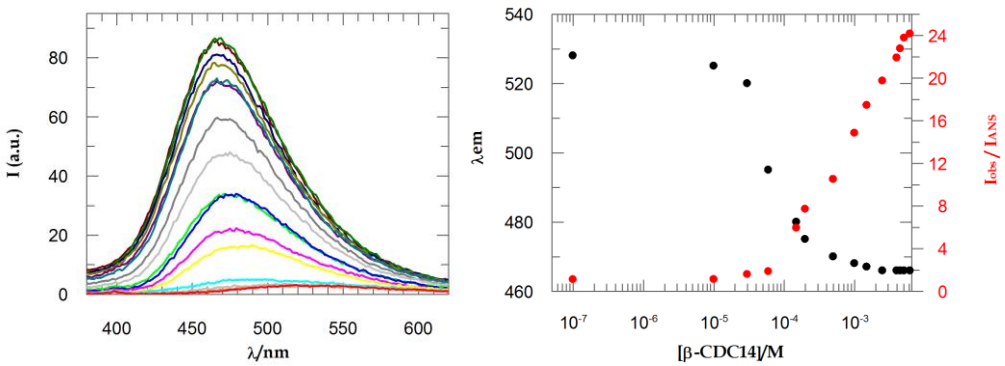

Figure 2.3.1.13. (Left) Fluorescence spectra of ANS (2 x 10^{-5} M) upon addition of increasing concentrations of β-CDC_{14} in aqueous solution, ranging from 0 (bottom) to 6.2 x 10^{-3} M (top spectrum). (Right) Plot of emission maximum position (λ_{max}) and normalised fluorescence intensity at 505.07 nm (I_{obs}/I_{ANS}).

Since the long chain self-inclusion might hinder the inclusion of the guest inside the cavity, while favourable electrostatic interactions beetween the ANS solfonate group SO_3^- and the ammonium group of β-CDC_{14} can be established, in our opinion the ANS guest is located in the lipophylic region of the aggregates.

2.4. Conclusions

This chapter reported the experimental results on the synthesis and aggregation properties of macrocycles based surfactants of different nature (calixarenes, cyclodextrins) together with different applications that make them good candidates as carriers for different substrates (drugs, fluorescence probe *etc.*).

2.5. Experimental section

2.5.1. Materials

THF, CH_3CN and DMF were dried by standard methods prior to use; β-CD, 8-Anilino-1-naphthalenesulfonic acid (ANS), Pyrene, *N*,*N*-Dimethyltetradecylamine, Rose Bengal, Amantadine, Naproxen and Flurbiprofen were reagent grade and were used without further purification. *p-tert*-Butylcalix[4]arene, *p*-methylcalix[5]arene were synthesized according to literature procedures.[57]

2.5.2. Experimental methods

NMR experiments. ^1H and ^{13}C NMR spectra were recorded at 500 or 300 and 125 or 75 MHz respectively. Diffusion Ordered NMR Spectroscopy (DOSY) and NOESY studies were performed on a Varian 500 MHz spectrometer equipped with a pulse-field gradient probe. DOSY spectra were recorded at 25 °C using a Doneshot pulse sequence. Experimental parameters were optimized according to the sample under investigation. Diffusion gradients were incremented in 30 steps with gradient pulse amplitudes varying from 1.6 to 50 gauss/cm, the number of transients acquired for each increment ranging from 16 to 128, with a diffusion gradient length of 2–4 ms and diffusion delays in the 150–200 ms range. All measurements were performed in triplicate and the reported values are the mean ± standard deviation of the mean. The hydrodynamic radii (R_h) were obtained using the Stokes-Einstein equation: $D_{obs} = k_BT/6\pi\eta R_h$, where k_B is the Boltzmann constant, T is the temperature (K) and η is the viscosity of the solvent (Pa s). 2D NOESY experiments were carried out

using a 500 ms mixing time, 16 transients for each increment (512 in total) and a relaxation time of 3 s.

Drug solubility. The solubility of the drugs naproxen (**4**) and flurbiprofen (**5**) in D_2O surfactant solution of different concentrations (2.5, 5.0 and 10.0 mM) was measured by NMR. A fixed amount of solid **4** or **5** (5 mmol) was added to 1 mL of the surfactant solution previously filtered through a 0.1 mm Millipore filter and the sample was equilibrated at room temperature for at least 24 h. The solutions were centrifugated (6000 rpm) for 10 minutes to remove undissolved solid. The "detectable" concentrations of the remaining calixarene and micelle-encapsulated naproxen/flurbiprofen in the supernatant were determined from the integral of selected peaks by using the quantitative qNMR software *Varian Vnmrj 3.2.*

UV solubility measurements were performed using a Varian Cary 50 Scan UV-Visible spectrophotometer. 2 mL of naproxen/surfactant solution ([**2**] = 5.0 mM) were prepared as described above. After centrifugation, one half of the supernatant solution was filtered through a 0.1 mm Millipore filter. Aliquots of filtered and unfiltered solutions (0.5 mL each) were allowed to stir for 24 h with 1 mL of $CHCl_3$. Finally 0.5 mL of the organic solutions were diluted with $CHCl_3$ (1 mL) and Naproxen concentration was determined by UV spectroscopy at λ = 318 nm.

Dynamic light scattering (DLS) for calixarenes aggregates. DLS measurements were carried out using a 35 mW polarized He-Ne laser source (l = 632.8 nm). The polarized scattered light was collected at 90°, in a self-beating mode, using an Avalanche Photodiode (Single Photon

Counting Module) by Excelitas Technologies. The signal was sent to a Malvern 4700 submicrometer particle analyzer system to measure the intensity autocorrelation function, $g_2(t)$. The intensity autocorrelation function is related to the scattered electric field correlation function $g_1(t)$ through the Siegert's relation: $g_1(t) \propto [g_2(t)-1]^{1/2}$. Determination of the size distribution from the field correlation function $g_1(t)$ was obtained through a Laplace inversion:

$$g_1(t) = \int \tau A(\tau) \exp(-t/\tau) d(\ln \tau)$$

where $\tau=1/(DQ^2)$, D and Q being the diffusion coefficient of the particle and the exchanged momentum of the scattered light, respectively. The diffusion coefficient D is related to the hydrodynamic radius through the Einstein-Stokes relation. A discrete multi-exponential non-negative least-squares fit (NNLS) was used to perform this inversion procedure.

The spectral amplitude τA is related to the scattered intensity of each species (with radius R), which, in turn, depends on its number concentration, n, on the radius R and on its form factor P(QR). By using the Rayley-Gans form factor of a sphere it is possible to obtain the number distribution as:

$$n(R) = a \frac{\tau A}{[\sin(QR) - QR\cos(QR)]^2}$$

where a is a constant giving the normalization to unity of the number-weighted size distribution.

Dynamic light scattering (DLS) for cyclodextrin aggregates. The hydrodynamic diameters were determined with a Malvern-ZetaSizer ZS90 apparatus, which uses dynamic light scattering at a 90° dispersion angle to measure the particle size. Particle diffusion in Brownian motion

is converted to a size distribution using the Stokes-Einstein equation. **AFM.** Atomic force microscopy was performed using an Ntegra probe NanoLaboratory from NT-MDT working in tapping mode and employing a Vit-p as probe. The sample was prepared dropping 10 μL of a solution of **2** (0.1 μM) on the 110 surface of an electronic grade silicon wafer and the sample was dryed under vacuum.

Cryo-TEM. Cryo-TEM experiments were performed by using a Holey Carbon support film on a 400-mesh copper grid. After glow-discharge to make hydrophilic the carbon film, a 3 μL drop of the sample was deposited onto the grid. Then the grid was mounted on a plunger (Leica EM-CPC) and blotted with a Whatman No.1 filter paper. The aqueous suspension containing exosomes was immediately vitrified by rapid immersion in liquid ethane. The grid with the vitrified samples was mounted on a Gatan 626 cryo-transfer system and inserted into the microscope. Images were obtained using a Jeol JEM 2011 cryo-electron microscope operated at 200 kV, under low-dose conditions, and using different degrees of defocus (500–900 nm) to obtain an adequate phase contrast. 32 Images were recorded on a Gatan Ultrascan US1000 CCD camera. The images were acquired and analyzed with the Digital Micrograph 1.8.

Rose Bengal micellization method. A fixed amount of Rose Bengal (10 μM) was added to different solutions of PEGylated surfactants (in the range 0 – 1 mM). The mixtures were stirred overnight and then UV measurements were performed using a Varian Cary 50 Scan UV-Visible spectrophotometer.

Surface tension. Surface tension experiments were performed by using a tensiometer K10-Kruss and the temperature was maintained at 25 ± 1°C through an external circuit.

Turbidity. UV measurements for the detection of turbidity (τ) values were performed using a Varian Cary 50 Scan UV-Visible. Samples were contained in square 1 × 1 cm^2 quartz cells of L = 1 cm optical path. The spectra recorded in the 400-800 nm wavelength range and baseline corrected by the absorbance of pure water did not show absorption bands. The turbidity (τ) was calculated from the absorbance A taken at 500 nm wavelength as Aln(10)/L.

Conductivity. Conductivity measurements of surfactant solutions were done using a Radiometer conductivity meter MeterLab CDM210 equipped with a CDC565 electrode of cell constant 0.929 cm^{-1}. The conductivity was measured in a double jacketed sample holder thermostated at 25 ± 1°C.

Fluorescence experiments: β-CDs and Pyrene. A stock solution of Pyrene (8 x 10^{-5} M) was prepared in ethanol; a stock solution of adamantyl (1.33 x 10^{-1} M) was prepared in Milli-Q water; β-CDs solutions were prepared in Milli-Q water and aliquots of Pyrene and Adamantyl stock solution were added. The concentration of Pyrene was maintained at 8 x 10^{-7} M in all the solutions. The samples prepared for spectroscopic measurements were used immediately after preparation. The excitation wavelength was 334 nm and the solution temperature was maintained at 298 ± 0.1 K by means of an external circulating water bath.

Fluorescence experiments: β-CDs and ANS. A stock solution of ANS (1 x 10^{-3} M) was prepared in Milli-Q water; β-CDs solutions were prepared

in Milli-Q water and an aliquot of the ANS stock solution was added. The concentration of ANS was maintained at 2 x 10^{-5} M in all the solutions. The samples prepared for spectroscopic measurements were used immediately after preparation. The excitation wavelength was 350 nm and the solution temperature was maintained at 298 ± 0.1 K by means of an external circulating water bath.

2.5.3. Synthetic procedures

Sodium *p-tert*-butyl-calix[4]arene-tetra-*O*-(4-butoxysulfonato) (2):

p-tert-Butylcalix[4]arene (400 mg, 0.61 mmol), an excess of NaH (177.5 mg, 7.4 mmol) and 1,4-butane sultone (1 g, 7.4 mmol) were mixed in anhydrous THF (40 mL) and refluxed for 48 h. The mixture was allowed to cool to room temperature and MeOH (10 mL) was added. The precipitate was collected by filtration, washed with EtOH, dissolved in 10 mL of water and finally precipitated by the salting-out method with sodium acetate. After centrifugation, the solid was separated and refluxed in EtOH (40 mL) for 24 h. The white powder (508 mg, 64%) was collected by filtration.

M.p. 305–310 °C (dec.). ^{1}H NMR (0.2 mM, D_2O) δ 0.97 (s, $C(CH_3)_3$, 36 H), 1.79–2.03 (m, $OCH_2(CH_2)_2$, 16 H), 2.89 (t, J = 7.9 Hz, SCH_2, 8 H), 3.13 and 4.31 (AX, J = 12.5 Hz, $ArCH_2Ar$, 8 H), 3.83 (br t, OCH_2, 8 H), 6.87 (s, Ar, 8 H) ppm; ^{13}C NMR (5.0 mM, D2O) δ 23.7, 31.5, 33.2, 34.1, 36.4, 53.9, 77.3, 127.9, 136.9, 147.5, 156 ppm. Anal. Calcd for $C_{60}H_{84}Na_4O_{16}S_4$: C, 56.23; H, 6.61; S, 10.01; Found: C, 55.93; H, 6.61; S, 9.97.

Sodium *p*-methylcalix[5]arene-tetra-O-(4-butoxysulfonato) (3):

p-methylcalix[5]arene (200 mg, 0.33 mmol), an excess of NaH (119 mg, 4.95 mmol) and 1,4-butane sultone (674 mg, 4.95 mmol) were mixed in anhydrous THF (25 mL) and refluxed for 48 h. The mixture was allowed to cool to room temperature and MeOH (5 mL) was added. The precipitate was collected by filtration, washed with EtOH, dissolved in 5 mL of water and finally precipitated by the salting-out method with sodium acetate. After centrifugation, the solid was separated and refluxed in EtOH (20 mL) for 24 h. The white powder (257 mg, 56%) was collected by filtration.

M.p. 300–310 °C (dec.). ^{1}H NMR (1 mM, D_2O) δ 1.76-1.90 (m, $OCH_2(CH_2)_2$, 20 H), 1.96 (s, $C(CH_3)$, 15 H), 2.87 (t, J = 7.9 Hz, SCH_2, 10 H), 3.25 e 4.33 (AX, J = 14.4 Hz, Ar-CH_2-Ar, 10 H), 3.79 (br t, OCH_2, 10 H) e 6.71 (s, Ar 10H) ppm. ^{13}C NMR (D_2O, 10 mM) δ 22.6, 23.6, 31.7, 53.7, 69.3, 76.2, 126.8, 132.1, 136.9 e 155.18 ppm. Anal. Calcd for $C_{60}H_{75}Na_5O_{20}S_5$: C, 51.79; H, 5.43; S, 11.52; Found: C, 51.63; H, 5.44; S, 11.49.

PEGylated-*p-tert*-butyl-calix[5]arene (6):

p-tert-Butylcalix[5]arene (200 mg, 0.25 mmol), an excess of K_2CO_3 (605 mg, 4.38 mmol) and MeOPEG550-OTs (2.64 g, 3.75 mmol) were mixed in anhydrous CH_3CN (25 mL) and refluxed for 72 h under inert atmosphere. After evaporating the solvent, the mixture was dissolved in deionized water (20 mL) and extracted with CH_2Cl_2 (2 x 100 mL). The combined organic extracts were evaporated under reduced pressure to afford a yellowish paste, which was purified by column chromatography (CH_2Cl_2/CH_3OH from 98:1 to 9:1, v/v). The purified product was obtained as a yellow liquid (347 mg, 40%).

^{1}H NMR (8 mM, $CDCl_3$) δ 1.00 (s, $C(CH_3)_3$, 45 H), 3.23 and 4.51 (AX, J = 14.2 Hz, $ArCH_2Ar$, 10 H), 3.37 (s, 15H, OCH_3), 3.53-3.81 (m, 260 H, OCH_2CH_2O), 6.87 (s, Ar, 10 H). ^{13}C NMR (8 mM, $CDCl_3$) δ 29.5, 31.3, 33.9, 59, 70.5, 70.6, 71.9, 72.4, 125.4, 133.7, 144.8, 152.4 ppm.

PEGylated-*p*-methyl-calix[5]arene (7):

p-methyl-calix[5]arene (200 mg, 0.33 mmol), an excess of K_2CO_3 (798 mg, 5.77 mmol) and MeOPEG550-OTs (3.49 g, 4.95 mmol) were mixed in anhydrous CH_3CN (25 mL) and refluxed for 72 h under inert atmosphere. After evaporating the solvent, the mixture was dissolved in deionized water (20 mL) and extracted with CH_2Cl_2 (2 x 100 mL). The combined organic extracts were evaporated under reduced pressure to afford a yellowish paste, which was purified by column chromatography (CH_2Cl_2/CH_3OH from 98:1 to 9:1, v/v). The purified product was obtained as a yellow liquid (473 mg, 44%).

^{1}H NMR (13 mM, $CDCl_3$) δ 2.03 (s, *p*-Me, 15 H), 3.18 and 4.46 (AX, J = 14.3 Hz, $ArCH_2Ar$, 10 H), 3.37 (s, 15 H, OCH_3), 3.53-3.86 (m, 260 H, OCH_2CH_2O), 6.58 (s, Ar, 10 H). ^{13}C NMR (13 mM, $CDCl_3$) δ 20.8, 29.9, 59, 70.5, 71.9, 72, 129.1, 131.7, 133.8, 152.8 ppm.

***N*-tetradecyl-*N*,*N*-dimethylammonium-β-cyclodextrin[49a] (β-CDC_{14}) (8):**

To a stirred solution of mono-iodo-β-CD[51] (1 g, 0.8 mmol) in dry DMF (40 mL) N,N-Dimethyltetradecylamine was added (3.86 g, 16 mmol). The reaction mixture was stirred for 72 h at 80 ˚C under inert atmosphere. After removal of the solvent, the residue was washed several times (3 - 4 times) under stirring in a mixture of acetone–chloroform. The insoluble

powder was recovered by filtration and precipitated in a mixture water-acetone (872 mg, 74%).

^{1}H NMR (300 MHz, D_2O) δ4.96 (d, 1 H, H-1 ammonium–glucose), 4.89 (s, 6 H, H-1 β-CD), 3.94 (t, 1 H, H-5 ammonium–glucose), 3.71–3.34 (m, 43 H, H-2, H-3, H-4, H-5, H-6, H-6′ β-CD, H-2, H-3, H-4, H-6, H-6′ ammonium–glucose and $CH_2\alpha$), 3.16 (s, 3 H, CH_3–N+), 2.99 (3 H, CH_3–N^+) 1.69-1.75 (m, 2 H, $CH_2\beta$), 1.33–1.02 (m, 22 H, -CH_2 $(CH_2)_9CH_2$-), 0.72 (t, 3 H, CH_3). ^{13}C NMR (75 MHz, D_2O) δ102.4, 101.9, 100.2 82.9, 81.1, 79.2 73.7–71.6 67.1, 63.6, 61.5, 60.1, 54.1, 53.2, 24.73, 19.55, 13.43, 12.9, 12.2, 11.9.

***N,N,N*-trimethyl-1-adamantyl-iodide (12):**

N,N,N-trimethyl-1-adamantyl quaternary ammonium salt was synthesized from amantadine by two-steps reactions according the method already reported in literature.[58]

References

[1] Sorrenti A., Illa O., Ortuño R.M., *Chem. Soc. Rev.,* **2013**, 42, 8200.

[2] Zhang W., Gao C., *J. Mater. Chem. A*, **2017**, 5, 16059.

[3] (a) Matile S., Jentzsch A.V., Montenegro J., Fin A., *Chem. Soc. Rev.,* **2011**, 40, 2453; (b) McIntosh T.J., Simon S.A., *Annu. Rev. Biophys. Biomol. Struct.,* **1994**, 23, 27; (c) Zhang S., *Nat. Nanotechnol.*, **2006**, 1, 169.

[4] (a) Wang M., Alberti K., Sun S., Arellano C.L., Xu Q., *Angew. Chem. Int. Ed.,* **2014**, 53, 2893; (b) Soussan E., Cassel S., Blanzat M., Rico-Lattes I., *Angew. Chem. Int. Ed.,* **2009**, 48, 274; (c) Yao J., Yang M., Duan Y., *Chem. Rev.,* **2014**, 114, 6130; (d) Kelley E.G., Albert J.N.L., Sullivan, Epps III T.H., *Chem. Soc. Rev.,* **2013**, 42, 7057.

[5] (a) Calama M.C., Timmerman P., Reinhoudt D.N., *Angew. Chem., Int. Ed.,* **2000**, 39, 755; (b) Guo D.S., Liu Y., *Acc. Chem. Res.,* **2014**, 47, 1925; (c) Kumar R., Lee Y.O., Bhalla V., Kumar M., Kim J.S., *Chem. Soc. Rev.,* **2014**, 43, 4824; (d) Sameni S., Jeunesse C., Matt D., Harrowfield J., *Chem. Soc. Rev.,* **2009**, 38, 2117; (e) Guo D.S., Liu Y., *Chem. Soc. Rev.,* **2012**, 41, 5907.

[6] Shinkai S., Mori S., Koreishi H., Tsubaki T., Manabe O., *J. Am. Chem. Soc.*,**1986**, 108, 2409.

[7] Arduini A., Pochini A., Reverberi S., Ungaro R., *J. Chem. Soc. Chem. Commun.,* **1984**, 981.

[8] Markowitz M.A., Bielski R., Regen S.L., *Langmuir*, **1989**, 5, 276.

[9] Shahgaldian P., Coleman A.W., Kalchenko V.I., *Tetrahedron Lett.*, **2001**, 42, 577.

[10] (a) Basílio N., García-Río L., *Chem. Phys. Chem.,* **2012**, 13, 2368; (b) Guo D.S., Wang K., Liu Y., *J. Inclusion Phenom. Macrocyclic Chem.*, **2008**, 62, 1; (c) Gaeta C., Caruso T., Mincolelli M., Troisi F., Vasca E., Neri P., *Tetrahedron*, **2008**, 64, 5370.

[11] (a) Shinkai S., Kawabata H., Arimura T., Matsuda T., Satoh H., Manabe O., *J. Chem. Soc., Perkin Trans. 1*, **1989**, 1073; (b) Shinkai S., Arimura T., Araki K., Kawabata H., Satoh H., Tsubaki T., Manabe O., Sunamoto J., *J. Chem. Soc., Perkin Trans. 1,* **1989**, 2039.

[12] (a) Tauran Y., Brioude A., Shahgaldian P., Cumbo A., Kim B., Perret F., Coleman A.W., Montasserf I., *Chem. Commun.,* **2012**, 48, 9483; (b) Jebors S., Fache F., Balme S., Devoge F., Monachino M., Cecillon S., Coleman A.W., *Org. Biomol. Chem.*, **2008**, 6, 319.

[13] (a) Colston M.J., Hailes H.C., Stavropoulos E., Hervé A.C., Hervé G., Goodworth K.J., Hill A.M., Jenner P., Hart P.D., Tascon R.E., *Infect. Immun.,* **2004,** 72, 6318; (b) Loiseau F.A., Hill A.M., Hii K.K., *Tetrahedron*, **2007**, 63, 9947.

[14] Tu C., Zhu L., Li P., Chen Y., Su Y., Yan D., Zhu X., Zhou G., *Chem. Commun.,* **2011**, 47, 6063.

[15] James E., Eggers P.K., Harvey A.R., Dunlop S.A., Fitzgerald M., Stubbs K.A., Raston C.L., *Org. Biomol. Chem.,* **2013**, 11, 6108.

[16] Gattuso G., Notti A., Pappalardo A., Pappalardo S., Parisi M.F., Puntoriero F., *Tet. Lett.,* **2013**, 54, 188.

[17] (a) Gutsche C.D., *Calixarenes - An Introduction, in Monographs in Supramolecular Chemistry. The Royal Society of Chemistry, Cambridge, 2nd,* **2008**, 6; (b) Jaime C., de Mendoza J., Prados P., Nieto P.M., Sanchez C., *J. Org. Chem.,* **1991**, 56, 3372.

[18] (a) Basilio N., García-Río L., Martín-Pastor M., *J. Phys. Chem. B*, **2010**, 114, 4816; (b) Sansone F., Dudic M., Donofrio G., Rivetti C., Baldini L., Casnati A., Cellai S., Ungaro R., *J. Am. Chem. Soc.*, **2006**, 128, 14528.

[19] Cohen Y., Avram L., Frish L., *Angew. Chem., Int. Ed.,* **2005**, 44, 520.

[20] Ding W., Bai W.Q., Qu G.M., Ma L., Yu T., *Appl. Chem. Ind.,* **2007**, 36, 1092.

[21] Cui X., Mao S., Liu M., Yuan H., Du Y., *Langmuir,* **2008**, 24, 10771.

[22] (a) Gattuso G., Notti A., Pappalardo S., Parisi M.F., Pisagatti I., Patanè S., *New J. Chem.,* **2014**, 38, 5983; (b) Denkova P.S., Van Lokeren L., Verbruggen I., WillemR., *J. Phys. Chem. B,* **2008**, 112, 10935.

[23] Gattuso G., Notti A., Pappalardo S., Parisi M.F., Pisagatti I., *Supramol. Chem.,* **2014**, 26, 597.

[24] Denkova P.S., Van Lokeren L., Verbruggen I., Willem R., *J. Phys. Chem. B,* **2008**, 112, 10935.

[25] D'Urso A., Cristaldi D.A., Fragalà M.E., Gattuso G., Pappalardo A., Villari V., Micali N., Pappalardo S., Parisi M.F., Purrello R., *Chem. Eur. J.,* **2010**, 16, 10439.

[26] Consoli G.M.L., Granata G., Lo Nigro R., Malandrino G., Geraci C., *Langmuir,* **2008**, 24, 6194.

[27] Zhuang L.H., Yu K.H., Wang G.W., Yao C., *J. Colloid Interface Sci.,* **2007**, 408, 94.

[28] (a) Bhat P.A., Rather G.M., Dar A.A., *J. Phys. Chem. B,* **2009**, 113, 997; (b) Zhang J., Tozuka Y., Uchiyama H., Higashi K., Moribe K., Takeuchi H., Yamamoto K., *J. Pharm. Sci.,* **2011**, 100, 4421.

[29] Dutta P., Dey J., Perumal V., Mandal V., *Int. J. Pharm.,* **2011**, 407, 207.

[30] Bhat P.A., Rather G.M., Dar A.A., *J. Phys. Chem. B,* **2009**, 113, 997.

[31] Caetano W., Tabak M., *Spectrochim. Acta, Part A,* **1999**, 55, 2513.

[32] (a) Shalaeva M., Kenseth J., Lombardo F., Bastin A., *J. Pharm. Sci.,* **2008**, 97, 2581. (b) Meloun V., Bordovská S., Galla L., *J. Pharm. Biomed. Anal.,* **2007**, 45, 552.

[33] (a) Jevsevar S., Kunstelj M., *Biotechnol. J.,* **2010**, 5, 113; (b) Veronese F.M., Pasut G., *Drug Discov. Today,* **2005**, 10, 145.

[34] Webber J.M., Appel E.A., Vinciguerrac B., Cortinas A.B., Thapa L.S., Jhunjhunwala S., Isaacsc L., Langer R., Anderson D.G., *PNAS,* **2016**, 113, 14189.

[35] Stewart D.R., Krawiec M., Kashyap R.P., Watson W.H., Gutsche C.D., *J. Am. Chem. Soc.*, **1995**, 117, 586.

[36] Suradkar Y.R., Bhagwat S.S., *J. Chem. Eng. Data,* **2006**, 51, 2026.

[37] Rosen M.J., *Surfactant and interfacial phenomena, 2nd ed.; John Wiley & Sons: New York,* 3, **1989**.

[38] Lombardo D., Longo A., Darcy R., Mazzaglia A., *Langmuir*, **2004**, 20, 1057.

[39] Doughty M.J., *Contact Lens & Anterior Eye,* **2013**, 36,272.

[40] Chang C.C., Yang Y.T., Yang J.C., Wu H.D.,Tsai T., *Dyes and Pigmenmts*, **2008**, 79, 170.

[41] (a) Connors K.A., *Chem. Rev.,* **1997**, 97, 1325; (b) Harada A., *Acc. Chem. Res.,* **2001**, 34, 456; (c) Uekama K., Hirayama F., Irie T., *Chem. Rev.,* **1998**, 98, 2045; (d) Crini G., *Chem. Rev.,* **2014**, 114, 10940.

[42] (a) Szejtli J., *Chem. Rev.,* **1998**, 98, 1743; (b) Hu Q.D., Tang G.P., Chu P. K., *Acc. Chem. Res.*, **2014,** 47, 2017; (c) Zhao Y., Sakai F, Su L., Liu Y., Wei K., Chen G., Jiang M., *Adv. Mater.,* **2013**, 25, 5215.

[43] Parrot-Lopez H., Ling C.C., Zhang P., Baszkin A., Albrecht G., De Rango C., Coleman A.W., *J. Am. Chem. Soc.,* **1992**, 114, 5479.

[44] Auzély-Velty R., Djedaıni-Pilard F., Deésert S., Perly B., Zemb T., *Langmuir*, **2000**, 16, 3727.

[45] Gulik A., Delacroix H., Wouessidjewe D., Skiba M., *Langmuir*, **1998**, 14, 1050.

[46] (a) Uekama K., Hirayama F., Irie T., *Chem. Rev.,* **1998**, 98, 2045; (b) Duchene D., Wouessidjewe D., Ponchel G., *J. Controlled Release,* **1999**, 62, 263.

[47] Sallas F., Niikura K., Nishimura S.I., *Chem. Commun.,* **2004**, 0, 596.

[48] (a) Donohue R., Mazzaglia A., Ravoo B.J., Darcy R., *Chem. Commun.,* **2002**, 2864; (b) Cryan S.A., Holohan A., Donohue R., Darcy R., O'Driscoll C.M., *Eur. J. Pharm. Sci.,* **2004**, 21, 625.

[49] (a) Binkowski C., Hapiot F., Lequart V., MartinP., Monflier E., *Org. Biomol. Chem.,* **2005** , 3, 1129; (b) Baâzaoui M., Béjaoui I., Kalfat R., Amdouni N., Hbaieb S., Chavelier Y., *RSC Adv*., **2016**, 6, 72044.

[50] Petter R.C., Salek J.S., *J. Am. Chem. Soc.,* **1987**, 109, 7897.

[51] Bonomo R.P., Cucinotta V., D'Alessandro F., Impellizzeri G., Maccarrone G., Vecchio G., Rizzarelli E., *Inorg. Chem.,* 1991, **30**, 2708.

[52] (a) Winnik F.M., *Chem. Rev*., **1993**, 93, 587; (b) Duhamel J., *Polymers,* **2012**, 4, 211; (c) Duhamel J., *Langmuir*, **2012**, 28, 6527; (d) Duhamel J., *Langmuir*, **2014**, 30, 2307.

[53] De la Pena A.M., Ndou T., Zung J.B.,Warner I.M., *J Phys Chem*, **1991**, 95, 3330.

[54] Kuhn H., Breitzke B., Rehage H., *Colloid Polym Sci,* **1998**, 276, 824.

[55] (a) Eftink M.R., Andy M.L., Bystrom K., Perlmutter H.D., Kristol D.S.J., *J. Am. Chem. Soc.*, **1989**, 111, 6765; (b) Harries D., Rau D.C., Parsegian V.A., *J. Am. Chem. Soc.,* **2005**, 127, 2184.

[56] Pereira Vilar A., Martin-Pastor M., Pessêgo M., García-Río L., *J. Org. Chem.,* **2016**, 81, 6587.

[57] (a) Gutsche C.D., Iqbal M., *Org. Synth.,* **1990**, 68, 234; (b) Stewart D.R., Gutsche C.D., *Org. Prep. Proc. Int.,* **1993**, 25, 137; (c) Gutsche C.D., *Calixarenes, Monograph in Supramolecular Chemistry, V*ol. 1; *(Ed. J.F. Stoddart), The Royal Society of Chemistry, Cambridge,* **1989**.

[58] Hu J., Yang F., Huang M., *Adv. Mat. Res.,* **2012**, 391, 1159.

Chapter 3

Calix[5]arene-based Supra-amphiphiles

3.1. Supramolecular amphiphiles (supra-amphiphiles)

In contrast to conventional amphiphiles, the field of supramolecular amphiphiles was developed on the basis of noncovalent interactions and dynamic covalent bonds (Figure 3.1.1).

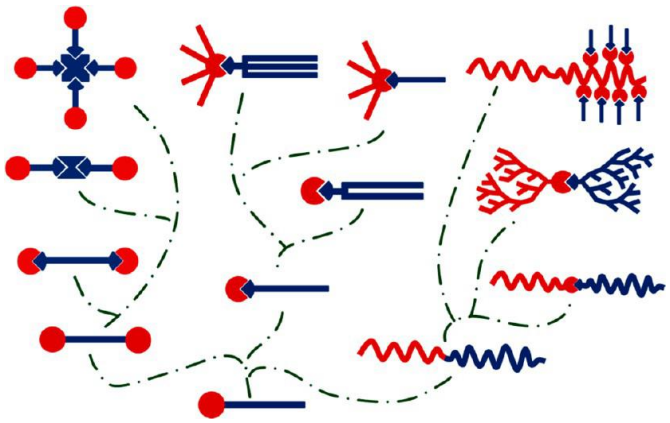

Figure 3.1.1. Evolution from amphiphiles to supra-amphiphiles. (Adapted from ref. 1).

Indeed, supramolecular amphiphiles[1] (supra-amphiphiles) are a new class of surfactants where the hydrophilic head and the hydrophobic tail are connected by means of noncovalent interactions such as electrostatic interactions, π–π stacking, hydrogen bonding, charge-transfer interactions and host-guest recognition. In contrast with conventional amphiphiles, supra-amphiphiles display some advantages.

First of all an easier chemical synthesis, since different functionalities can be introduced separately on the hydrophobic and hydrophilic components. Secondly, but not less important, the possibility of a fine modulation of their self-assembling with a large variety of chemical or physical stimuli (pH, redox properties, light, host-guest recognition, *etc.*) that can easily affect the dynamic nature of noncovalent interactions, thus promoting reversible assembling-disassembling and structural transitions in the colloidal systems under investigation.

There are two main strategies for fabricating supra-amphiphiles according to the structure of the building blocks. One is to create amphiphilicity by the combination of the hydrophilic and the hydrophobic parts through noncovalent interactions or dynamic covalent bonds. The other strategy is to modulate amphiphilicity by modifying conventional covalent amphiphiles with the techniques of noncovalent synthesis. So far, various topologies of supra-amphiphiles have been achieved, such as single-chain head-to-tail, multi-chain head-to-tail and bolaform ones.

In the emerging field of supra-amphiphiles, water soluble or amphiphilic macrocycles represent very promising candidates for the construction of novel supramolecular surfactants, thanks to the unique recognition properties of the macrocyclic cavity and the reversibility of the host-guest interactions. Recently, numerous examples with the most popular classes of macrocycles (cyclodextrins,[2] cucurbiturils,[3] pillararenes[4]) have been reported. For example, as shown in Figure 3.1.2.a., Jeon *et al*[5] utilized an amphiphilic viologen derivative, naphthalene diol, and curcubit[8]uril (CB[8]) to prepare a supra-amphiphile in a facile manner.

The amphiphilic alkyl viologen itself self-assembled in aqueous solution to form micelles. However, when naphthalene diol was added, a 1:1 charge-transfer complex was formed inside the cavity of CB[8], leading to the formation of a supra-amphiphile with single-chain head-to-tail topology. After complexation, the size of the hydrophilic viologen headgroup increased, leading to a decrease in the packing parameter and further resulting in the transformation from micelles to vesicles. The single-chain head-to-tail topology can be logically extended to the multichain head-to-tail structure.

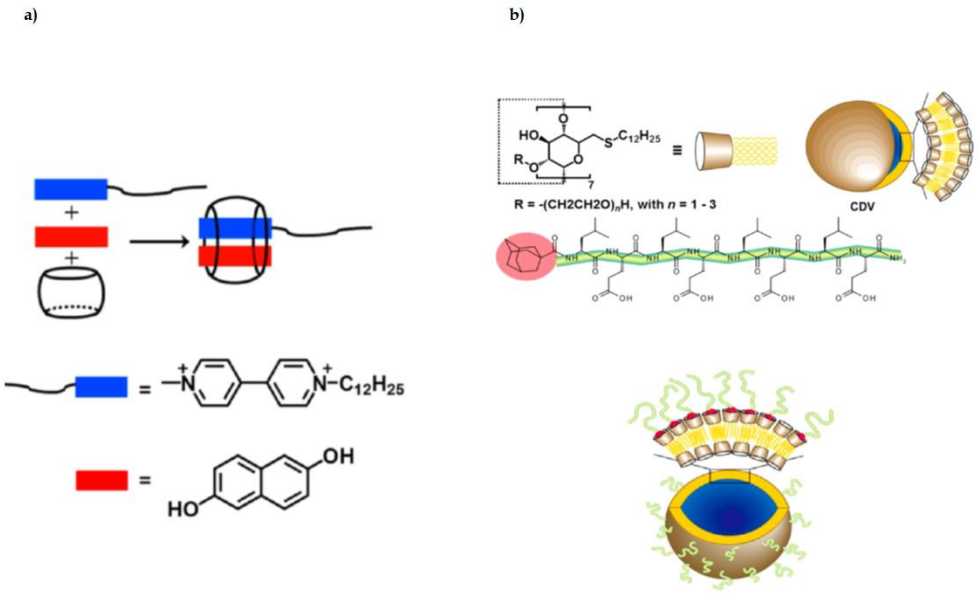

Figure 3.1.3. a) Single-chain head-to-tail supra-amphiphiles; b) Schematic illustration of a peptide-containing multichain head-to-tail supra-amphiphile with pH responsiveness. (Adapted from ref. 5,6).

As depicted in Figure 3.1.3.b, Versluis *et al* [6] utilized a modified amphiphilic β-CD and an adamantane-terminated octapeptide to form multichain head-to-tail supra-amphiphile via the strong and specific

host−guest interaction between β-CD and adamantane groups. The octapeptide contained valine and aspartic acid moieties alternately. Under neutral and basic conditions, the aspartic acid groups would deprotonate and repulse each other, and the supra-amphiphiles self-assembled to form vesicles. As far as the calixarene family is concerned, the complexation-induced aggregation of water-soluble derivatives has been largely exploited with anionic *p*-sulfonatocalix[4]arenes[7] and *p*-sulfonatocalix[6]arenes.[8]

Complexation of the smaller anionic calix[4]arene with cationic guests afforded several examples of supra-amphiphiles which led to vesicle assemblies with drug-delivery potentials and enzyme and photolytic responsiveness.[7] It has been further demonstrated that, when mixing aqueous solutions of cationic conventional surfactants and water soluble (but non amphiphilic) *p*-sulfonato anionic calixarene[9] the latter efficiently modulate the aggregational properties of the surfactants lowering their critical micellar concentration (cmc) as a result of the combined formation of a new host-guest amphiphile and of catanionic mixed system.

When ionic gemini guests (bolaform surfactants) are used to induce the host-guest interaction with oppositely charged not amphiphilic *p*-sulfonatocalix[*n*]arenes, [10] a number of different complexation-mode have been postulated depending on numerous factors: stoichiometry of the complex (H/G 1:1 or 2:1), length of the spacer in the gemini guests, number of charges and volume of the guest head-groups (Figure 3.1.4.).

Figure 3.1.4. Possible Inclusion Manners between *p*-sulfonatocalix[*n*]arenes and gemini guests. (Adapted from ref. 10c).

In contrast to bolaform amphiphiles based on covalent bonds, it's possible to fabricate bolaform supra-amphiphiles by modulating various intermolecular interactions. Recently, Huang at al.[11] constructed a bola-type supra-amphiphile from a water-soluble pillar[5]arene (**WP5**) and an imidazolium functionalized rod–coil molecule driven by the **WP5**–imidazolium molecular recognition (Figure 3.1.5).

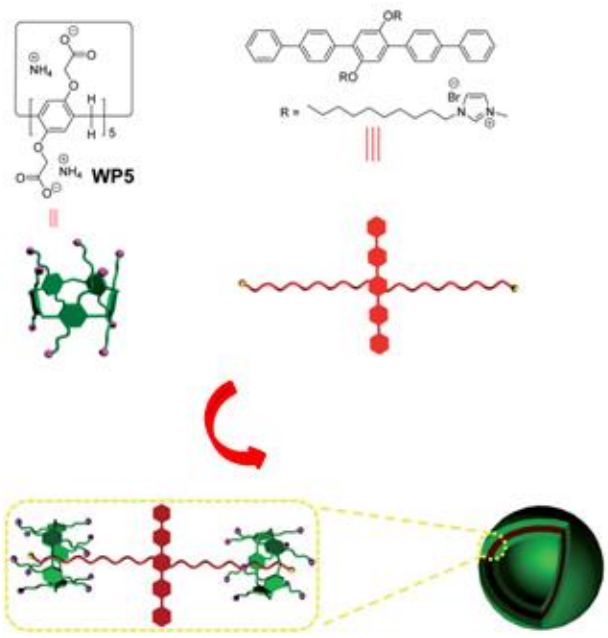

Figures 3.1.5. A bola-type supra-amphiphile from a water-soluble pillar[5]arene (**WP5**). (Adapted from ref. 11).

3.2. Calix[5]arenes and n-alkylammonium ions

Over the past decades, calixarene[12] have attracted considerable attention in the field of host–guest and supramolecular chemistry. These cyclic oligomers of phenol possess robust frameworks that can safely undergo most organic transformations,[13] allowing the synthesis of molecular receptors and tailor-made building blocks for the self-assembly of complex supramolecular architectures. The remarkable host–guest properties of the less accessible calix[5]arenes were initially revealed by Fukazawa and Haino, in the mid-nineties, with a series of reports on calix[5]arene/fullerene complexes, formed as a result of the excellent stereoelectronic matching between the π–electron rich concave cavity of the calixarene and the π-electron deficient convex surface of C60.[14] In the same period, my research group showed that penta-*O*-alkylated *p-tert*-butylcalix[5]arenes **1**, frozen in a C_{5v}-symmetric cone conformation, can recognize and bind (in an *endo*-cavity fashion) linear primary alkylammonium ions[15] (Figure 3.2.1) thus paving the way for the attainment of different supramolecular systems such as capsular assemblies, [16] supramolecular-oligo/polymer, [17] hetero(poly)topic receptors,[18] or sensing devices.[19]

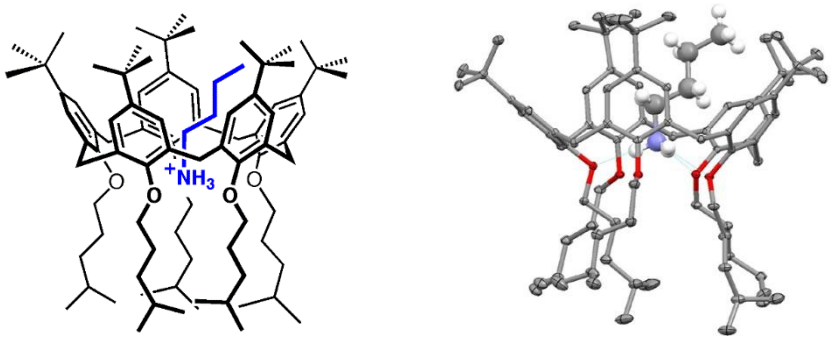

1⊃*n*-BuNH$_3^+$

Figure 3.2.1. *Endo*-cavity complexation of *n*-BuNH$_3^+$: (left) chemical structure and (right) X-Ray structure. (Adapted from Ref. 15d).

In solution, complexation is unambiguously supported by typical ^{1}H NMR spectral features: the appearance of resonances in the high-field region of the spectra, typically assigned to the alkylammonium moieties included within the aromatic cavity of a calix[5]arene molecule and the down-field shift of the aromatic protons. This kind of complex is held together by the cooperative action of a number of weak non-covalent intermolecular forces, including ammonium cation-π and CH-π interactions of the included alkyl chain with the aromatic wall of the calixarene cavity, as well as hydrogen-bond formation between the ammonium head and the ethereal oxygens.[15d,20]

As an extension of this previous investigation, subsequent studies of the group have been directed to test the ability of *p*-*tert*-butylcalix[5]arenes (in the cone conformation) to act as *endo*-cavity receptors toward α,ω-alkanediyldiammonium ions (H_3N^+-$(CH_2)_n$-NH_3^+, **NC$_n$N**, *n* = 8, 9, 10, 12). Beside the expected formation of 1:1 H/G inclusion complexes (Figure 3.2.2), ditopic α,ω-diammonium ions featuring a spacer of at least ten carbon atoms (**NC$_n$N**, n = 10, 12) between the two polar heads display a

remarkable tendency to coordinate a pair of calix[5]arene units, which are oriented rim-to-rim to form a closed cavity encapsulating the shape-complementary dication. As a consequence, the guest is symmetrically included inside the two cavities and, in the case of **$NC_{10}N$,** only five resonances are observed in the high field region of the ^1H NMR spectrum (Figure 3.2.2a). With shorter spacers the formation of the capsule in solution is hindered by severe steric repulsions between the upper rim substituents.[16,17b,21]

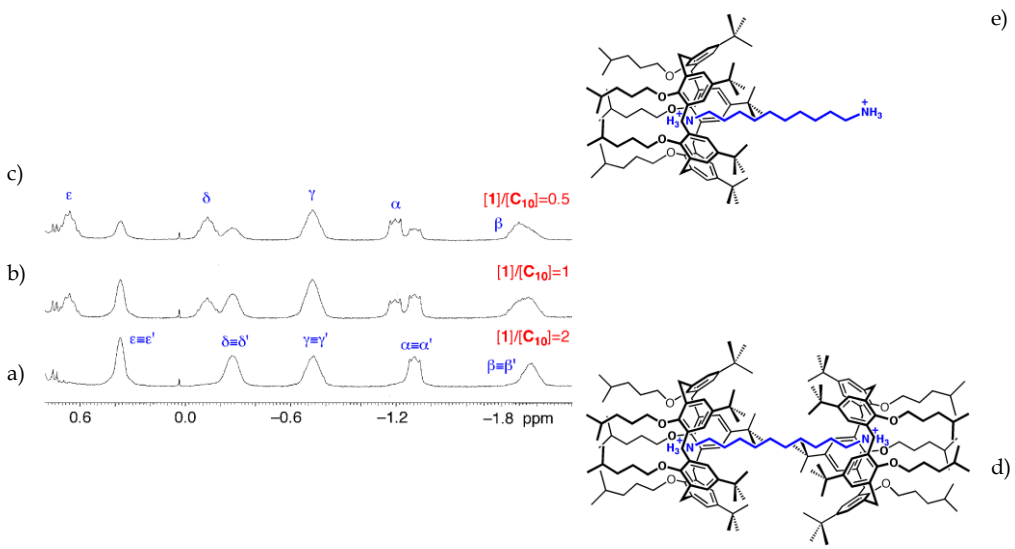

Figure 3.2.2. (left) The high field region of the ^1H NMR spectra (300 MHz, 295 K, $CDCl_3/CD_3OD$, 2:1) of mixtures of **1** and **$NC_{10}N$** at different H/G molar ratios: (a) H/G=2; (b) H/G=1; (c) H/G=0.5. (right) (d) the 2:1 capsular assembly and (e) the 1:1 inclusion complex.

3.3. A calix[5]arene-based supra-amphiphile

Recently, my research group reported on the synthesis of a new water-soluble *p-tert*-butylcalix[5]arene **2** (Figure 3.3.1) bearing *O*-4-butylsulfonato groups at the lower rim[22] together with the evidence of its

amphiphilic nature and its application in the construction of a supra-amphiphile upon complexation of linear *n*-dodecylammonium chloride salt (**NC$_{12}$**) in water.

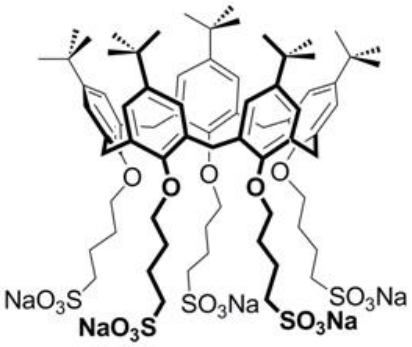

2

Figure 3.3.1. Chemical structure of *p-tert*-butylcalix[5]arene **2**.

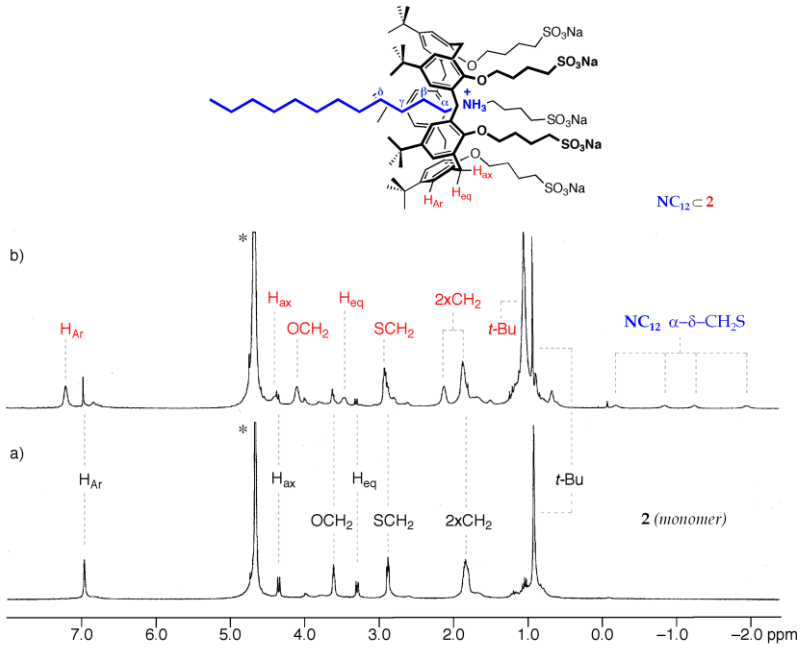

Figure 3.3.2. ^{1}H NMR spectra (500 MHz, D_2O, 298 K) of a 0.4 mM solution of calixarene **2** (a) before and (b) after the addition of **NC$_{12}$** (1 equiv.).

The formation of the **2⊃NC$_{12}$** supra-amphiphile was unambiguously proven by the broadening of the ^{1}H NMR resonances relative to the host-guest complex (Figure 3.3.2) and further corroborated by Diffusion Ordered NMR Spectroscopy (DOSY) data.[22]

The data reported were in agreement with the formation of a catanionic micelle[23] in which alkylammonium ions are not only included inside the calixarene cavities, but also take part in the micelle formation process (Figure 3.3.3.).

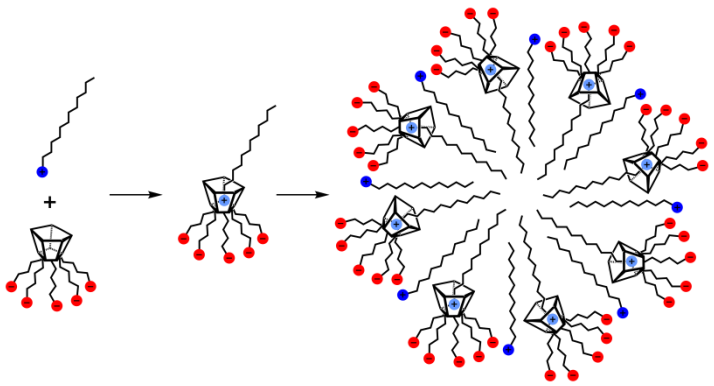

Figure 3.3.3. Schematic representation of the likely pathway leading to the formation of the **NC$_{12}$⊂2** supra-amphiphile and its aggregation in a catanionic micelle.

Later, further investigations unveiled an apparent discrepancy between the nominal and the calculated concentrations of the amphiphilic *O*-butylsulfonato-calix[5]arene monomer **2**, the latter concentration being always nearly half than the former,[24] when examined by quantitative ^{1}H NMR analysis[25] below its cmc (0.64 mM in D_2O). Preliminary dynamic light scattering (DLS) measurements demonstrated the presence of large aggregates with a hydrodynamic radius (R_h) of about 100 nm, "invisible" by the NMR technique (R_h = 10.0 Å for monomer **2** from DOSY

experiments), even in aqueous solutions below their estimated values of cmc. This finding is in line with the reported tendency of amphiphilic calixarene-type surfactants to aggregate below the cmc in large infinite "open model" structures.[26]

In this chapter is described a deeper insight into the aggregation properties of calixarene **2**. Moreover, considering previous results on the *endo*-cavity complexation of ammonium guests inside the cavity of monomer **2,**[22,25] the next objective was to verify whether the water soluble calixarene **2** retained, also in aqueous media, the ability to encapsulate a molecule of gemini α,ω-alkanedyildiammonium ion in the hydrophobic space provided by the two head-to-head opposite calix[5]arene cavities.[16]

3.4. Results and discussion

3.4.1. Insight into the aggregation properties of calix[5]arene **2** *and structures of the supra-amphiphiles*

The morphologies of colloidal systems (micelles, vesicles, bilayers) are closely related to the packing parameter of the surfactant ($P_s = v_c / a_o l_c$, where v_c and l_c are the volume and the length of the hydrophobic portion of the surfactant, and a_o is the head group area), which is largely dictated by the molecular shape of the surfactant and the polar-head area. Conical shaped surfactants assemble into micelles whereas cylindrical surfactants form vesicles or linear bilayers. In the case of penta-anionic surfactant **2**, ignoring for a moment the precise contribution of the electrostatic repulsions between head-groups to the overall structure, it is reasonable to imagine that this macrocycle would

either adopt a truncated-cone or a cylindrical shape (Figure 3.4.1.1). As a result, upon self-assembly, it is predicted the formation of either micelles or lower-curvature layered structures (vesicles). These considerations may then explain the presence in solution of large aggregates ($R_h \approx 100$ nm), even below the cmc, as the only species detected by DLS analysis.

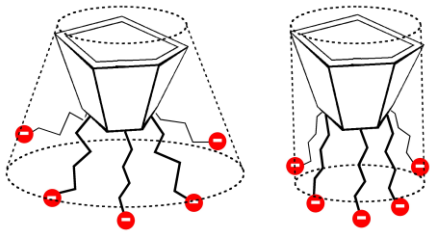

Figure 3.4.1.1. Possible shapes of amphiphilic calix[5]arene **2**.

A complete scenario of the aggregates formed was finally offered by SEM investigations. Together with small spherical objects,[27] SEM images showed the presence of nanograins (around 20 nm) aggregated to form elongated structures, relatively uniform in size (about 100 nm in length) and spatial distribution (Figure 3.4.1.2).

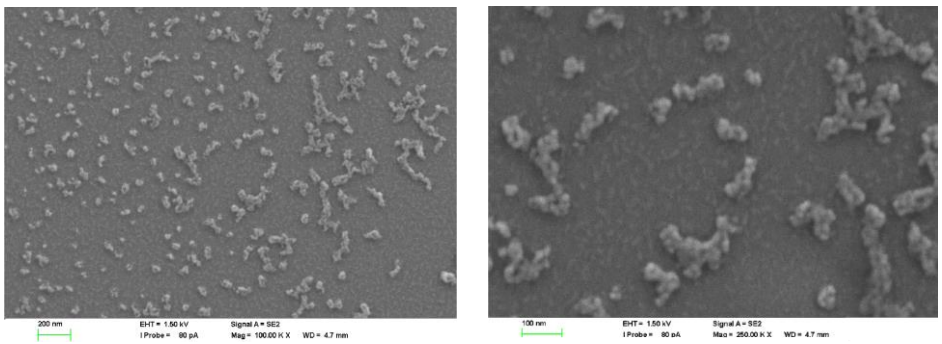

Figure 3.4.1.2. SEM images of [**2**] = 0.1 mM.

To evaluate the ability of derivate **2** to bind α,ω-alkanedyildiammonium ions we performed a series of ^{1}H NMR experiments with H_3N^+-$(CH_2)_n$-NH_3^+ bis-chlorides of different lengths (n = 8, 10, 12, 16, **NC$_n$N**) at [**2**] = 0.4 mM in D_2O, that is below its cmc, in a 2:1 and 1:1 **2**/ **NC$_n$N** ratio, in order to assess, also in the aqueous medium, the slow mode of complexation on the NMR timescale, and to determine the optimal guest chain length capable of triggering the capsular assembly. The diagnostic high field and aromatic regions of the ^{1}H NMR spectra of the 2:1 ratio ([**2**] = 0.4 mM, [**NC$_n$N**] = 0.2 mM), which should favour the 2:1 capsular complex, are reported in Figure 3.4.1.3.

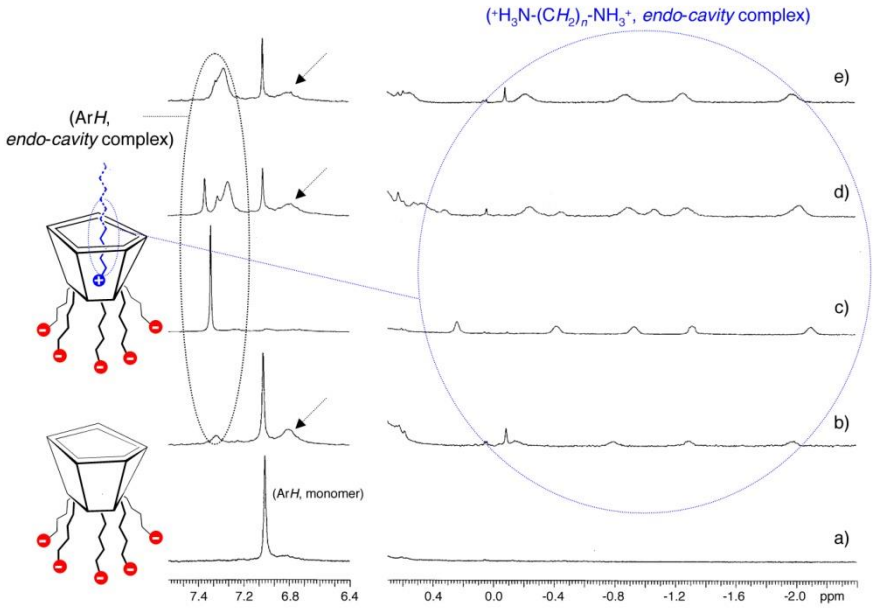

Figure 3.4.1.3. Selected aromatic and high-field regions of the ^{1}H NMR spectra (D_2O, 500 MHz, 298 K) of: a) [**2**] = 0.4 mM; b) [**2**] = 0.4 mM and [**NC$_8$N**] = 0.2 mM; c) [**2**] = 0.4 mM and [**NC$_{10}$N**] = 0.2 mM; d) [**2**] = 0.4 mM and [**NC$_{12}$N**] = 0.2 mM; e) [**2**] = 0.4 mM and [**NC$_{16}$N**] = 0.2 mM.

The high field region (0.5 to - 2.5 ppm) of traces b–e display, as a common feature, diagnostic sets of resonances, assigned to the *endo*-cavity included methylene groups of the different gemini guests, strongly shielded by the aromatic rings of the calixarene host. On the contrary, two distinctive scenarios can be observed when looking at the aromatic region of the spectra in Figure 3.4.1.3: (i) the δ 6.96 ppm resonance relative to monomer **2** co-existed with other sharp and broad signals (traces b, d, e); (ii) monomer **2** is no longer present, having been replaced by a sharp signal at δ 7.32 ppm (trace c).

When dealing with ^{1}H NMR spectroscopy of amphiphiles, sharp resonances are indicative of the presence of small or discrete species, whereas broadening of the signals is indicative of the presence of bigger aggregates. On the basis of previous results, the broad aromatic upfield-shifted signal at δ 6.80 ppm (arrows in Figure 3.4.1.3) was attributed to the aggregation of **2**, induced by the addition of the cationic guest but without inclusion of the guest itself inside the macrocyclic cavity (electrostatic interaction/catanionic system). The low-field shift of the other aromatic resonances is instead consistent with the aromatic calixarene cavity involved in an *endo*-type recognition process of the cationic guests.

Under our experimental conditions, depending on the spacer length and the host/guest ratio, two modes of complexation can be envisaged: a 1:1 head-to-tail complex and a 2:1 capsule (type-I and type-II complexes respectively, Figure 3.4.1.4.).

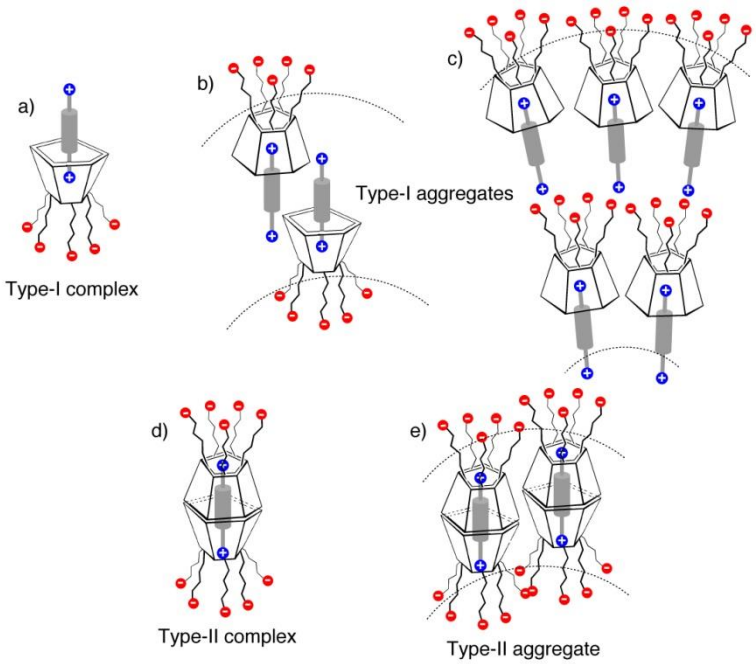

Figure 3.4.1.4. Cartoons of the possible complexes and of the resulting aggregates in **2/NC$_n$N** systems.

These two kinds of complexes still posses hydrophilic charged head-groups at both ends and can be considered as an oppositely charged bolaform head-to-tail supramolecular surfactant (type I) and a capsular bolaform supramolecular surfactant (type II) which, in turn, may further aggregate. It is well known that bolaform surfactants display, when compared with conventional surfactants with similar hydrophobic portions, an increased water solubility, due to the presence of charged head-groups on both ends, and higher cmc values. The presence of both sharp and broad signals in our experiments suggested that, under the experimental conditions adopted, the supramolecular species formed displayed different aggregational features.

A combined ^{1}H NMR and ^{1}H NMR Diffusion Ordered (DOSY) study provided a deeper insight into the different species present in solution. As mentioned earlier, after the addition of 0.5 equivalents of **NC$_{10}$N** the aromatic signal of monomer **2** (singlet at δ 6.96 ppm) completely disappeared in favor of a sharp singlet at δ7.32 ppm (Figure 3.4.1.3, trace b). The ^{1}H NMR Diffusion Ordered (DOSY) experiment run on this sample ([**2**] = 0.4 mM, [**NC$_{10}$N**] = 0.2 mM, D_2O) (Figure 3.4.1.5) clearly showed the same diffusion coefficient (D_{obs} = 1.56 x 10^{-10} m^2 s^{-1}) for the calixarene and the high-field guest resonances.

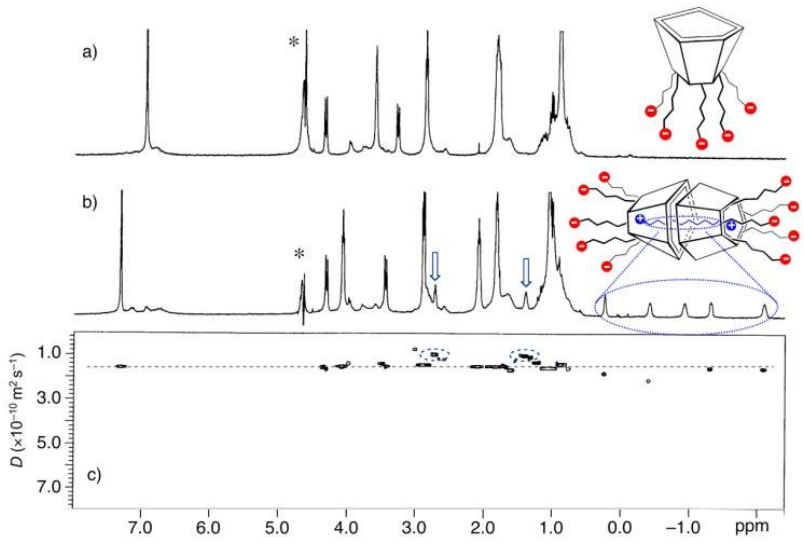

Figure 3.4.1.5. a) ^{1}H NMR spectrum of [**2**] = 0.4 mM (D_2O, 500 MHz, 298 K); b) DOSY spectrum (D_2O, 500 MHz, 298 K) of [**2**] = 0.4 mM and [**NC$_{10}$N**] = 0.2 mM.

Assuming a spherical shape for both monomer **2** and its complex with **NC$_{10}$N**, by using equation (eq. 1)[28]

$$D_{complex}/D_{monomer} = (M_{monomer}/M_{complex})^{1/3} \quad \textbf{(eq. 1)}$$

which correlates the diffusion coefficients of the species under investigation and their molecular masses, and knowing $D_{monomer}$ = 1.98 x 10^{-10} m^2 s^{-1}, a value of $M_{complex}$ that is the double of $M_{monomer}$ ($M_{complex}/M_{monomer}$ = 2.05) was calculated. This is consistent with the formation of a capsular 2:1 **2**⊃**NC$_{10}$N**⊂**2** complex (type-II). In the capsule **NC$_{10}$N** is symmetrically included inside the two calixarene cavities and, as a consequence, only five resonances are observed in the region δ 0.24 – -2.10 ppm. From previous observation on the effective concentration of monomer **2** below the cmc, considering that the solutions under investigation were [**2**] = 0.4 mM (but a 0.2 mM concentration of monomer could effectively be detected) and [**NC$_{10}$N**] = 0.2 mM, and given the formation of a capsular complex, the presence of free guest was expected in solution. Closer inspection of the DOSY spectrum showed no free guest ($D_{NC10N,free}$ = 5.81 x 10^{-10} m^2 s^{-1}) while the resonances at δ 2.81 and 1.47 ppm are ascribable to guest molecules interacting with bigger species and therefore diffusing slower (D_{obs} = 0.97 x 10^{-10} m^2 s^{-1}).

Contrary to the case of **NC$_{10}$N**, the addition of 0.5 equiv. of either the shorter (**NC$_8$N**) or the longer (**NC$_{16}$N**) gemini guest to a 0.4 mM solution of **2** caused the formation of **NC$_n$N**⊂**2**-type supramolecular bolaamphiphiles. The ^{1}H NMR spectra of these solutions showed a broad low field signal (δ 7.20–7.30 ppm; of low intensity in the case of **NC$_8$N**) together with a single set of high field guest-included methylene resonances, all of them displaying comparable diffusion coefficients (Table 3.4.1.1). In line with our findings in organic solvents[16] **NC$_8$N** is too short to promote the formation of a capsular assembly, being this guest only able to generate a 1:1 *endo*-cavity complex (**NC$_8$N**⊂**2**). On the other

hand, given the close similarity of the spectral patterns of Figure 3.4.1.3 (traces b and e), it is reasonable to conclude that in the case of the longer guest a similar 1:1 *endo*-cavity complex (*i.e.* **NC$_{16}$N⊂2**) has also been formed. In solution **NC$_8$N⊂2** and **NC$_{16}$N⊂2** complexes behave as oppositely-charged supra-bolaamphiphiles aggregating, in turn, with each other. In the case of the shorter guest, only a modest amount (10%) of **NC$_8$N⊂2** is formed. Subsequent addition of 0.5 equivalents of **NC$_8$N** ([**2**] = [**NC$_8$N**] = 0.4 mM) caused the self-assembly of **2** to increase, but did not induce any further *endo*-cavity inclusion of the guest (δ = 6.80 ppm; D_{obs} = 1.04 x 10^{-10} m^2 s^{-1}, Figure 3.4.1.6.).

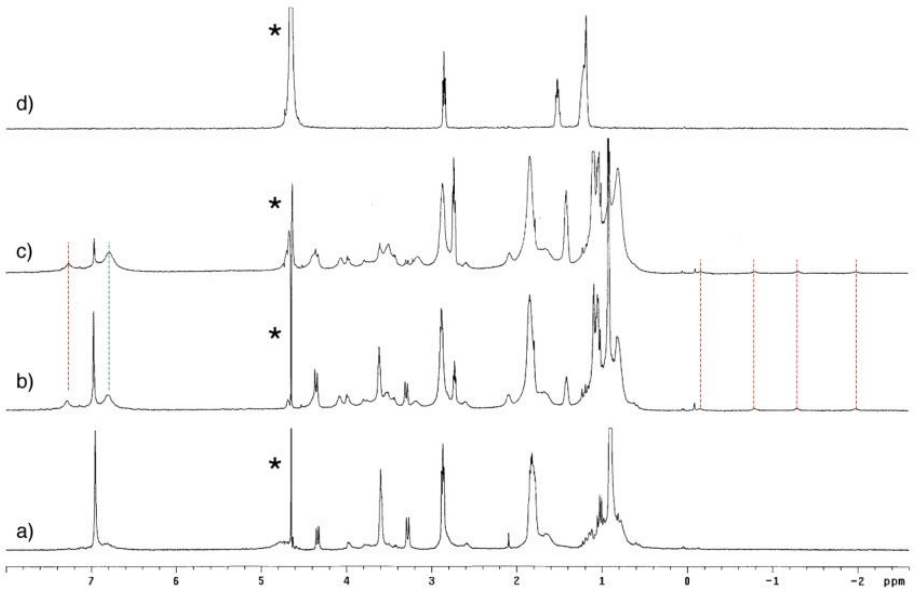

Figure 3.4.1.6. ^{1}H NMR spectra (D_2O, 500 MHz, 298 K) of (a) [**2**] = 0.4 mM; (b) [**2**] = 0.4 mM, [**NC$_8$N**] = 0.2 mM; (c) [**2**] = [**NC$_8$N**] = 0.4 mM; (d) [**NC$_8$N**] = 0.4 mM. Dashed lines indicate selected resonances for: red) type-I aggregate; green) aggregate without *endo*-cavity complexation. Asterisks indicates residual solvent peaks.

On the contrary, in tha case of **NC$_{16}$N,** nearly quantitative type I

aggregate was obtained when a stoichiometric amount of guest was added, indicating that with the longer guest the distance between the oppositely charged head-groups allows favorable electrostatic interactions in type-I aggregates (Figure 3.4.1.7).

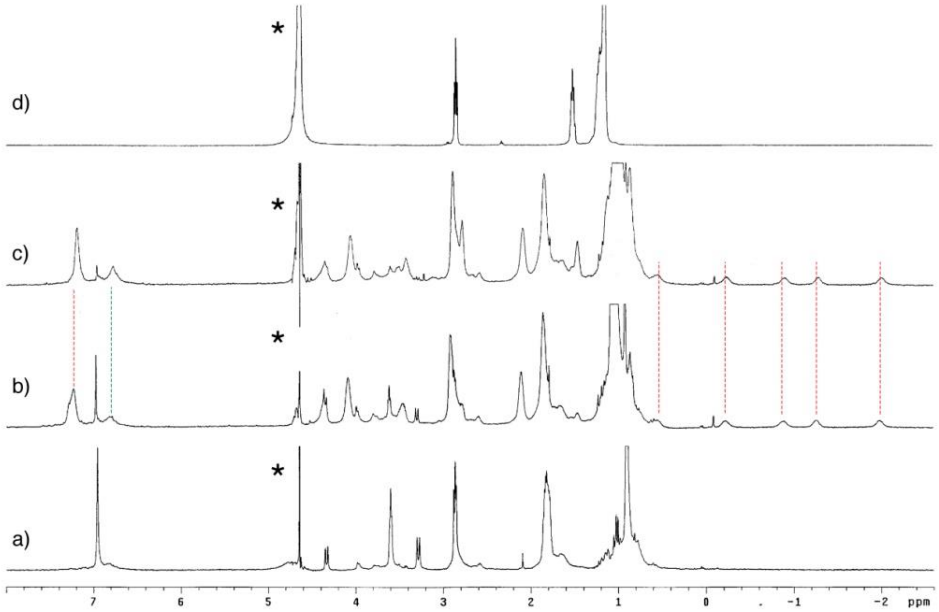

Figure 3.4.1.7. ^{1}H NMR spectra (D_2O, 500 MHz, 298 K) of (a) [**2**] = 0.4 mM; (b) [**2**] = 0.4 mM, [**NC$_{16}$N**] = 0.2 mM; (c) [**2**] = [**NC$_{16}$N**] = 0.4 mM; (d) [**NC$_{16}$N**] = 0.4 mM. Dashed lines indicate selected resonances for: red) type-I aggregate; green) aggregate without *endo*-cavity complexation. Asterisks indicates residual solvent peaks.

Finally, experiments with **NC$_{12}$N** were pivotal to understand the stoichiometry and self-assembly features of these calix[5]arene-based supraamphiphiles. When 0.5 equiv. of **NC$_{12}$N** were used, at least three different species, apart from monomer **2**, can be identified in the aromatic region and two different sets of upfield-shifted methylene resonances for the guest (Figure 3.4.1.8, trace b). A comparison of the

different traces in figure 3.4.1.3 suggested that in this case both 1:1 and capsular bolaamphiphiles were formed. To verify our hypothesis we performed a series of additional experiments. When 1 equiv. of **$NC_{12}N$** was added, in order to force the complexation event towards the 1:1 complex, the sharp signal at δ 7.36 ppm disappeared, the spectrum in figure 3.4.1.8, trace c, closely resembling that with **$NC_{16}N$** (broad signal at δ = 7.20 ppm). An 8-fold dilution of this sample did not show any significant change in the spectral patterns (Figure 3.4.1.9). On the contrary, when experimental conditions favouring the formation of the capsular complex were adopted (**2**/**$NC_{12}N$** 4:1 molar ratio, see figure 3.4.1.10), the sharp signal at δ 7.36 ppm was predominant. These observations allowed us to assign the δ 7.36 ppm resonance to the capsular **2**⊃**$NC_{12}N$**⊂**2** complex, the broad signal at δ = 7.20 ppm (D_{obs} = 1.11 x 10^{-10} m^2 s^{-1}) to the type-I aggregate, while the sharp aromatic resonance (δ 7.27 ppm) overlapping with the broad 1:1 aggregate might be assigned to the monomeric **2**⊃**$NC_{12}N$** supramolecular amphiphile (Figure 3.4.1.8).

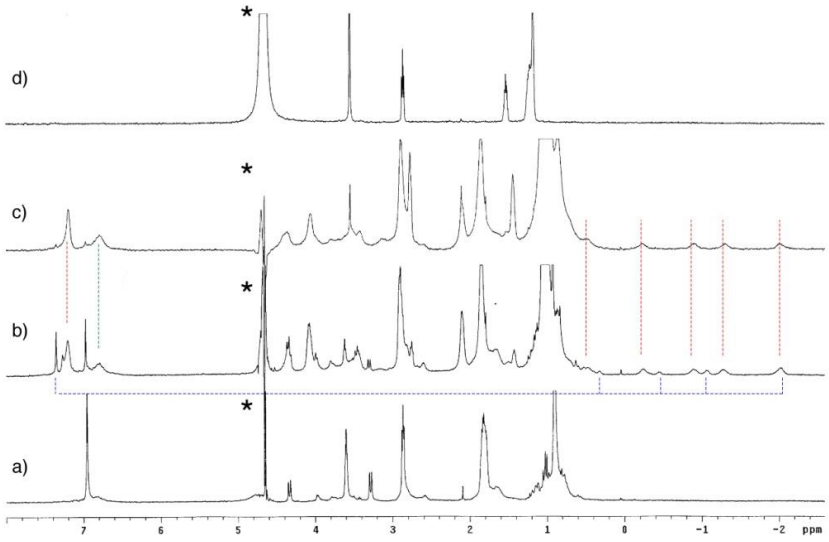

Figure 3.4.1.8. ^{1}H NMR spectra (D_2O, 500 MHz, 298 K) of (a) **[2]** = 0.4 mM; (b) **[2]** = 0.4 mM, **[$NC_{12}N$]** = 0.2 mM; (c)) **[2]** = **[$NC_{12}N$]** = 0.4 mM; (d) **[$NC_{12}N$]** = 0.4 mM. Dashed lines indicate selected resonances for: red) type-I aggregate; blu) type-II complex; green) aggregate without *endo*-cavity complexation. Asterisks indicates residual solvent peaks.

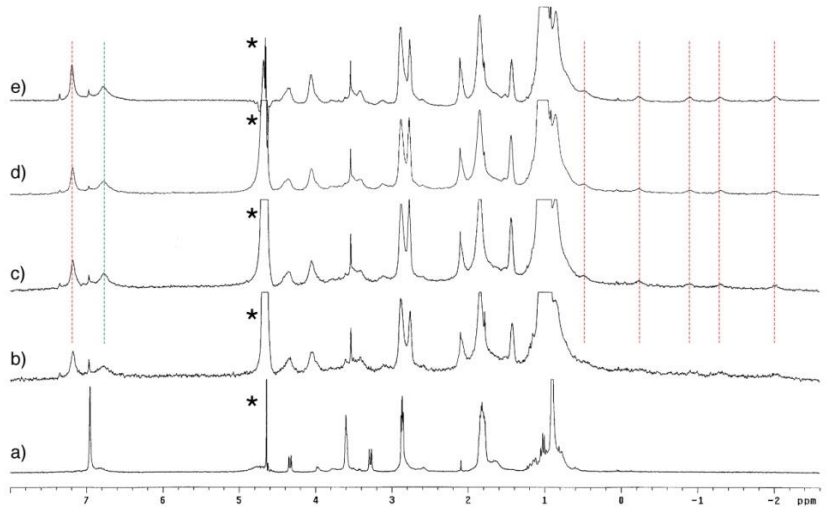

Figure 3.4.1.9. ^{1}H NMR spectra (D_2O, 500 MHz, 298 K) of (a) **[2]** = 0.4 mM; (b) **[2]** = **[$NC_{12}N$]** = 0.05 mM; (c) **[2]** = **[$NC_{12}N$]** = 0.1 mM; (d) **[2]** = **[$NC_{12}N$]** = 0.2 mM; (e) **[2]** = **[$NC_{12}N$]** = 0.4 mM. Dashed lines indicate selected resonances for: red) type-I aggregate; green) aggregate without *endo*-cavity complexation. Asterisks indicates residual solvent peaks.

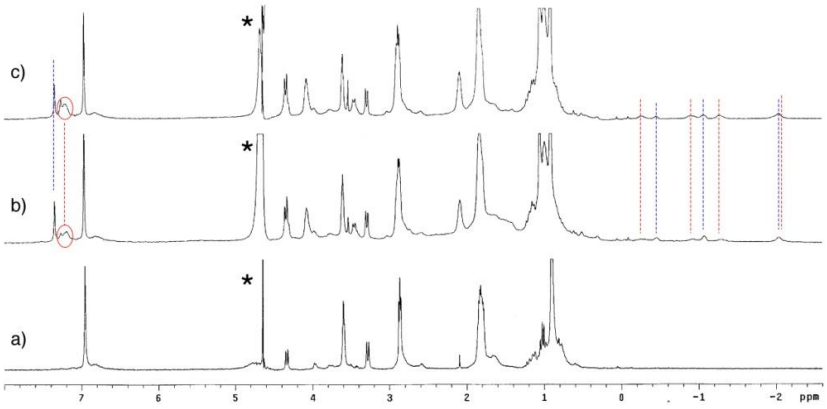

Figure 3.4.1.10. ^{1}H NMR spectra (D_2O, 500 MHz, 298 K) of (a) [**2**] = 0.4 mM; (b) [**2**] = 0.2 mM, [**NC$_{12}$N**] = 0.05 mM; (c)) [**2**] = 0.4 mM, [**NC$_{12}$N**] = 0.1 mM. Dashed lines indicate selected resonances for: red) type-I aggregate; blu) type-II complex. Asterisks indicates residual solvent peaks.

n	**2**	type-II complex	type-I aggregate	*exo-cavity* aggregate	**NC$_n$N**
	1.98 ± 0.07 (10.0 Å)				
8			1.27 ± 0.1 (15.7 Å)	1.04 ± 0.09 (19.2 Å)	6.32 ± 0.02 (3.2 Å)
10		1.56 ± 0.01 (12.8 Å)		0.90 ± 0.06 (22.2 Å)	5.81 ± 0.09 (3.4 Å)
12		1.54	1.11 ± 0.05	1.0± 0.03	1.0± 0.06
16			1.13 ± 0.03 (17.6 Å)		4.21 ± 0.01 (4.7 Å)

Table 3.4.1.1. Self-diffusion coefficients D_{obs} (x 10^{-10} m^2 s^{-1}) and corresponding hydrodynamic radii R_h (in parentheses) of **2**, **2**/**NC$_n$N** and **NC$_n$N**.

Overall the NMR studies on **2** and **NC$_n$N** showed: a) a peak selectivity of **2** for **NC$_{10}$N** (quantitative bis-*endo*-cavity inclusion of the gemini guest to

afford capsular complexes), as a consequence of the exceptional stereo- and electronic complementarity between the calix[5]arene cavity and the 1,10-decanediammonium guest and b) that the hydrophilic/amphiphilic properties of type I- or type-II complexes depends on a fine modulation of the hydrophilic and hydrophobic portions which in turn can be tuned by a gemini guest of appropriate length.

3.4.2. Determination of the cmc

The amphiphilic nature of **2⊃NC$_{10}$N⊂2** bola-amphiphile was further proved by ^{1}H NMR experiment carried out at different **2**/**NC$_{10}$N** concentrations.

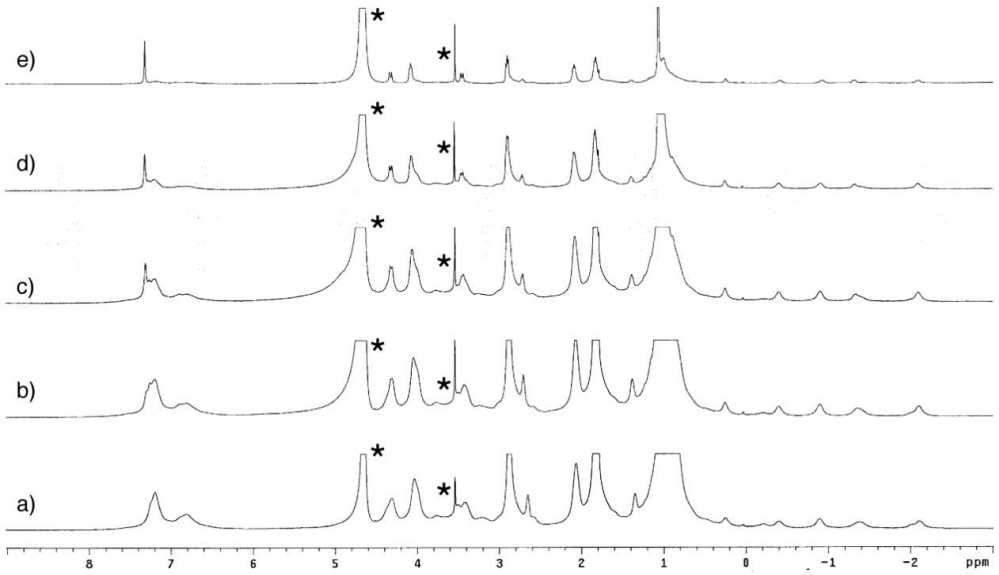

Figure 3.4.2.1. ^{1}H NMR spectra (D_2O, 500 MHz, 298 K) of (a) [**2**] = 6.2 mM, [**NC$_{10}$N**] = 3.1 mM; (b) [**2**] = 4.0 mM, [**NC$_{10}$N**] = 2.0 mM; (c) [**2**] = 2.5 mM, [**NC$_{10}$N**] = 1.25 mM; (d) [**2**] = 1.0 mM, [**NC$_{10}$N**] = 0.5 mM. Asterisks indicates residual solvent peaks.

^{1}H NMR spectra (Figures 3.4.2.1) show sharp signals for the more diluted solutions, while increasing the concentration, the resonances broaden, indicating that an aggregation process is taking place. Moreover traces b, c, and d (Figure 3.4.2.1) show three different resonances in the aromatic region, indicating that by increasing the concentration different aggregation phenomena are taking place in a slow exchange on the NMR time-scale. Finally the cmc value of **2⊃NC$_{10}$N⊂2** bola-amphiphile (0.77 mM, in D_2O) was determined by DOSY NMR spectroscopy (Figure 3.4.2.2).

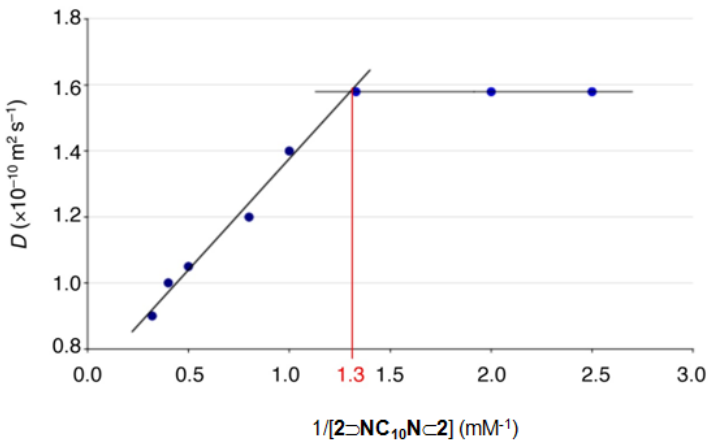

Figure 3.4.2.2. Plot of the self-diffusion coefficients (*D*) *vs* the inverse of concentration of **2⊃NC$_{10}$N⊂2**.

NMR spectroscopy, however, was found to be unsuitable to determine the very low cmc value for the **2⊃NC$_{16}$N** supra-amphiphile, the latter requiring the alternative use of a dye (Sudan I) solubilization experiment[29] performed at increasing concentrations of **2⊃NC$_{16}$N**. A remarkable increase of the absorbance at λ 485 nm demonstrated the

formation of **2⊃NC$_{16}$N** aggregates with lipophilic domains starting from concentration of [**2**] = [**NC$_{16}$N**] = 17 μM (Figure 3.4.2.3).

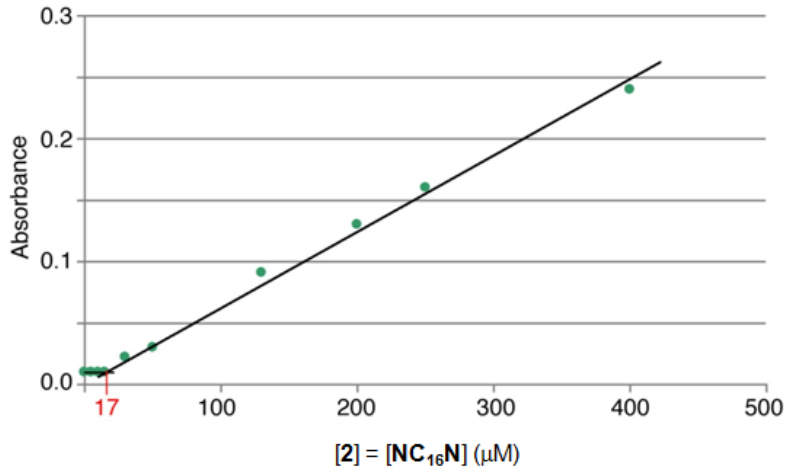

Figure 3.4.2.3. Plot of absorbance of Sudan I *vs* the concentration of **2⊃NC$_{16}$N**.

3.4.3. Comparison of DOSY NMR and DLS data

Self-diffusion coefficients (D_{obs}) and hydrodynamic radii (R_h) of **2** and **NC$_n$N** together with those of the complexes/aggregates detected by DOSY NMR in the 2:1 **1**/**NC$_n$N** solutions (D_2O) are listed in Table 3.4.1.1. R_h values were routinely calculated using the Stokes-Einstein equation ($D_{obs} = k_BT/6\pi\eta R_h$), assuming an overall spherical shape for all the species considered.

The D_{obs} data in Table 3.4.1.1 indicate that among type-I aggregates, the one formed in the presence of the longest guest (**NC$_{16}$N**) diffuses slower, hence, is the biggest of the lot (R_h = 17.6 Å).

According to DOSY data (Table 3.4.1.1), the dimensions of monomers, complexes and aggregates fall all within the 3–22 Å range. On the other

hand, DLS measurements carried out on a solution of calixarene **2** below the cmc ([**2**] = 0.1 mM) showed the presence of "NMR-invisible" aggregates of R_h = 100–120 nm with a negative superficial charge (□-potential = -25 mV) and electrophoretic mobility μ = -1.5 μm/s V cm^{-1} (Table 3.4.3.1). Titration of aqueous solutions of calixarene **2** (0.1 mM) with the three gemini dications **NC*n*N** (*n* = 8, 10, 16) produced, according to DLS measurements, large aggregates with R_h = 100–300 nm.

Progressive addition of the best-fitting **NC$_{10}$N** guest to an unfiltered solution of the calixarene, within the 0.5 to 8 to **NC$_{10}$N/2** ratio interval (Figure 3.4.3.1), produced insignificant changes to the hydrodynamic radius of the species already present in solution. In particular, the electrophoretic mobility and the related ζ-potential of the aggregates (Table 3.4.3.1) hardly varied in the course of the addition of the **NC$_{10}$N**, with appreciable variation of these parameters, towards less negative values, observed only after addition of an excess of guest, most likely because of an opposite-charge neutralization process.

	R_h (nm)	μ (μm/s V cm^{-1})	ζ-potential (mV)
[**2**] = 0.1 mM	100–120	-1.5	-25
[**2**] = 0.1 mM + [**NC$_8$N**] = 0.05 mM	≈ 100	-0.7	-10
[**2**] = 0.1 mM + [**NC$_{10}$N**] = 0.05 mM	≈ 120	-1.5	-25
[**2**] = 0.1 mM + [**NC$_{10}$N**] = 0.8 mM	≈ 120	-0.2	-3
[**2**] = 0.1 mM + [**NC$_{16}$N**] = 0.05 mM	200–300	-3.5	-50

Table 3.4.3.1. Hydrodynamic radii (R_h), electrophoretic mobilities (μ) and ζ-potentials for aggregates of **2** and **2/NC$_n$N.**

This trend is in agreement with our previous considerations on *p-tert*-butylcalixarene-*O*-butylsulfonato aggregating, below the cmc, in large "open model" structures with a head-to-head arrangement (Figure 3.4.3.4a). When 0.5 equivalents of **$NC_{10}N$** are added, the guest molecules are encapsulated in the calixarene bilayer with the positive ammonium heads "hidden" inside the calixarene cavities. As a consequence, the overall dimension of the aggregate does not change (Figure 3.4.3.1b) and the dicationic gemini guest does not alter the superficial charge of the aggregates (ζ-potential and μ do not vary). Partial neutralization of the negatively charged surface of the aggregates finally occurs upon addition of an excess of **$NC_{10}N$** ions (Figure 3.4.3.1d).

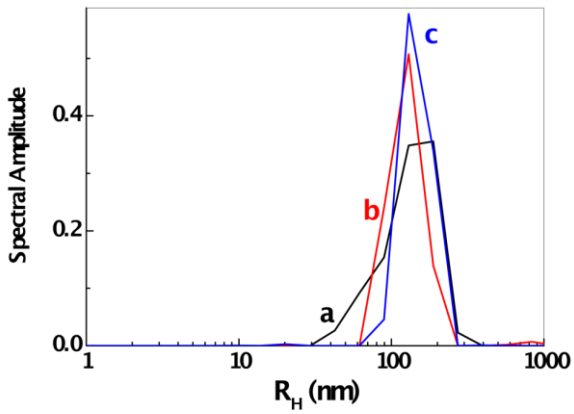

Figure 3.4.3.1. Size distribution of aggregates in aqueous solution of (a) **[2]** = 0.1 mM; (b) **[2]** = 0.1 mM, **[$NC_{10}N$]** = 0.05 mM; (c) **[2]** = 0.1 mM, **[$NC_{10}N$]** = 0.8 mM.

The addition 0.5 equivalents of the shorter guest did not produce appreciable variation of the dimension of nanosized aggregates (Figure 3.4.3.2), while ζ-potential and electrophoretic mobility (Table 3.4.3.1) immediately increased, suggesting that the anionic shell around the calixarene aggregates has been partially neutralized by electrostatically

interacting with the diammonium guest. These findings are consistent with previous NMR observation: **NC$_8$N** is too short to be encapsulated, only a small amount of aggregating 1:1 supra-amphiphile is formed, the rest of guest electrostatically interacts with the sulfonato moieties of **2** (Figure 3.4.3.4c).

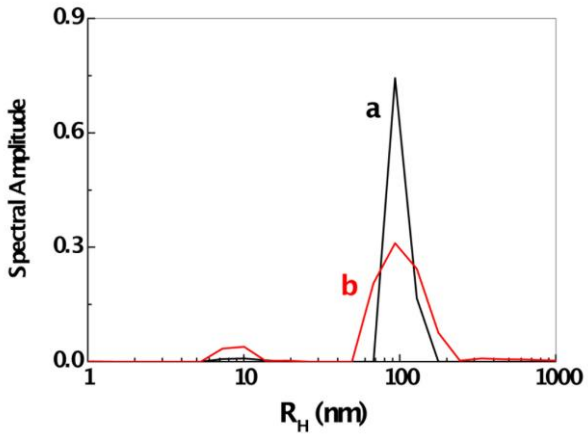

Figure 3.4.3.2. Size distribution of aggregates in aqueous solution of (a) [**2**] = 0.1 mM; (b) [**2**] = 0.1 mM, [**NC$_8$N**] = 0.05 mM.

The addition of **NC$_{16}$N** afforded, as already seen by NMR results, the formation of bigger aggregates (R_h 200–300 nm, Figure 3.4.3.3.). Interestingly, more negative ζ-potential (–50 mV) and μ (–3.5 μm/s V/cm) values were detected this time (Table 3.4.3.1). This is consistent with an increased negative superficial charge of the aggregates, which might be explained by taking into account the presence of "free" ammonium head groups of single bola-amphiphile (**2**⊂**NC$_{16}$N**) acting as supramolecular linkers, via electrostatic interactions, with the sulfonate groups of nearby aggregates (Figure 3.4.1.4c). Such a process may also account for the increased dimensions of the aggregates.

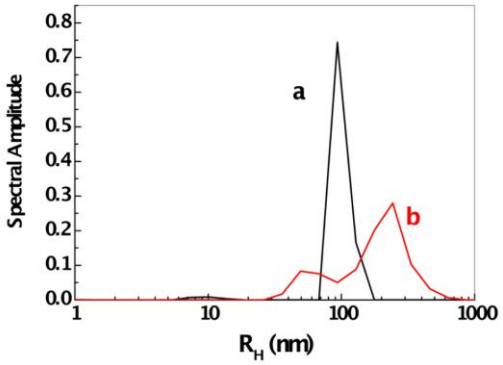

Figure 3.4.3.3. Size distribution of aggregates in aqueous solution of (a) [**2**] = 0.1 mM; (b) [**2**] = 0.1 mM, [**NC$_{16}$N**] = 0.05 mM.

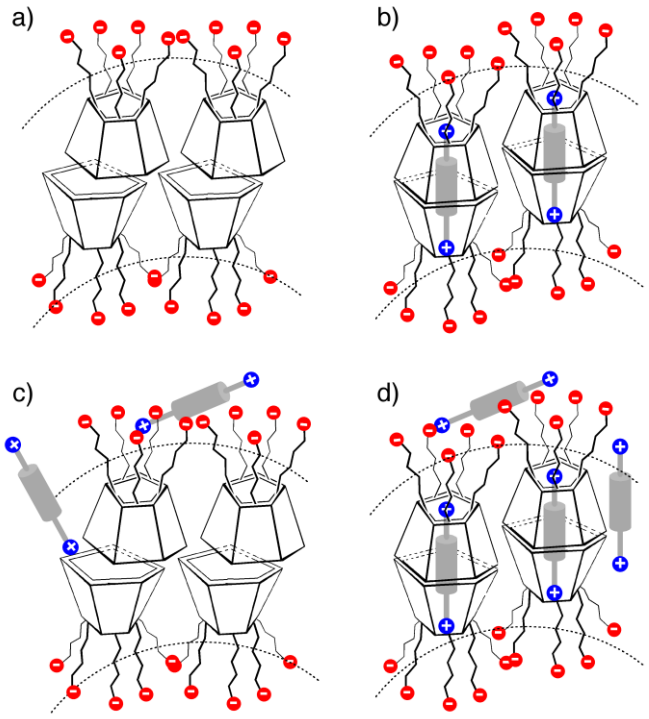

Figure 3.4.3.4. Cartoons.

Finally, the considerable morphological change after addition of **$NC_{16}N$** was also evidenced by means of SEM microscopy. The nanoaggregates show sizes ranging between 80-200 nm (Figure 3.4.3.5.). Moreover, some donuts-like structures, results of the coalescence of smaller nanoaggregates, are also evident.

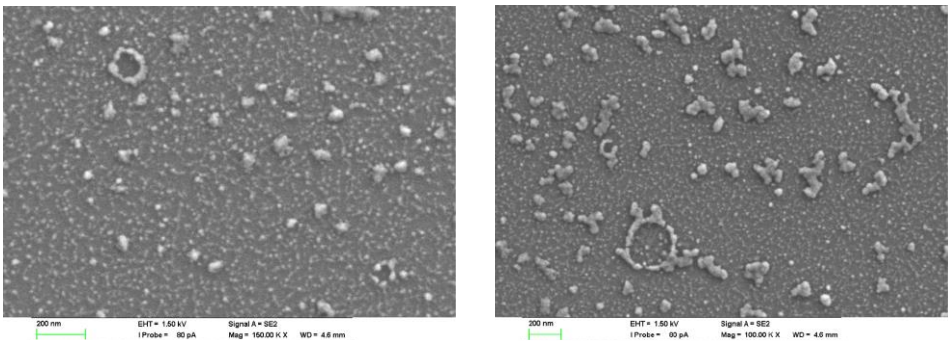

Figure 3.4.3.5. SEM images of **[2]** = 0.1 mM, **[$NC_{16}N$]** = 0.05 mM.

3.4.4. Drug solubilising studies

Colloidal systems are currently used as drug-solubilising and drug-delivering agents in pharmacological formulation for oral, parenteral and transdermal adminstration of actives.[30]

Recently coassemblies of amphiphilic calixarenes and resorcarenes with organic hydrophobic acids[31] and anticancer drugs have been reported to show great potentials in the solubilisation of insoluble drugs and in drug-delivery strategies. The fine modulation of the structural transitions of our calixarene-based colloids prompted us to verify the solubilising properties of the different assemblies deriving from calixarene **2**. To this end, three different D_2O solutions of calixarene **2** (**[2]** = 0.4 mM; **[2]** = 0.4 mM and **[$NC_{10}N$]** = 0.2 mM; **[2]** = 0.4 mM and

[**NC$_{16}$N**] = 0.4 mM) were used to solubilise the water-insoluble antitumoral drug tamoxifen (water solubility as free base 0.1 μg/ml). Preliminary ^{1}H NMR data (Figure 3.4.4.1) revealed that only the bigger aggregates formed upon inclusion of **NC$_{16}$N** were able to dissolve the insoluble drug. The trace 3.4.4.1b clearly shows the upfield-shifted aromatic protons of tamoxifen partially overlapping with the calixarene species. Back exctraction into chloroformic phase allowed us to determine a 1400-fold (140 μg/ml) increase of solubilised drug, both by using the quantitative qNMR software *Varian Vnmrj 3.2* and UV analyses (the concentration of extracted tamoxifen was determined from the absorbance value at λ = 275 nm).

Considering the very low cmc value determined for **2⊃NC$_{16}$N** supraamphiphile, we believe that supraamphiphilc systems based on calixarene amphiphiles can be considered relevant candidates for the construction of "drug-chaperones"[32] for poor soluble drugs.

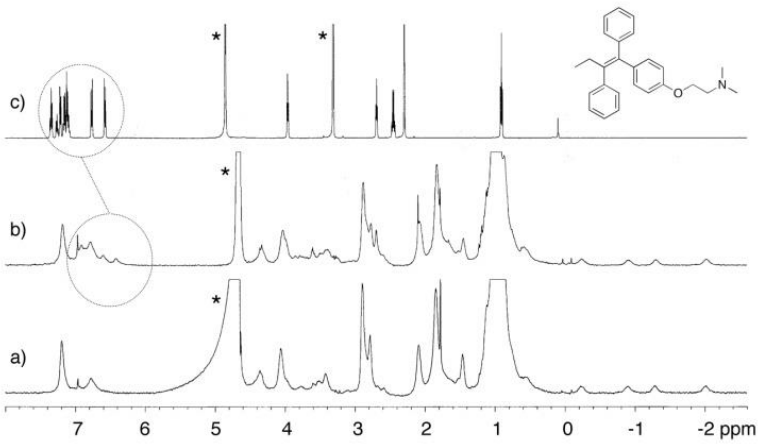

Figure 3.4.4.1. ^{1}H NMR spectra (D_2O, 500 MHz, 298 K) of: a) [**2**] = [**NC$_{16}$N**] = 0.4 mM (D_2O, 500 MHz, 298 K); b) after exctraction of tamoxifen; c) tamoxifen in CD_3OD.

3.5. Conclusions

In this chapter I have demonstrated that calix[5]arene **2** maintain also in water the host-guest chemistry already reported in organic solvents. Moreover, the aggregational features of the calix[5]arene-*O*-butylsulfonato derivative can be efficiently modulated by the formation of supra-amphiphiles obtained through the *endo*-cavity recognition of α,ω–alkanediyldiammonium ions of different lengths. NMR spectroscopy gave a direct insight into the interactions (*endo*-cavity or electrostatic) taking place during the recognition phenomena, thus allowing the identification (modeling) of two different bola-supraamphiphiles with extremely different aggregating properties. ^{1}H NMR evidences together with DOSY experiments were essential to understand the morphological changes, observed by complementary techniques such as DLS and SEM, of "NMR invisible" aggregates. The bigger aggregates formed by **2**⊃**NC$_{16}$N** supraamphiphile were able to increase the water-solubility of the antitumoral drug tamoxifen of a factor of 1400. Finally, the results herein reported demonstrate the great potentials of calixarene-based supraamphiphiles in the design of novel drug-solubilisation and delivery systems.

3.6. Experimental section

3.6.1. General experimental methods

^{1}H and ^{13}C NMR spectra were recorded at room temperature in D_2O, at 500 and 125 MHz respectively. The solvent residual peak (δ_H 4.65 ppm) was used as an internal standard for ^{1}H NMR spectra, while the ^{13}C NMR spectrum was referenced to internal dioxane (δ_C 69.3 ppm). THF was dried by a standard method prior to use; other chemicals were reagent grade and were used without further purification. *p-tert*-Butylcalix[5]arene was synthesized according to a literature procedure.[33]
Diffusion Ordered NMR Spectroscopy (DOSY) studies were performed on a Varian 500 MHz spectrometer equipped with a pulse-field gradient probe. Spectra were recorded at 25 °C using a DgcsteSL pulse sequence. Experimental parameters were optimized according to the sample under investigation. Diffusion gradients were incremented in 30 steps with gradient pulse amplitudes varying from 1.8 to 58.5 gauss/cm, the number of transients acquired for each increment ranging from 16 to 128, with a diffusion gradient length of 2 ms and diffusion delays in the 150–200 msrange. All measurements were performed in triplicate and the reported values are the mean ± standard deviation of the mean. The hydrodynamic radii (R_h) were obtained using the Stokes-Einstein equation: $D_{obs} = k_B T/6\pi\eta R_h$, where k_B is the Boltzmann constant, T is the temperature and η is the viscosity of the solvent.
SEM analyses were carried out with a Zeiss (model Merlin Gemini 2) filed emission electron microscope, operating at 150 kV and a working distance of 4 mm.

UV measurements were performed using a Varian Cary 50 Scan UV-Visible spectrophotometer.

DLS measurements were carried out using a 35 mW polarized He-Ne laser source (l = 632.8 nm). The polarized scattered light was collected at 90°, in a self-beating mode, using an Avalanche Photodiode (Single Photon Counting Module) by Excelitas Technologies. The signal was sent to a Malvern 4700 submicrometer particle analyzer system to measure the intensity autocorrelation function, $g_2(t)$. The intensity autocorrelation function is related to the scattered electric field correlation function $g_1(t)$ through the Siegert's relation: $g_1(t) \propto [g_2(t)-1]^{1/2}$. Determination of the size distribution from the field correlation function $g_1(t)$ was obtained through a Laplace inversion:

$$g_1(t) = \int \tau A(\tau) \exp(-t/\tau) d(\ln \tau)$$

where $\tau=1/(DQ^2)$, D and Q being the diffusion coefficient of the particle and the exchanged momentum of the scattered light, respectively. The diffusion coefficient D is related to the hydrodynamic radius through the Einstein-Stokes relation. A discrete multi-exponential non-negative least-squares fit (NNLS) was used to perform this inversion procedure.

The spectral amplitude τA is related to the scattered intensity of each species (with radius R), which, in turn, depends on its number concentration, n, on the radius R and on its form factor P(QR). By using the Rayley-Gans form factor of a sphere it is possible to obtain the number distribution as:

$$n(R) = a \frac{\tau A}{[\sin(QR) - QR\cos(QR)]^2}$$

where *a* is a constant giving the normalization to unity of the number-weighted size distribution.

3.6.2. Synthetic procedure

Sodium *p-tert*-butyl-calix[5]arenepenta-*O*-(4-butoxysulfonato)[22] (**2**)
p-tert-Butylcalix[5]arene (186 mg, 0.23 mmol), an excess of NaH (83 mg, 3.45 mmol) and 1,4-butane sultone (470 mg, 3.45 mmol) were mixed in anhydrous THF (20 mL) and refluxed for 48 h. The mixture was allowed to cool to room temperature and MeOH (5 mL) was added. The precipitate was collected by filtration, washed with EtOH, dissolved in 5 mL of water and finally precipitated by the salting-out method with sodium acetate. After centrifugation, the solid was separated and refluxed in EtOH (20 mL) for 24 h. The white powder (172 mg, 47%) was collected by filtration. M.p. 255–258 °C (dec.). ^{1}H NMR (0.5 mM) δ 0.91 (s, C(CH3)3, 45 H), 1.79–1.85 (m, OCH2(CH2)2, 20 H), 2.87 (t, J = 8.1 Hz, SCH2, 10 H), 3.29 and 4.34 (AX, J = 14 Hz, ArCH2Ar, 10 H), 3.60 (bt, OCH2, 10 H), 6.96 (s, Ar, 10 H) ppm; ^{13}C NMR (5.0 mM) δ 23.7, 31.6, 33.4, 34.0, 36.5, 54.0, 76.5, 128.3, 136.7, 147.7, 154.9 ppm. Anal. Calcd for $C_{75}H_{10}5Na_5O_{20}S_5$: C, 56.23; H, 6.61; S, 10.01; Found: C, 55.92; H, 6.63; S, 9.95.

3.*6.3. Determination of the cmc*

The cmc of **2**⊃**NC$_{16}$N** amphiphile was determined by dye solubilisation experiments. The experiments were performed by adding an excess of crystalline dye Sudan I to equimolar solutions of **2** and **NC$_{16}$N** of different concentrations ([**2**] = [**NC$_{16}$N**] = 0 – 400 μM). After equilibrating

for 24 h at room temperature, the solutions were centrifugated (6000 rpm) for 10 minutes to remove undissolved dye, and their absorbance was measured at λ = 485 nm. Absorbance values were plotted *vs* the sample concentrations and the cmc was derived from the intersection between the two lines best fitting the experimental data points.

3.6.4. *Drug solubilisation*

Tamoxifen solubilization experiments were performed by adding solid tamoxifen (1μmol) to 1 mL of 0.4 mM solution of **2** and **$NC_{16}N$** (1:1) in ultrapure H_2O. After equilibrating for 24 h at room temperature in the dark, the solution was centrifugated (6000 rpm) for 10 minutes to remove undissolved solid. 900 μL of the supernatant were extracted with 900 μL of $CHCl_3$ in a closed vial for 12 h. The organic phase was diluited 10 times before UV analysis. The concentration of extracted tamoxifen was determined from the absorbance value at λ = 275 nm. 200 μL of $CDCl_3$ were added to 300 μL of the tamoxifen chloroformic solution and the concentration of recovered tamoxifen was determined from the integral of selected peaks by using the quantitative qNMR software *Varian Vnmrj 3.2.*

References

[1] Kang Y., Liu K., Zhang X., *Langmuir*, **2014**, 30, 5989.

[2] (a) Zhang Z., Ding J., Chen X., Xiao C., He C., Zhuang X., Chen L., Chen X., *Polym. Chem*., **2013**, 4, 3265; (b) Zhang H., Liu Z., Xin F., An W., Hao A., Li J., Li Y., Sun L., Sun T., Zhao W., Li Y., Kong L., *Carbohydr. Res*., **2011**, 346, 294; (c) Wang Y., Ma N., Wang Z., Zhang X., *Angew. Chem. Int. Ed.,* **2007**, 46, 2823.

[3] (a) Yu Y., Li J., Zhang M., Cao L., Isaacs L., *Chem. Commun*., **2015**, 51, 3762; (b) Liu K., Yao Y., Kang Y., Liu Y., Han Y., Wang Y., Li Z., Zhang X., *Sci. Rep.,* **2013**, 3, 2372; (c) Jiao D., Geng J., Loh X.J., Das D., Lee T.C., Scherman O.A., *Angew. Chem. Int. Ed*., **2012**, 51, 9633; (d) Jeon Y.J., Bharadwaj P.K, Choi S.W., Lee J.W., Kim K., *Angew. Chem. Int. Ed.,* **2002**, 41, 4474.

[4] (a) Gao L., Wang T., Jia K., Wu X., Yao C., Shao W., Zhang D., Hu X.Y., Wang L., *Chem. A. Eur. J.,* **2017**, 27, 6605; (b) Liu X., Jia K., Wang Y., Shao W., Yao C., Peng L., Zhang D., Hu X.Y., Wang L., *ACS Appl. Mater. Interfaces,* **2017**, 9, 4843; (c) Meng L.B., Zhang W., Li D., Li Y., Hu X.Y., Wang L., Li G., *Chem. Commun*., **2015**, 51, 14381; (d) Yao Y., Li J., Dai J., Chi X., Xue M., *RSC Adv*., **2014**, 4, 9039; (e) Cao Y., Hu X.Y., Li Y., Zou X., Xiong S., Lin C., Shen Y.Z., Wang L., *J. Am. Chem. Soc.,* **2014**, 136, 10762.

[5] Jeon Y.J., Bharadwaj P.K., Choi S., Lee J.W., Kim K., *Angew. Chem., Int. Ed.,* **2002**, 41, 4474.

[6] Versluis F., Tamatsu I., Kehr S., Fregonese C., Tepper A.W.J.W., Stuart M.C.A., Ravoo B.J., Koning R.I., Kros A., *J. Am. Chem. Soc.,* **2009**, 131, 13186.

[7] (a) Peng S., Gao J., Liu Y., Guo D.S., *Chem. Commun.,* **2015**, 51, 16557; (b) Wang Y.X., Zhang Y.M., Liu Y., *J. Am. Chem. Soc.,* **2015**, 137, 4543; (c) Qin Z., Guo D.S., Gao X.N., Liu Y., *Soft Matter,* **2014**, 10, 2253; (d) Guo D.S., Wang K., Wang Y.X., LiuY., *J. Am. Chem. Soc*., **2012**, 134, 10244; (e) Wang K., Guo D.S., Liu Y., *Chem. Eur. J.,* **2012**, 18, 8758; (f) Basilio N., Martín-Pastor M., García-Río L., *Langmuir,* **2012**, 28, 6561; (g) Francisco V., Basilio N., Garcia-Rio L., Leis J.R., Maques E.F., Vázquez-Vázquez C., *Chem. Commun*., **2010**, 46, 6551.

[8] Wintgens V., Miskolczy Z., Guigner J.M., Amiel C., Harangozo J.G., Biczók L., *Langmuir,* **2015**, 31, 6655.

[9] (a) Costa C., Francisco V., Silva S.G., do Vale M.L.C., García-Río L., Marques E.F., *Colloids Surf. A: Physicochem. Eng. Aspects,* **2015**, 480, 71; (b) Basilio N., García-Río L., *Chem. Eur. J.,* **2009**, 15, 9315; (c) Guo D.S., Liu Y., *Acc. Chem. Res*., **2014**, 47, 1925; (d) Guo D.S., Wang K., Wang Y.X., Liu Y., *J. Am. Chem. Soc.,* **2012**, 134, 10244; (e) Cao Y., Wang Y.X., Guo D.S., Liu Y., *Sci. China Chem*., **2014**, 57, 371.

[10] (a) Francisco V., García-Río L., *Langmuir,* **2014**, 30, 6748; (b) Bonaccorso C., Brancatelli G., Forte G., Arena G., Geremia S., Sciotto D., Sgarlata C., *RSC Adv.*, **2014**, 4, 53575; (c) Zhao H.X., Guo D.S., Liu Y., *J. Phys. Chem. B*, **2013**, 117, 1978.

[11] Yao Y., Chi X., Zhou Y., Huang F., *Chem. Sci.,* **2014**, 5, 2778.

[12] Gutsche C.D., *Calixarenes – an Introduction, in Monographs in Supramolecular Chemistry*, ed. J.F. Stoddart, The Royal Society of Chemistry, Cambridge, *2nd* **2008**, 6.

[13] Asfari Z., Böhmer V., Harrowfield J. and VicensJ., *Calixarenes*, Kluwer Academic Publisher, Dordrecht, **2001**.

[14] (a) Haino T., Yanase M., Fukazawa Y., *Angew. Chem., Int. Ed. Engl.,* **1997**, 36, 259; (b) Haino T., Yanase M., Fukazawa Y., *Angew. Chem., Int. Ed.,* **1998**, 37, 997; (c) Yanase M., Haino T., Fukazawa Y., *Tetrahedron Lett.*, **1999**, 40, 2781; (d) Haino T., YamanakaY., Araki H., Fukazawa Y., *Chem.Commun*., **2002**, 402.

[15] (a) Pappalardo S., Parisi M.F., *J. Org. Chem.*, **1996**, 61, 8724; (b) Arnaud-Neu F., Fuangswasdi S., Notti A., Pappalardo S., Parisi M.F., *Angew. Chem., Int. Ed*., **1998**, 37, 112; (c) Ferguson G., Notti A., Pappalardo S., Parisi M.F., Spek A.L., *Tetrahedron Lett.,* **1998**, 39, 1965; (d) Gattuso G., Notti A., Pappalardo S., Parisi M.F., Pilati T., Resnati G., Terraneo G., *Cryst. Eng. Comm.,* **2009**, 11, 1204.

[16] Garozzo D., Gattuso G., Kohnke F.H., Malvagna P., Notti A., Occhipinti S., Pappalardo S., Parisi M.F., Pisagatti I., *Tetrahedron Lett.,* **2002**, 43, 7663.

[17] (a) Pappalardo S., Villari V., Slovak S., Cohen Y., Gattuso G., Notti A., Pappalardo A., Pisagatti I., Parisi M.F., *Chem. Eur. J.,* **2007**, 13, 8164; (b) Gattuso G., Notti A., Pappalardo A., Parisi M.F., Pisagatti I., Pappalardo S., Garozzo D., Messina A., Cohen Y., Slovak S., *J. Org. Chem.,* **2008**, 73, 7280; (c) Capici C., Cohen Y., D'Urso A., Gattuso G., Notti A., Pappalardo A., Pappalardo S., Parisi M.F., Purrello R., Slovak S., Villari V., *Angew. Chem., Int. Ed.,* **2011**, 50, 11956.

[18] (a) Garozzo D., Gattuso G., Notti A., Pappalardo A., Pappalardo S., Parisi M.F., Perez M., Pisagatti I., *Angew. Chem., Int. Ed.,* **2005**, 44, 4892; (b) Gargiulli C., Gattuso G., Liotta C., Notti A., M. F. Parisi, I. Pisagatti and S. Pappalardo, *J. Org. Chem.,* **2009**, 74, 4350; (c) Capici C., De Zorzi R., Gargiulli C., Gattuso G., Geremia S., Notti A., Pappalardo S., Parisi M.F., Puntoriero F., *Tetrahedron,* **2010**, 66, 4987.

[19] (a) Giannetto M., Mori G., Notti A., Pappalardo S., Parisi M.F., *Anal. Chem.,* **1998**, 70, 4631; (b) Lupo F., Capici C., Gattuso G., Notti A., Parisi M.F., Pappalardo A., Pappalardo S., Gulino A., *Chem. Mater.,* **2010**, 22, 2829.

[20] De Salvo G., Gattuso G., Notti A., Parisi M.F., Pappalardo S., *J. Org. Chem.***, 2002**, 67, 684.

[21] (a) Garozzo D., Gattuso G., Kohnke F.H., Notti A., Pappalardo S., Parisi M.F., Pisagatti I., White J P., Williams D.J., *Org. Lett.*, **2003**, 5, 4025; (b) Gargiulli C., Gattuso G., Notti A., Pappalardo S., Parisi M.F., *Tetrahedron Lett.,* **2011**, 52, 7116.

[22] Gattuso G., Notti A., Pappalardo A., Pappalardo S., Parisi M.F., Puntoriero F., *Tetrahedron Lett*., **2013**, 54, 188.

[23] Mahiuddin S., Zech O, Raith S., Tourand D., Kunz W., *Langmuir,* **2009**, 25, 12516.

[24] Gattuso G., Notti A., Pappalardo S., Parisi M.F., Pisagatti I., *Supramol. Chem.,* **2014**, 26, 597.

[25] Henderson T.J., *Anal. Chem.,* **2002**, 74, 191.

[26] (a) Zakharova L.Y., Kudriashova Y.R., Selivanova N.M., Voronin M.A., Ibragimova A.R., Solovieva S.E., Gubaidullin A.T., Litvinov A.I., Nizameev I.R, Kadirov M.K., Galyametdinov Y.G., Antipin I.S., Konovalov A.I., *J. Membr. Sci*., **201**0, 364, 90; (b) Pashirova T.N., Gibadullina E.M., Burilov A.R., Kashapov R.R., Zhiltsova E.P., Syakaev V.V., Habicher W.D., Rümmeli M.H., Latypov S.K., Konovalev A.I., Zakharova L.Y., *RSC Adv*., **2014**, 4, 9912.

[27] Gattuso G., Notti A., Pappalardo S., Parisi M.F., Pisagatti I., Patanè S., *New J. Chem*.**, 2014**, 38, 5983.

[28] Waldeck A.R., Kuchel P.W., Lennon A.J., Chapman B.E., *Prog. Nucl. Magn. Reson. Spectrosc.,* **1997**, 30, 39.

[29] (a) Gaynanova G.A., Bekmukhametova A.M., Kashapov R.R., Ziganshina A.Y., Zakharova L.Y., *Chem. Phys. Lett.,* **2016**, 652, 190; (b) Pashirova T.N., Ziganshina A.Y.,

Sultanova E.D., Lukashenko S.S., Kudryashova Y.R., Zhiltsova E.P., Zakharova L.Y., Konovalov A.I., *Colloid. Surf. A,* **2014**, 448, 67.

[30] *Colloids in Drug Delivery*, *Surfactant Science Series, vol. 148*, (Ed.: M. Faunn), Taylor and Francis/CRC press, Boca Raton, **2010**.

[31] Barbera L., Gattuso G., Kohnke F.H., Notti A., Pappalardo S., Parisi M.F., Pisagatti I., Patanè S., Norberto M., Villari V., *Org. Biomol. Chem*., **2015**,13, 6468.

[32] Wang Y.X., Guo D.Sh., Duan Y.Ch., Wang Y.J., Liu Y., *Sci. Rep*., **2015**, 5, 9019.

[33] Stewart D.R., Gutsche C.D., *Org. Prep. Proc. Int*., **1993**, 25, 137.

Chapter 4

Self-sorting of supramolecular systems in water

4.1. Introduction

The term self-sorting[1] is used to describe spontaneous and high fidelity self and/or non-self-recognition of two or more species within a multicomponent mixture.

In 2003, Isaacs *et al*. classified artificial self-sorting into two categories: social self-sorting and narcissistic (asocial) self-sorting.[2] Social self-sorting occurs between different species whereas a narcissistic self-sorting process[3] takes place between the same species (Scheme 4.1.1).

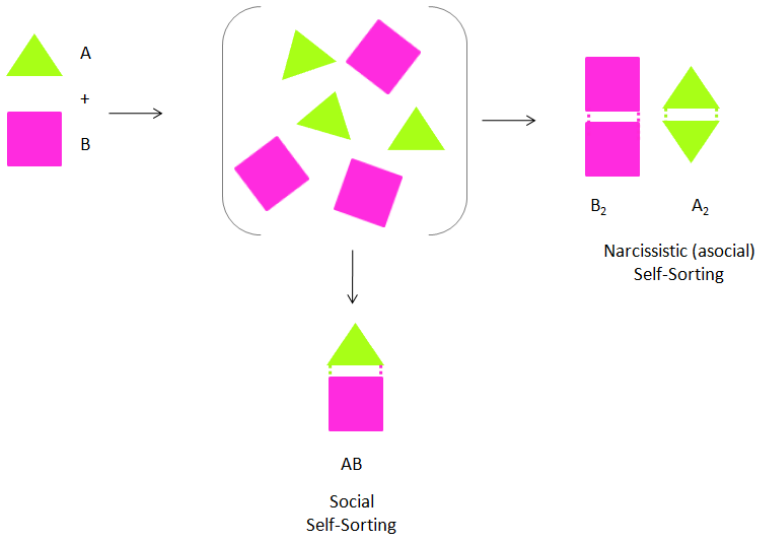

Scheme 4.1.1. Self-sorting in a 2-component system.

Recently, Schalley and co-workers[4] divided social self-sorting systems in integrative and nonintegrative. In nonintegrative systems, the components of the mixture combine to yield more than one final complex, whereas in integrative systems all species present in the mixture are integrated into one more complicated assembly.

Self-sorting phenomena have manifold appearances in Nature and in biological processes[5]: adenine (A), thymine (T), guanine (G), and cytosine (C) automatically self-sort to form two base pairs (AT and GC)[6] allowing to store an immense amount of information in a specific sequence of the DNA; carbohydrates, peptides and fatty acids undergo self-sorting in the construction of a cell. When trying to replicate these exceptional properties in laboratory host-guest chemistry, researchers have to face with two fundamentals supramolecular interactions, *i.e.* directional and non-directional forces. Directional forces (hydrogen bonds,[7] metal-ligand interactions,[8] π–π stacking,[9]) secure geometrical requirements which allow high affinities and specificities in supramolecular complexes, while non-directional attractive or repulsive van der Waals interactions play important roles in determining the distances between the interacting species.

In the field of calixarenes chemistry, Böhmer and Schalley reported efficient self-sorting processes relative to mixtures of tetraurea calix-[4]arenes which are noted to form dimeric capsules under controlled conditions.[10]

More recently, Talotta *et al*.[11] have demonstrated that calix[6]arene-based pseudo[3]rotaxanes with bisammonium axles have intriguing self-

sorting capabilities. In details, by mixing two different symmetrical axles and two wheels, among twenty possible homo- and heteropseudo[3]rotaxanes (Figure 4.1.1b) only two are stereospecifically formed, while in a three component mixture of two wheels and one asymmetrical axle, among 16 possible species only one heteropseudo[3]rotaxane was observed (red box, Figure 4.1.1c).

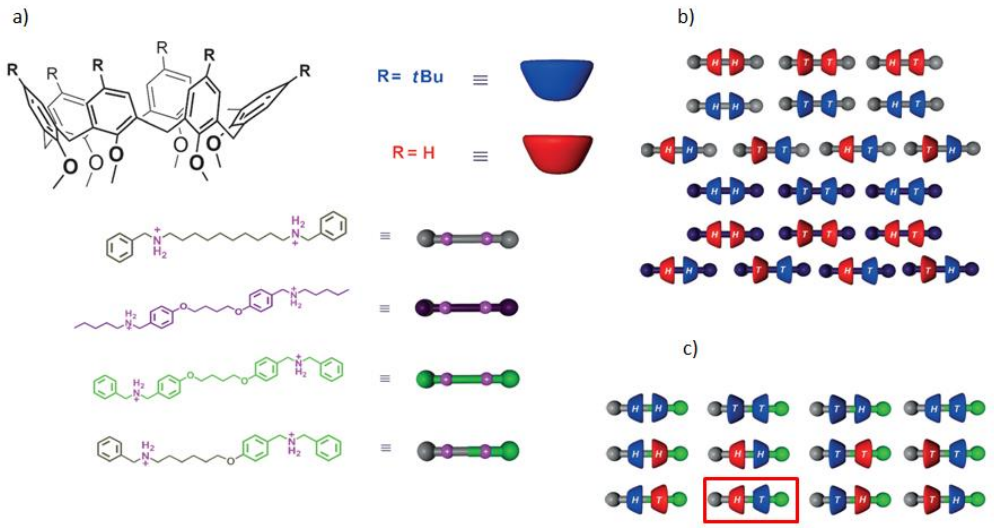

Figure 4.1.1. a) Structures of calix[6]arene wheels and dibenzyl- and alkylbenzylammonium axles; b) all species that can form in mixtures of two different wheels and two different axles; c) all species that can form in mixtures of two calix wheels and a directional axle. (Adapted from Ref.11).

Our research group has been involved for a long time in the study of the optimal requirements needed for the (poly)capsular[12] formation of calix[5]arene derivatives induced by long-chained bis(poly)-ammonium ions in solution and in the solid state.[13] All these studies showed that an efficient capsule formation depends on the length of the guest, the

degree of penetration inside the host cavity and attractive van der Waals interactions between the upper rims of the hosts. In particular precedent experiments carried out with calix[5]arenes bearing bulkier *tert*-butyl groups at the upper rim highlighted that a chain-lenght of at least ten-carbon atoms is necessary to position two calixarene cups at the right distance to ensure favorable attracting van der Waals interactions, while a shorter eight-carbon chain is preferred for capsular arrangements of *p*-methyl derivatives.[12]

In the next section, I will report a fascinating example of social (non integrative) self-sorting based on a four component system (Figure 4.1.2) consisting of two water-soluble calix[5]arene derivatives differently substituted at the upper rim (**1** and **2**) and two α,ω-alkanediyldiammonium ions of different lengths (H_3N^+-$(CH_2)_n$-NH_3^+, *n* = 8, 10, **NC$_8$N** and **NC$_{10}$N**).

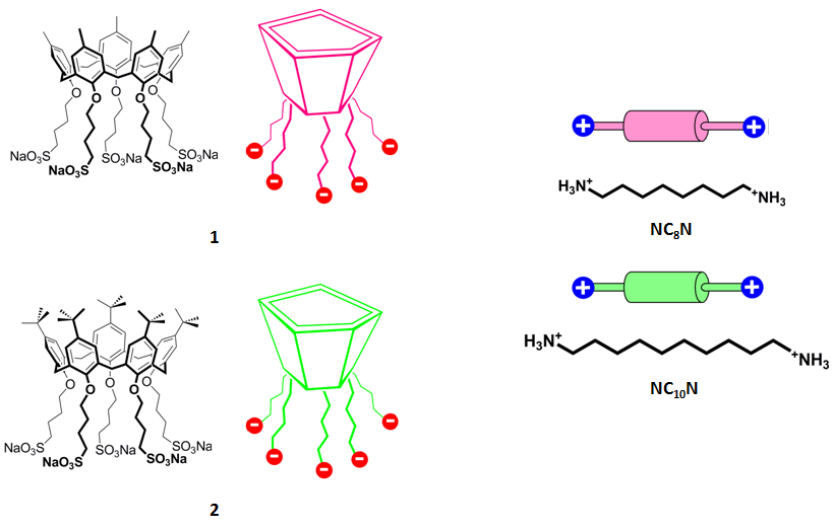

Figure 4.1.2. Schematic representation of the four-component system based on hosts **1** and **2** and guests **NC$_8$N** and **NC$_{10}$N**.

4.2. Results and discussion

p-Methyl-calix[5]arene **1** was synthesized as reported in paragraph 2.2.1. As previously reported for *p-tert*-butylcalix[5]arene and *p-tert*-butylcalix[4]arene[14] analogues, ^{1}H NMR spectra recorded in D_2O at different concentration of **1** (Figure 4.2.1) showed broad resonances for concentrated samples ([**1**]≥ 7.5 mM) and sharp ones for diluted solutions, in agreement with the amphiphilic nature of this macrocycle. However, in contrast with previous results with *p-tert*-butyl derivative **2** and the *p-tert*-butylcalix[4]arene analogous described in chapter 2,[14] but in line with traditional surfactants, only one aromatic resonance was observed in all spectra of Figure 4.2.1, indicating that the monomer-to-micelle exchange is fast on the NMR time-scale.

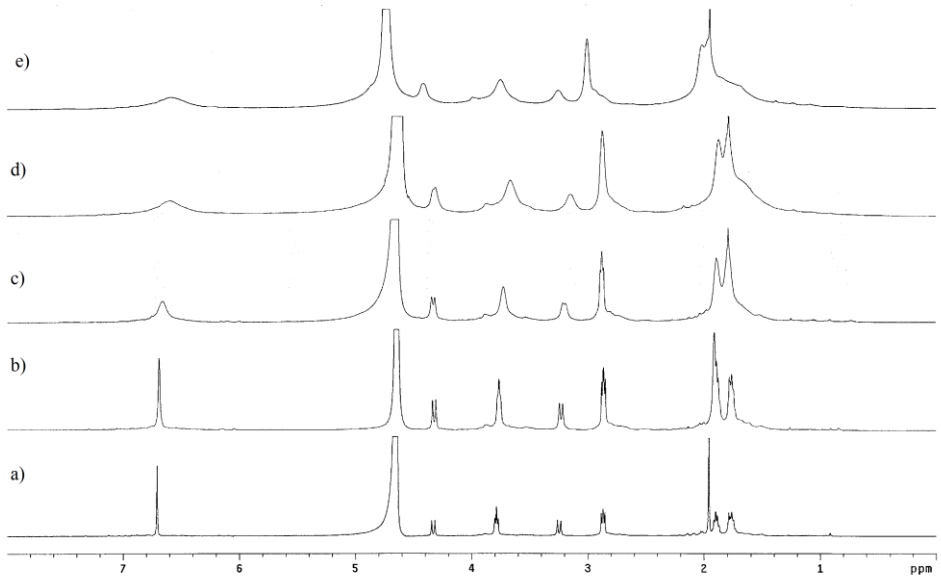

Figure 4.2.1. ^{1}H NMR spectra (500 MHz, 298 K, D_2O) of calix[5]arene **1** at different concentrations: (a) 3.0 mM, (b) 6.5 mM, (c) 10.0 mM, (d) 15.0 mM, (e) 20.0 mM.

A closer inspection of Figure 4.2.1 revealed that both aromatic and methyl resonances are up-field shifted as a result of the anisotropic shielding effect of the surrounding calixarene molecules in the micellar aggregate.

The critical micellar concentration (cmc) of the new amphiphilic derivative **1** was determined by a diffusion ordered NMR spectroscopy (DOSY) study carried out on D_2O solutions at different calixarene concentrations. A cmc value of 7.5 mM was estimated from the intersection of the two lines best-fitting the experimental data points obtained by plotting the diffusion coefficients (D_{obs}) *vs* the inverse of concentration (Figure 4.2.2). This value is almost 12 folds higher the one determined for *p-tert*-butylcalixarene **2** (0.64 mM),[14a] thus indicating that the amphiphlic properties of *O*-butylsulfonato calix[5]arenes can be simply modulated by changing the lipophilic character of the *para*-substituents.

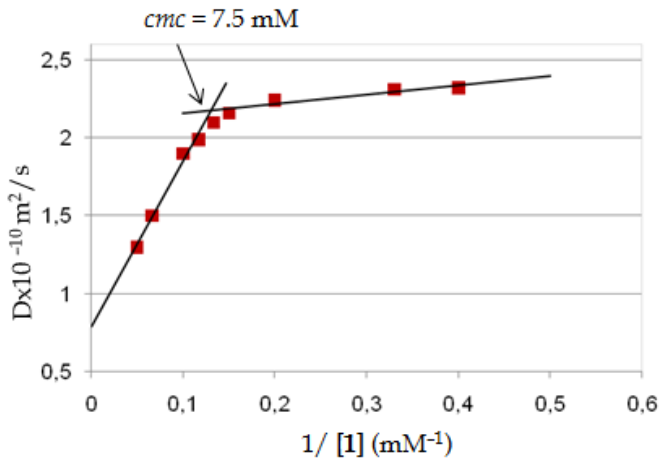

Figure 4.2.2. Plot of the self-diffusion coefficients (D) *vs.* the inverse of the concentration of calixarene **1** in D_2O at 298 K.

The optimal requirements needed for the capsular formation of *p-tert*-butylcalix[5]arene derivatives with α,ω-alkanedyildiammonium ions have already been described in chapter 3. Before studying the four component system, our first concern was to test whether derivative **1**, below its cmc value, retained in aqueous media the ability of forming capsular assemblies with the shorter **NC$_8$N** guest.[12b] The *endo*-cavity inclusion properties of derivative **1** were also studied in the presence of the longer **NC$_{10}$N**.

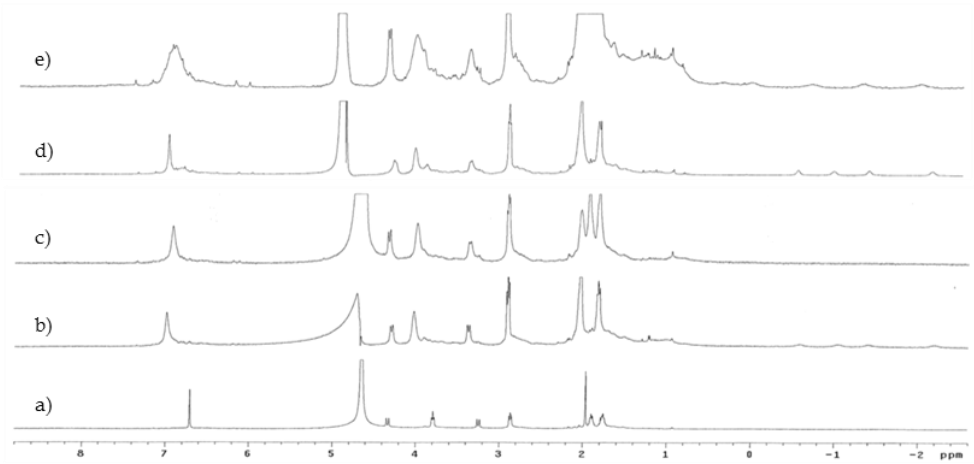

Figure 4.2.3. ^{1}H NMR spectra (D_2O, 500 MHz) of: a) [**1**] = 0.4 mM, 298 K; b) [**1**] = 0.4 mM and [**NC$_8$N**] = 0.2 mM, 298 K; c) [**1**] = 0.4 mM and [**NC$_{10}$N**] = 0.2 mM, 298 K; d) [**2**] = 0.4 mM and [**NC$_8$N**] = 0.2 mM, 278 K; e) [**2**] = 0.4 mM and [**NC$_{10}$N**] = 0.2 mM, 278 K.

^{1}H NMR experiments carried out in D_2O (Figure 4.2.3) at 298 K and 278 K confirmed the formation of *endo*-cavity complexes of *p*-methylcalix[5]arene **1** with guests **NC$_8$N** and **NC$_{10}$N**; the *endo*-cavity recognition event of the alkylammoium portion of the guests was unequivocally proven by the down-field shift of the aromatic resonances of the calixarene cavity and by the broad up-field signals (-3.0 – 0.2 ppm)

relative to the guest alkyl chain included inside the calixarene cavity, which especially in the case of **NC$_{10}$N**, became more evident when spectra were recorded at lower temperature (278 K, Figure 4.2.3e). In particular, only four distinct signals for the encapsulated guest were observed in the high-field region of the ^{1}H NMR spectrum of **1**/**NC$_8$N** 2:1 solution ([**1**]=0.4 mM; [**NC$_8$N**]=0.2 mM) as expected for the guest methylene protons symmetrically included inside the two calixarene cavities (Figure 4.2.4).

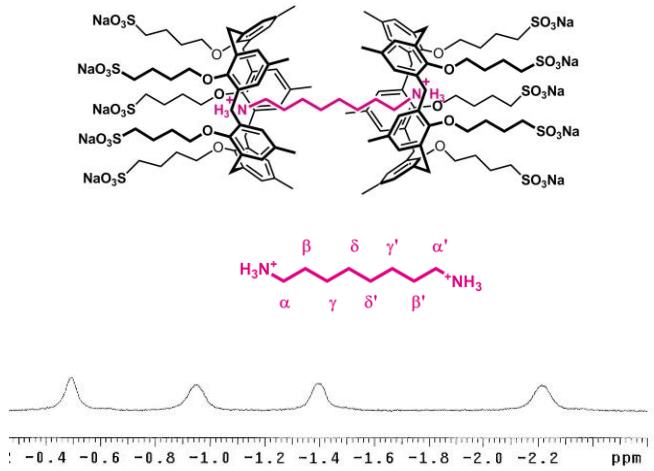

Figure 4.2.4. Selected high-field region of the ^{1}H NMR spectrum (D_2O, 500 MHz, 278 K) of [**1**] = 0.4 mM and [**NC$_8$N**] = 0.2 mM.

As previously described for derivative **2** and **NC$_{10}$N** (paragraph 3.4.1), the formation of the capsular complex **1⊃NC$_8$N⊂1** was further supported by a ^{1}H NMR Diffusion Ordered (DOSY) experiment ([**1**] = 0.4 mM, [**NC$_8$N**] = 0.2 mM, D_2O) that clearly showed the same diffusion coefficient ($D_{complex}$ = 1.75 x 10^{-10} m^2 s^{-1}) for the calixarene and the high-

field guest resonances. Assuming a spherical shape for both monomer **1** and its complex with **NC$_8$N**, by using equation 1[15] (eq. 1) which correlates the diffusion coefficients of the species under investigation and their molecular masses, and knowing $D_{monomer}$ = 2.39 x 10^{-10} m^2 s^{-1}, a value of $M_{complex}$ that is the double of $M_{monomer}$ ($M_{complex}/M_{monomer}$ = 2.55) was calculated. This is an additional evidence of the formation of the capsular complex.

$$D_{complex}/D_{monomer} = (M_{monomer}/M_{complex})^{1/3} \quad \textbf{(eq. 1)}$$

Furthermore the association constant for the capsular complex **1⊃NC$_8$N⊂1** (*K_{ass}* = 1.29 x 10^5 M^{-2}) was determined by integration of the signals relative to free and complexed host and guest of a diluted host-guest solution ([**1**]= 0.1 mM; [**NC$_8$N**]= 0.05 mM). Under this condition the only detectable complex was the capsular assembly and no 1:1 H/G complex was observed.

In order to analyse the self-sorting event in the capsular complexes formation, we performed a series of ^{1}H NMR experiments with the four components mixture **1**:**2**:**NC$_8$N**:**NC$_{10}$N** in 2:2:1:1 ratio. The experiments were carried out at 278 K to observe the methylene resonances of **NC$_{10}$N** eventually included in **1** (Figure 4.2.3e).

Statistically, by mixing in solution the four components **1, 2**, **NC$_8$N** and **NC$_{10}$N**, ten possible complexes can be formed as illustrated in Figure 4.2.5: four 1:1 H/G complex (**1⊃NC$_8$N**, **1⊃NC$_{10}$N**, **2⊃NC$_8$N**, **2⊃NC$_{10}$N**), two heterocapsules (relative to the hosts) (**1⊃NC$_8$N⊂2** and **1⊃NC$_{10}$N⊂2**)

and four homocapsules (**1**⊃**NC$_8$N**⊂**1**; **2**⊃**NC$_8$N**⊂**2**; **1**⊃**NC$_{10}$N**⊂**1**; **2**⊃**NC$_{10}$N**⊂**2**).

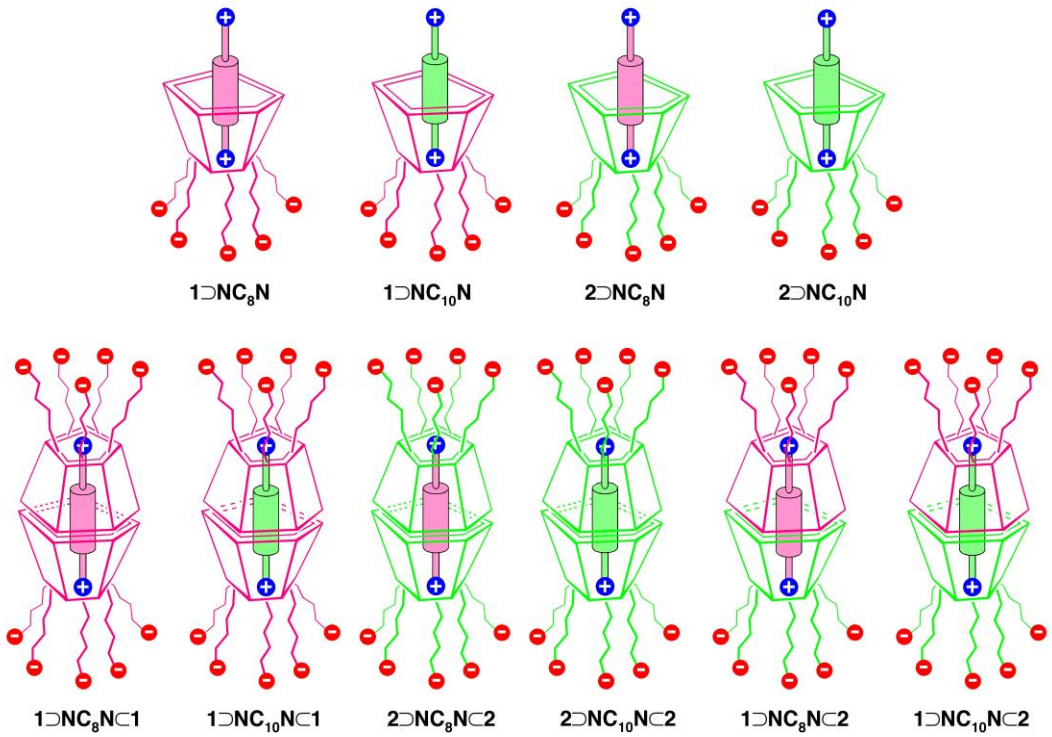

Figure 4.2.5. Cartoons of the ten possible complexes.

Knowing the amphiphilic properties of both derivatives **1** (cmc = 7.5 mM) and **2** (cmc = 0.64 mM),[14a] and in order to limit aggregation phenomena, ^{1}H NMR titration experiments were performed at hosts' concentrations of 0.4 mM. Since derivative **2** was found to form NMR "invisible" aggregates (see chapter 3), its effective concentration was corrected by careful addition of aliquots of **2** until a final 0.4 mM

concentration determined by NMR quantitative analysis (qNMR software *Varian Vnmrj 3.2*).

Upon addition of 0.5 equiv. of **$NC_{10}N$** to an equimolar mixture of **1** and **2,** ([**1**]=[**2**]=0.4 mM; [**$NC_{10}N$**]= 0.2 mM), only the homocapsule **2⊃$NC_{10}N$⊂2** was quantitatively obtained, as showed by the green coloured resonances in Figure 4.2.6b, while the signal relative to the aromatic hydrogens of compound **1** remained unchanged and no resonances relative to **$NC_{10}N$** included inside the cavity of calixarene **1** were observed (Figure 4.2.6b).

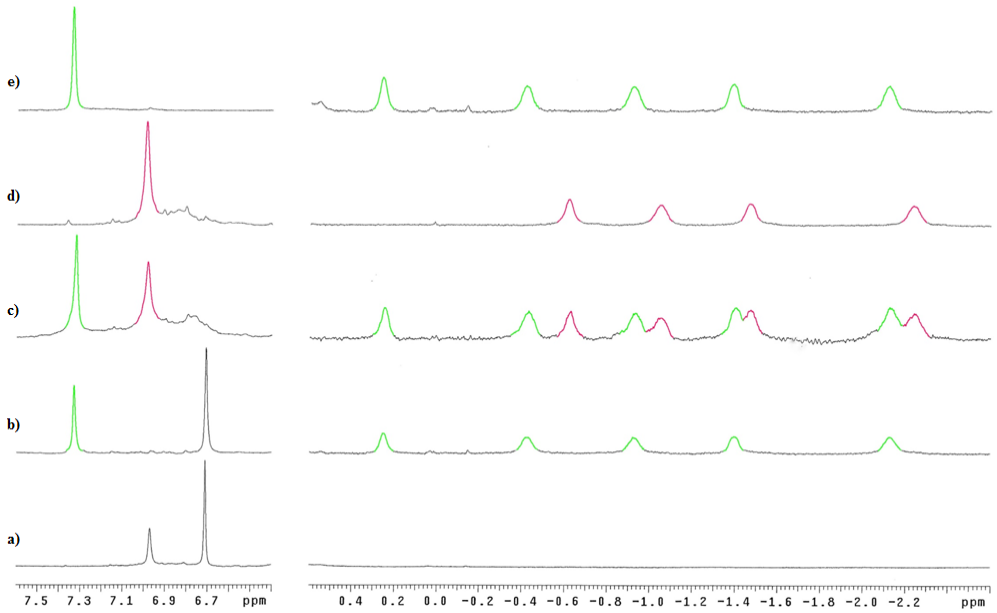

Figure 4.2.6. Selected aromatic and high-field regions of the ^{1}H NMR spectra (D_2O, 500 MHz, 278 K) of: a) [**1**] = 0.4 mM, [**2**] = 0.4 mM; b) [**1**] = 0.4 mM, [**2**] = 0.4 mM, [**$NC_{10}N$**] = 0.2 mM; c) [1] = 0.4 mM, [2] = 0.4 mM, [**$NC_{10}N$**] = 0.2 mM, [**NC_8N**] = 0.2 mM; d) [**1**] = 0.4 mM, [**NC_8N**] = 0.2 mM; e) [**2**] = 0.4 mM, [**$NC_{10}N$**] = 0.2 mM.

Further evidence of the homocapsule formation (**2⊃$NC_{10}N$⊂2**) was yielded by a DOSY NMR spectrum, which showed the five upfield

resonances of the guest having the same diffusion coefficient of the aromatic resonance of calixarene **2**, while the diffusion coefficient of **1** remained unaltered (Figure 4.2.7).

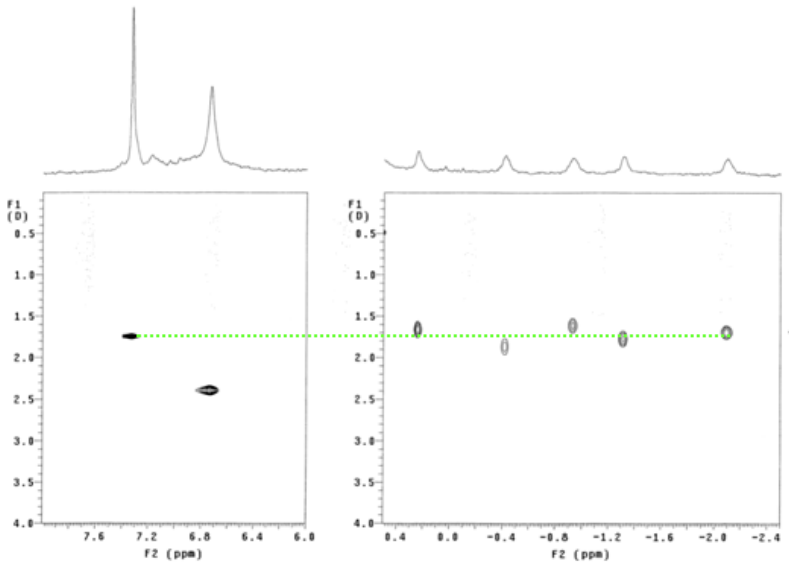

Figure 4.2.7. Sections of the DOSY spectrum (D_2O, 500 MHz, 298 K) of [**1**] = 0.4 mM; [**2**] = 0.4 mM; [**$NC_{10}N$**] = 0.2 mM.

Upon subsequent addition of **NC_8N** to this mixture, the aromatic resonance relative to the free calix[5]arene **1** readily disappeared in favor of a down-field shifted signal, while a new set of signals appeared in the high field region (fuchsia signals), which can be unambiguously ascribed to the **1**⊃**NC_8N**⊂**1** (see traces c and d in figure 4.2.6 for a comparison). Except for the broad signal at $\delta \sim$ 6.7 ppm, which suggests that some aggregation is occurring under these conditions, there isn't any NMR evidence of the presence of the other possible complexes.

According to these results, the four components "socially" combined in a non-integrative fashion to exclusively form the two "homocapsules" **2**⊃**NC$_{10}$N**⊂**2** and **1**⊃**NC$_{8}$N**⊂**1** (Figure 4.2.8).

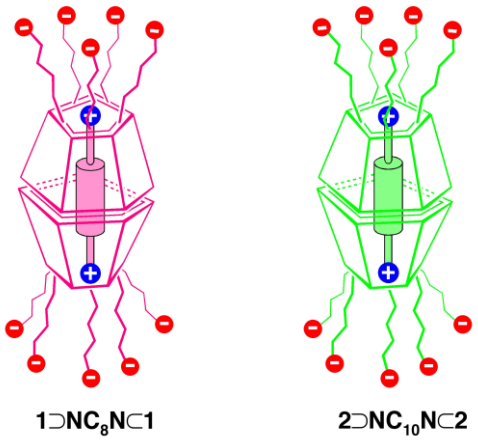

Figure 4.2.8. Cartoons of the two homocapules **1**⊃**NC$_{8}$N**⊂**1** and **2**⊃**NC$_{10}$N**⊂**2** formed in the four-components mixture.

A series of experiments were planned in order to understand if the self-sorting event was under thermodynamic or kinetic control and to evaluate the system response after external stimuli such as temperature, concentration or different stoichiometry of the components.

To this aim, two independent mixtures containing the "non-matching" host/guest pairs (**1**/**NC$_{10}$N** and **2**/**NC$_{8}$N**, 2:1 ratio each, Figure 4.2.9) where prepared to force alternative recognition events.

Upon mixing to the usual final concentration of the components, the best-matching **1**⊃**NC$_{8}$N**⊂**1** and **2**⊃**NC$_{10}$N**⊂**2** capsules were readily

formed and remained stable over the time, thus demonstrating the thermodynamic control of the self-sorting event.

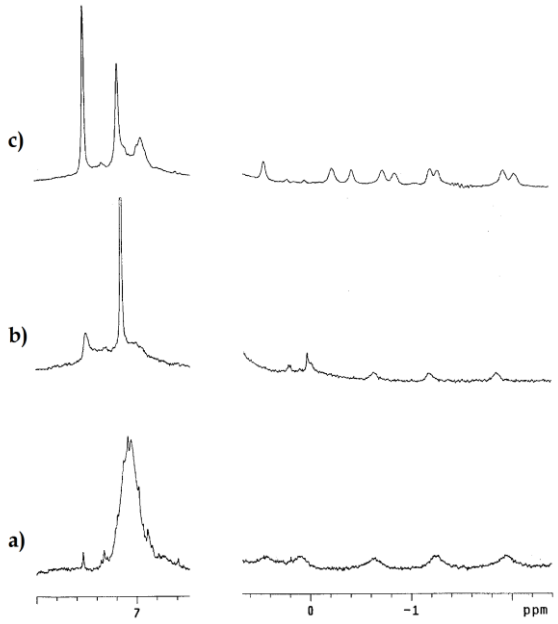

Figure 4.2.9. Selected aromatic and high-field regions of the ^{1}H NMR spectra (D_2O, 500 MHz, 278 K) of: a) [**1**] = 0.4 mM, [**NC$_{10}$N**] = 0.2 mM; b) [**2**] = 0.4 mM, [**NC$_8$N**] = 0.2 mM; c) after mixing a + b.

It is known that many variables can affect molecular recognition, and therefore influence the outcome of the self-sorting event (*i.e.*, temperature, concentration, stoichiometry). Preliminary VT NMR experiments (Figure 4.2.10), recorded with the two independent homocapsules showed that in the case of **1**⊃**NC$_8$N**⊂**1** the ^{1}H NMR resonances of the complex broadened at 298 K and at 328 K no signals relative to the guest included inner the cavity were detected (0 – -3 ppm). Furthermore the aromatic resonances relative to host **1** at 328 K in trace c

of figure 4.2.10 are high-field shifted, thus indicating that a disassembling event is taking place.

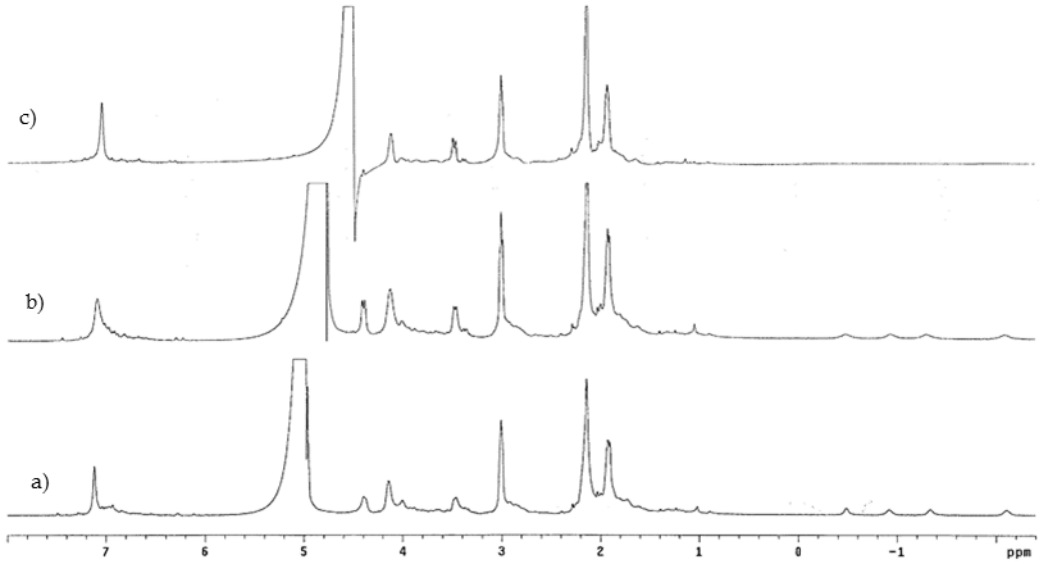

Figure 4.2.10. ^{1}H NMR spectra (D_2O, 500 MHz) of **[1]** = 0.4 mM and **[NC_8N]** = 0.2 mM at a) 278 K; b) 298 K; c) 328 K.

On the contrary, the **2⊃$NC_{10}N$⊂2** capsule was the only species also at higher temperature (353 K) as shown by the unchanged spectral patterns in the ^{1}H NMR spectra carried out at different temperatures (Figure 4.2.11).

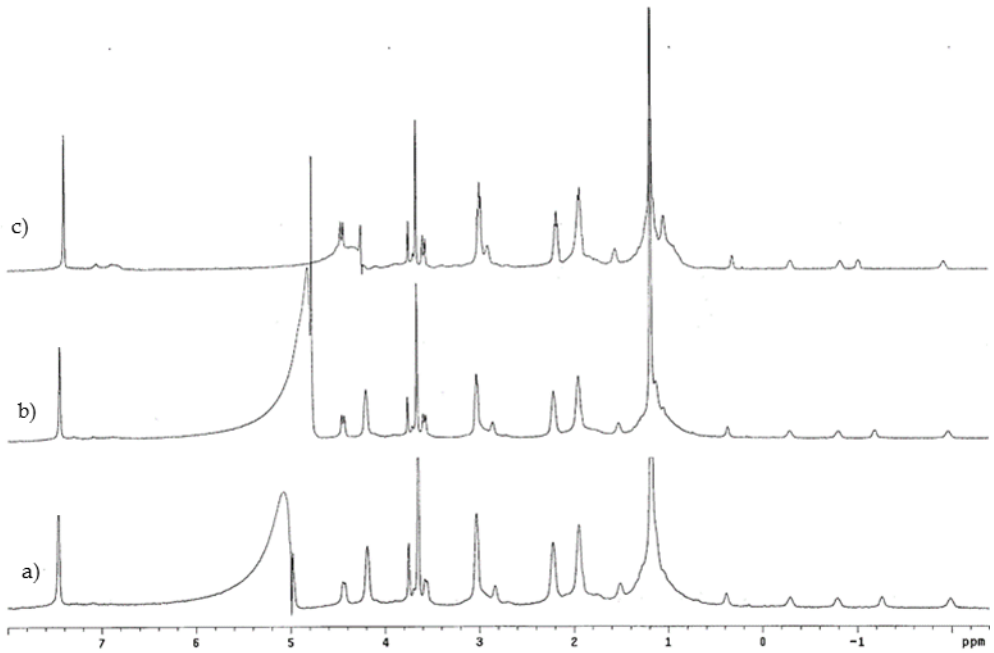

Figure 4.2.11. ^{1}H NMR spectra (D_2O, 500 MHz) of [**2**] = 0.4 mM and [**NC$_{10}$N**] = 0.2 mM at a) 278 K; b) 298 K; c) 353 K.

To our opinion these experiments highlighted the importance of the presence of *tert*-butyl groups at the upper rim of the calix[5]arene derivatives for efficient Van deer Waals interactions to take place with both the *upper*-rim of the facing calixarene and the alkyl chain of the guest.

VT NMR experiments recorded on the four-component mixture evidenced the stability of the **2⊃NC$_{10}$N⊂2** capsule (Figure 4.2.12).

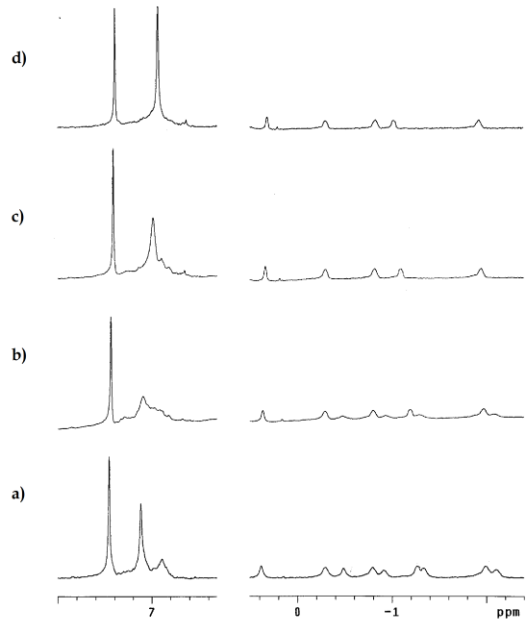

Figure 4.2.12. Selected aromatic and high-field regions of the ^{1}H NMR spectra (D_2O, 500 MHz) of [**1**] = 0.4 mM; [**2**] = 0.4 mM; [$\mathbf{NC_{10}N}$] = 0.2 mM; [$\mathbf{NC_8N}$] = 0.2 mM at a) 278 K; b) 298 K; c) 328 K; d) 353 K.

The stability of the **2**⊃$\mathbf{NC_{10}N}$⊂**2** capsule was further demonstrated by a 5-fold dilution experiment ([**1**] = [**2**] = 0.08 mM, [$\mathbf{NC_8N}$] = [$\mathbf{NC_{10}N}$] = 0.04 mM). As it can be observed in figure 4.2.13, also in these conditions the **2**⊃$\mathbf{NC_{10}N}$⊂**2** complex was quantitatively formed, while upon dilution **1**⊃$\mathbf{NC_8N}$⊂**1** disassemble to afford only 22% of complex.

To verify that the self-sorted capsules were preferred also in the presence of an excess of guests, a 1:1:1:1 mixture was prepared. Unfortunately, at the usual 0.4 mM concentration the excess of guests caused the aggregation of the *p-tert*-butyl derivative **2**. Nonetheless, by diluting all components to 0.1 mM, the high field region of the ^{1}H NMR spectrum showed the same spectral patterns for the included methylenes of $\mathbf{NC_8N}$

and **NC$_{10}$N** in the two usual self-sorted homocapsules, demonstrating that also under these conditions the self-sorting event is taking place (Figure 4.2.14)

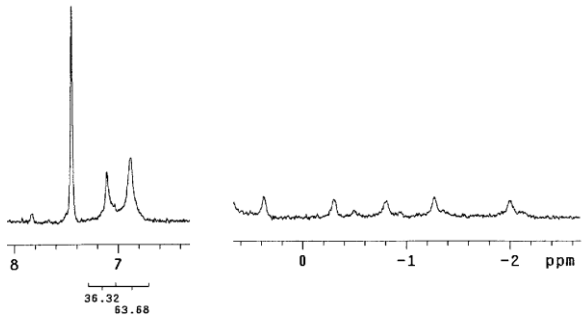

Figure 4.2.13. Selected aromatic and high-field regions of the ^{1}H NMR spectrum (D_2O, 500 MHz, 278 K) of [**1**] = 0.08 mM, [**2**] = 0.08mM; [**NC$_{10}$N**] = 0.04 mM, [**NC$_8$N**] = 0.04 mM.

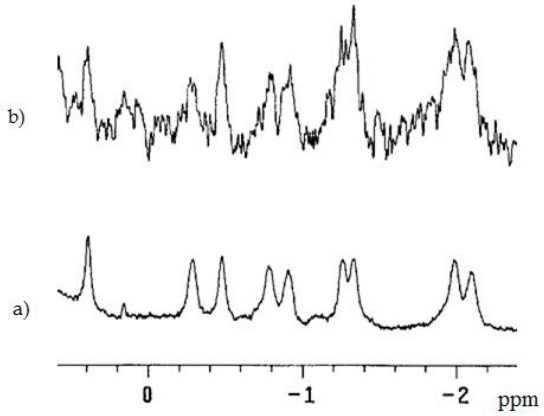

Figure 4.2.14. Selected high-field regions of the ^{1}H NMR spectra (D_2O, 500 MHz, 278 K) of: a) [**1**] = 0.4 mM, [**2**] = 0.4 mM, [**NC$_{10}$N**] = 0.2 mM, [**NC$_8$N**] = 0.2 mM; b) [**1**] = 0.1 mM, [**2**] = 0.1 mM, [**NC$_{10}$N**] = 0.1 mM, [**NC$_8$N**] = 0.1 mM.

Finally, the ^{1}H NMR titration experiment was repeated by changing the order in the addition of the guests. After adding the shorter **NC$_8$N** first

([**1**] = [**2**]=0.4 mM, [**NC$_8$N**]=0.2 mM), instead of the expected **1**⊃**NC$_8$N**⊂**1** capsule, four distinct signals were observed for the aromatic resonances together with a predominant set (up to six signals) of included methylenes in the high field region (see Figure 4.2.15b), which could not be ascribable neither to **1**⊃**NC$_8$N**⊂**1** capsule (which formed in a very small amount) nor to **2**⊃**NC$_8$N** 1:1 complex. A closer look at the aromatic region of the spectrum (figure 4.2.15b) showed the doubling of the aromatic resonances, two of which underwent, with respect to the chemical shifts of free hosts, a downfield shift similar to those observed in the individual titration experiments.

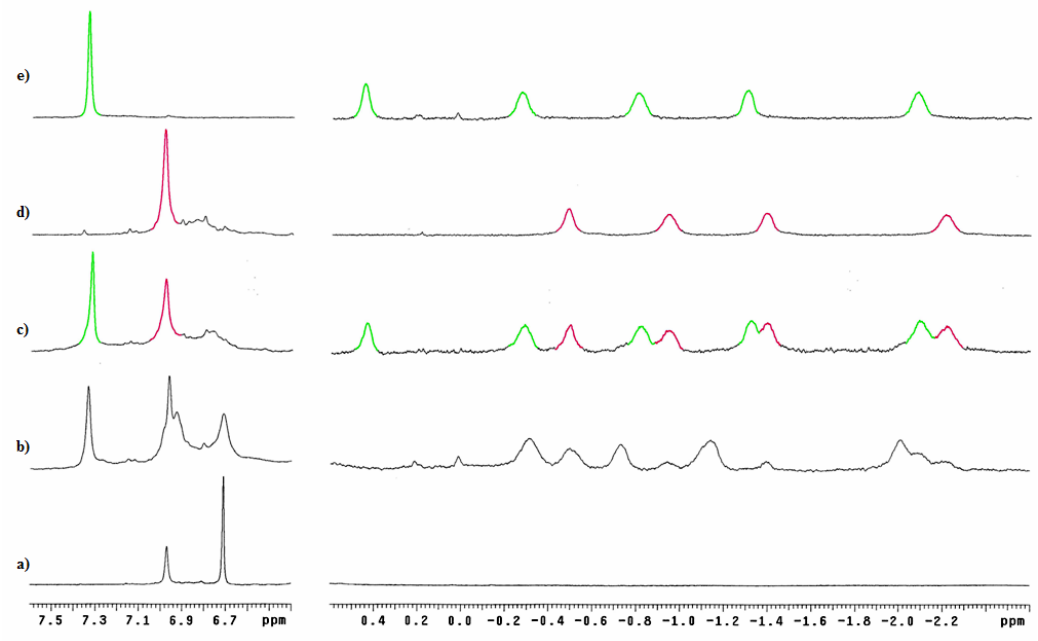

Figure 4.2.15. Selected aromatic and high-field regions of the ^{1}H NMR spectra (D_2O, 500 MHz, 278 K) of: a) [**1**] = 0.4 mM, [**2**] = 0.4 mM; b) [**1**] = 0.4 mM, [**2**] = 0.4 mM, [**NC$_8$N**] = 0.2 mM; c) [**1**] = 0.4 mM, [**2**] = 0.4 mM, [**NC$_8$N**] = 0.2 mM; [**NC$_{10}$N**] = 0.2 mM; d) [1] = 0.4 mM, [**NC$_8$N**] = 0.2 mM, e) [**2**] = 0.4 mM, [**NC$_{10}$N**] = 0.2 mM.

Integration of aromatic resonances demonstrated that half quantity of each host was involved in the complexation of the guest, and careful integration of the included methylenes of the guest suggested that under this condition the guest molecule was asymmetrically high-field shifted by the inclusion into the two different calixarene cups. This complex was also found to be stable over months at room temperature. Further addition of **$NC_{10}N$** restored the precedent homocapsules equilibrium (**1**⊃**NC_8N**⊂**1** and **2**⊃**$NC_{10}N$**⊂**2**, Figure 4.2.15c).

These experimental data demonstrated that in this three-component mixture, hosts **1** and **2**, and **NC_8N** socially combine in an integrative fashion leading to the heterocapsule **1**⊃**NC_8N**⊂**2**. In our four-component mixture the integrative/non-integrative self-sorting can be achieved by simply changing the order of addition of the α,ω-alkanediyldiammonium ions to the solution of the hosts.

Upon heating the **1/2/NC_8N (**2:2:1) mixture (Figure 4.2.16), the aromatic resonances relative to host **1** immediately merged and subsequently sharpened at 353 K, indicating a fast exchange on the NMR time scale between the free and complexed forms of calixarene **1**, even at 298K. On the contrary, resonances corresponding to free and complexed calixarene **2**, although of different intensities, remained well separated, thus showing a slower exchanging rate also at 353 K. Concurrently, the high-field ^{1}H NMR region showed an initial broadening of the resonances of the **NC_8N** portion included in the *p*-methylcalixarene **1**, which eventually disappeared.

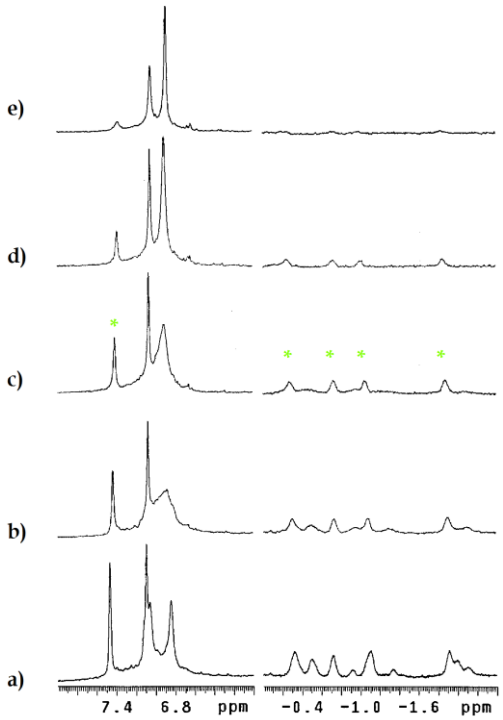

Figure 4.2.16. Selected aromatic and high-field regions of the ^{1}H NMR spectra (D_2O, 500 MHz) of [**1**] = 0.4 mM, [**2**] = 0.4 mM, [**NC$_8$N**] = 0.2 mM at a) 278 K; b) 298 K; c) 328 K; d) 338 K ; e) 353K. Green asterisks indicate the **NC$_8$N** portion included inside **2**.

Integration of the included guest portion *vs.* the aromatic signals of complexed derivative **2** in trace c of Figure 4.2.16, displayed a 8:10 relation, while the relative integration of the four included resonances showed a 1:1:1:1 ratio (asterisks in figure 4.2.16, trace c). The possibility of formation of the 1:1 **2**⊃**NC$_8$N** complex at 328 K was ruled out by a parallel VT NMR experiment on the **2**/**NC$_8$N** system. It comes out that the residual resonances for complexed species in figure 4.2.16, traces c–e, can be assigned to the **2**/**NC$_8$N** portion of the heterocapsule. The VT NMR experiment of the **1**⊃**NC$_8$N**⊂**2** complex highlighted the different exchange kinetics of the two hosts[11] towards the alkylammonium moiety

and once again confirmed the relevance of *tert*-butyl groups of **2** in determining effective attractive van deer Waals interactions both with the other calixarene cup and with the guest alkyl chain.

4.3 Conclusions

In this chapter I have reported a brief introduction about the self-sorting phenomena and then our experimental results on a four component system consisting of two water-soluble calix[5]arene derivatives differently substituted at the upper rim (**1** and **2**) and two α,ω–alkanediyldiammonium ions of different lengths (H_3N^+-$(CH_2)_n$-NH_3^+, n = 8, 10, **NC_8N** and **$NC_{10}N$**). The obtained results demonstrated that among the ten possible complexes with mixed/different stoichiometry, only the **1⊃NC_8N⊂1** and **2⊃$NC_{10}N$⊂2** capsules are formed, providing a fascinating example of social (non integrative) self-sorting based on water-soluble supramolecular systems. Furthermore, in this system the switching between an integrative and a non-integrative social self-sorting can be achieved by changing the order of addition of the guests to an equimolar solution of the hosts.

4.4 Experimetal section

Calixarenes **1** and **2** were synthesized as already described in chapter 2. ^{1}H NMR spectra were recorded in D_2O at 500 MHz using a Varian 500 MHz spectrometer equipped with a pulse-field gradient probe. The Dioxane solvent peak ($\delta_H = 3.53$ ppm) was used as an internal standard for ^{1}H NMR spectra.

Diffusion Ordered NMR Spectroscopy (DOSY) studies were performed at 298 K using a DONESHOT pulse sequence. Experimental parameters were optimized according to the sample under investigation. Diffusion gradients were incremented in 30 steps with gradient pulse amplitudes varying from 1.8 to 58.5 gauss/cm, the number of transients acquired for each increment ranging from 16 to 128, with a diffusion gradient length of 2 ms and diffusion delays in the 150–200 ms range.

References

[1] (a) Saha M.L., Schmittel M., *Org. Biomol. Chem.,* 2**012**, 10, 4651; (b) Safont-Sempere M.M., Gustavo Fernández, Würthner F., *Chem. Rev.,* **2011**, 111, 5784.

[2] (a) Wu A., Isaacs L., *J. Am. Chem. Soc.,* **2003**, 125, 4831; (b) Mukhopadhyay P., Wu A., Isaacs L., *J. Org. Chem.,* **2004**, 69, 6157.

[3] Krämer R., Lehn J.M., Marquis-Rigault A., *Proc. Natl. Acad.Sci. U. S. A.,* **1993**, 90, 5394.

[4] (a) Jiang W., Schalley C.A., *Proc. Natl. Acad. Sci. U. S. A.,* **2009**, 106, 10425; (b) Jiang W., Winkler H.D.F., Schalley C.A., *J. Am. Chem. Soc.,* **2008**, 130, 13852.

[5] Voet D., Voet J.G., *Biochemistry*, **1995**.

[6] Watson J.D., Crick F.H., *Nature*, **1953**, 171, 737.

[7] (a) Jolliffe K.A., Timmerman P., Reinhoudt D.N., *Angew. Chem., Int. Ed.*, **1999**, 38, 933; (b) Ma Y.G, Kolotuchin S.V., Zimmerman S.C., *J. Am. Chem. Soc.,* **2002**, 124, 13757.

[8] (a) Caulder D.L., Raymond K.N., *Angew. Chem., Int. Ed.*, **1997**, 36, 1440; (b) Nitschke J.R., *Acc. Chem. Res.*, **2006**, 40, 103.

[9] Shaller A.D., Wang W., Gan H.Y., Li A.D.Q., *Angew. Chem., Int. Ed.,* **2008**, 47, 7705.

[10] (a) Braekers D., Peters C., Bogdan A., Rudzevich Y., Böhmer V., Desreux J.F., *J. Org. Chem.,* **2008**, 73, 701; (b) Rudzevich Y., Rudzevich V., Klautzsch F., Schalley C.A., Böhmer V., *Angew. Chem., Int. Ed.*, **2009**, 48, 3867; (c) Rudzevich Y., Rudzevich V., Böhmer V., *Chem. Eur. J.*, **2010**, 16, 4541; (d) Mogck O., Paulus E.F., Böhmer V., Thondorf I., Vogt W., *Chem. Commun.*, **1996**, 2533.

[11] Talotte C., Gaeta C., Qi Z., Schalley C.A., Neri P., *Angew. Chem. Int. Ed.,* **2013**, 52, 7437.

[12] (a) Garozzo D., Gattuso G., Kohnke F.H., Malvagna P., Notti A., Occhipinti S., Pappalardo S., Parisi M.F., Pisagatti I., *Tetrahedron Lett.,* **2002**, 43, 7663; (b) Gargiulli C., Gattuso G., Notti A., Pappalardo S., Parisi M.F., *Tetrahedron Lett.*, **2011**, 52, 7116.

[13] (a) Pappalardo S., Villari V., Slovak S., Cohen Y., Gattuso G., Notti A., Pappalardo A., Pisagatti I., Parisi M.F., *Chem. Eur. J.,* **2007**, 13, 8164; (b) Gattuso G., Notti A., Pappalardo A., Parisi M.F., Pisagatti I., Pappalardo S., Garozzo D., Messina A., Cohen Y., Slovak S., *J. Org. Chem.,* **2008**, 73, 7280; (c) Capici C., Cohen Y., D'Urso A., Gattuso G., Notti A., Pappalardo A., Pappalardo S., Parisi M.F., Purrello R., Slovak S., Villari V.,

Angew. Chem., Int. Ed., **2011**, 50, 11956; (d) Garozzo D., Gattuso G., Notti A., Pappalardo A., Pappalardo S., Parisi M.F., Perez M., Pisagatti I., *Angew. Chem., Int. Ed.,* **2005**, 44, 4892; (e) Gargiulli C., Gattuso G., Liotta C., Notti A., Parisi M.F., Pisagatti I., Pappalardo S., *J. Org. Chem.,* **2009**, 74, 4350; (f) Capici C., De Zorzi R., Gargiulli C., Gattuso G., Geremia S., Notti A., Pappalardo S., Parisi M.F., Puntoriero F., *Tetrahedron,* **2010**, 66, 4987.

[14] (a) Gattuso G., Notti A., Pappalardo A., Pappalardo S., Parisi M.F., Puntoriero F., *Tetrahedron Lett.*, **2013**, 54, 188; (b) Barbera L., Gattuso G., Kohnke F.H., Notti A., Pappalardo S., Parisi M.F., Pisagatti I., Patanè S., Norberto M., Villari V., *Org. Biomol. Chem.*, **2015**,13, 6468.

[15] Waldeck A.R., Kuchel P.W., Lennon A.J., Chapman B.E., *Prog. Nucl. Magn. Reson. Spectrosc.,* **1997**, 30, 39.

Chapter 5

Drug carriers based on a water soluble pillar[5]arene

5.1. Introduction: synthesis and properties of pillar[n]arenes

In 2008 Tomoki Ogoshi *et al*.[1] while they were planning to synthesize a polymer by condensation of 1,4-dimethoxybenzene and paraformaldehyde, discovered new pillar-shaped macrocycles hosts named "pillar[*n*]arenes", where *n* is the number of aromatic units. These macrocycles contain hydroquinone units linked by methylene bridges at the para positions. Although the composition of pillararenes is similar to that of calixarenes, they have different structural characteristics (Figure 5.1.1). Historically, reaction of phenolic derivatives with aldehydes has afforded various macrocyclic compounds.[2] However, to obtain phenolic macrocyclic compounds, there are two key factors. One is controlling the reaction point of phenolic derivatives to inhibit the formation of three-dimensional network polymers. The other is the inhibition of the linear polymer formation and acceleration of macrocyclization.

Today, 9 years after Ogoshi initial report, pillar[*n*]arenes are recognized as key players in supramolecular chemistry; in fact the symmetrical pillar architecture and the electron-donating cavities of these macrocycles are particularly intriguing and confer them some special and interesting physical, chemical, and host-guest properties.

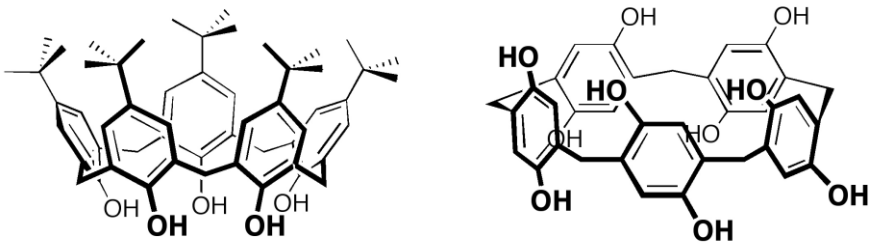

p-tert-Butylcalix[5]arene Pillar[5]arene

Figure 5.1.1. Pillararenes *vs.* Calixarenes.

The first synthesis of pillar[5]arene **1**, reported in 2008[1] is a condensation of 1,4-dimethoxybenzene with paraformaldehyde and an appropriate Lewis acid as a catalyst, therefore the symmetrical 1,4-dimethoxypillar[5]arene (DMpillar[5]arene) **2**, was selectively obtained (Scheme 5.1.1).

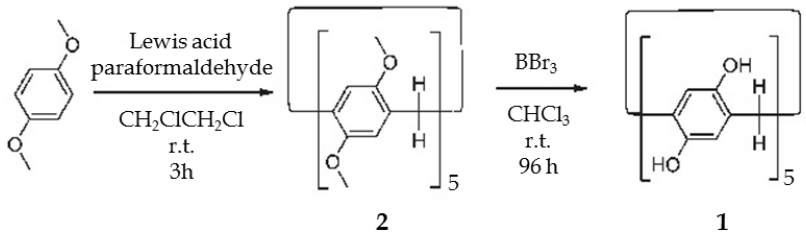

Scheme 5.1.1. Synthesis of DMpillar[5]arene (**2**) and Pillar[5]arene (**1**).

Various Lewis acids were used for this reaction, and with $BF_3 \cdot O(C_2H_5)_2$, the cyclic pentamer was selectively obtained in 22% yield. Then pillar[5]arene **1**, was obtained by deprotection of the methoxy groups of DMpillar[5]arene with a yield of 30%.[1]

Subsequently, many authors changed the first synthetic procedure to improve the yield of the cyclization reaction, decrease the reaction time

and obtain pillararenes with a different size of the cavity (*e.g.* pillar[6]arenes).[3] More recently different synthetic methodologies were developed in order to obtain mono- di- tetra- and per-functionalized pillar[*n*]arenes.[4]

Pillararenes have the following characteristics: (i) despite of their simple structures, pillararenes show outstanding host–guest properties and planar chirality (Figure 5.1.2);[5] (ii) viewed from the side, they have very symmetrical pillar-shaped architectures (Figure 5.1.3).

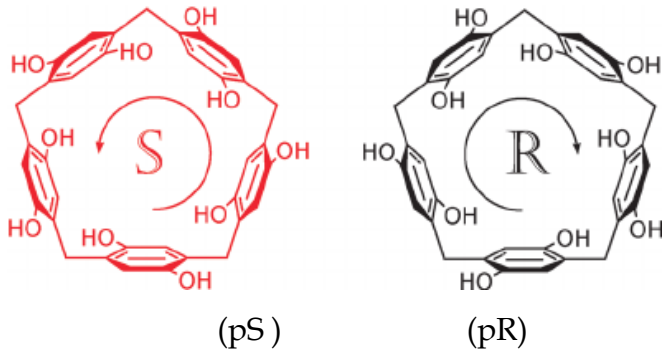

(pS) (pR)

Figure 5.1.2. Planar chiral of pillar[5]arenes: Sp (left) and Rp (right).

From the top, pillar[5]arenes and pillar[6]arenes display regular cyclic pentagonal and hexagonal structures, respectively. In terms of cavity size, pillar[5]arene (approximately 5.5 Å) is almost analogous to □-cyclodextrin (approximately 4.7 Å) and cucurbit[6]uril (approximately 5.8 Å). α-Cyclodextrin and cucurbit[6]uril bind linear alkanes and simple aromatic compounds.[6] These guests will also fit in the cavities of pillar[5]arenes. Pillar[5]arenes form complexes with linear alkanes containing electron-poor systems such as amine, ammonium, cyano, and

halogen groups, as well as simple aromatic compounds such as pyridinium and viologen derivatives.

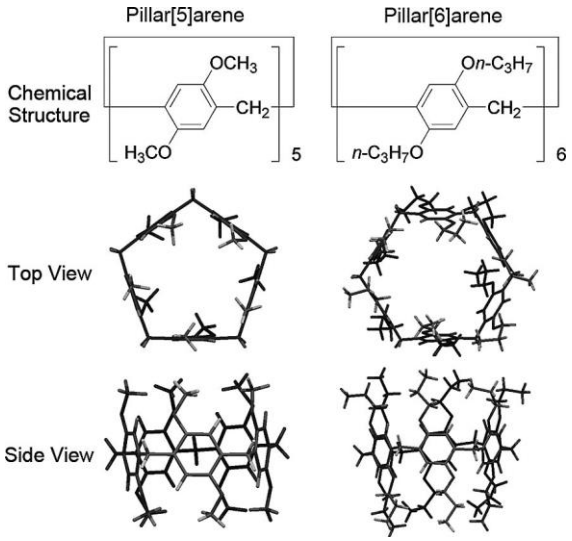

Figure 5.1.3. Chemical and X-ray crystal structures of permethylated pillar[5]arene and perpropylated pillar[6]arene. (Adapted from Ref. 4f).

(iii) Ease of functionalization at both rims by various synthetic approaches, which allows the construction of a variety of pillararene-based supramolecular assemblies.

Due to their high solubility in a large variety of solvents, low toxicity and specific recognition towards many model substrates, pillar[*n*]arenes have been widely used for the development of various interesting supramolecular systems, including nanomaterials,[7] chemosensors,[8] transmembrane channels,[9] and supramolecular polymers.[10]

5.1.1. Water soluble Pillar[5]arenes

Pillar[*n*]arenes are inherently water insoluble but, suitable functionalization at the rims furnished anionic[11] cationic[12] and neutral[13] water-soluble pillar[*n*]arenes. The first water-soluble pillar[5]arene was synthesized in 2010 (Figure 5.1.1.1) by the introduction of carboxylate anions at both upper and lower rims; this derivative was able to bind cationic viologen salt in water;[11a] the second one, a pillar[5]arene decaamine, was synthesized in 2011 and revealed to encapsulate linear diacids in neutral, alkaline and acidic conditions (Figure 5.1.1.2).[13a]

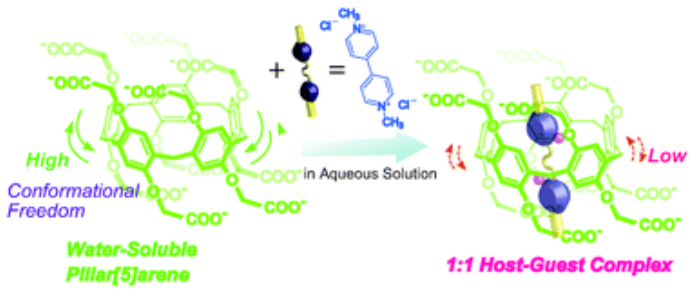

Figure 5.1.1.1. The first water-soluble pillar[5]arene. (Adapted from Ref. 11a).

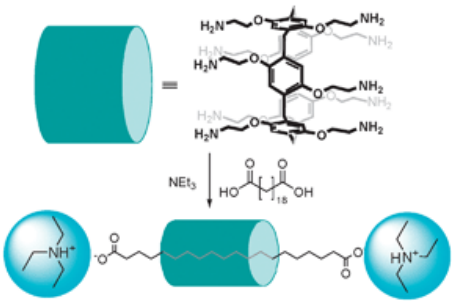

Figure 5.1.1.2. Pillar[5]arene decamine. (Adapted from Ref. 13a).

Subsequently, Huang *et al*. reported the synthesis of a cationic water-soluble pillar[5]arene prepared by the introduction of trimethylammonium groups at both upper and lower rims which forms a stable 1 : 1 host–guest complex with sodium 1-octanesulfonate in water (Figure 5.1.1.3).[12a]

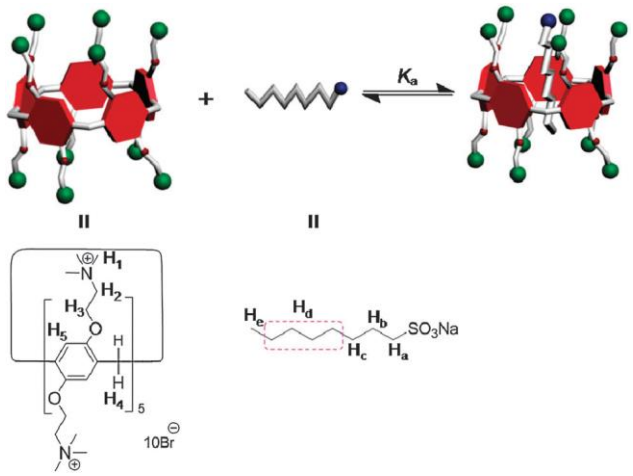

Figure 5.1.1.3. A cationic water-soluble pillar[5]arene. (Adapted from Ref. 12a).

Among various derivatives, carboxylatopillar[*n*]arenes (*n* = 5–10, **WP**) **WP5** and **WP6** (*n* = 5, 6) represent a class of water soluble pillar[*n*]arene derivatives which have gained great popularity in the last years, comparable to that of *p*-sulfonatocalix[*n*]arenes.[14]

Carboxylatopillar[*n*]arenes have a π-electron rich hydrophobic cavity and anionic carboxylate groups at the portals useful for molecular recognition of cationic guests. Hydrophobic analytes of appropriate sizes can accommodate inside the cavity of **WP** with the cationic end projecting outside for favourable electrostatic interactions with the anionic groups (Figure 5.1.1.4). As a result, carboxylatopillar[*n*]arenes

are ideal candidates for host-guest binding with cationic guests, and find application in fabricating responsive supramolecular systems for trapping and releasing cargo molecules.[15]

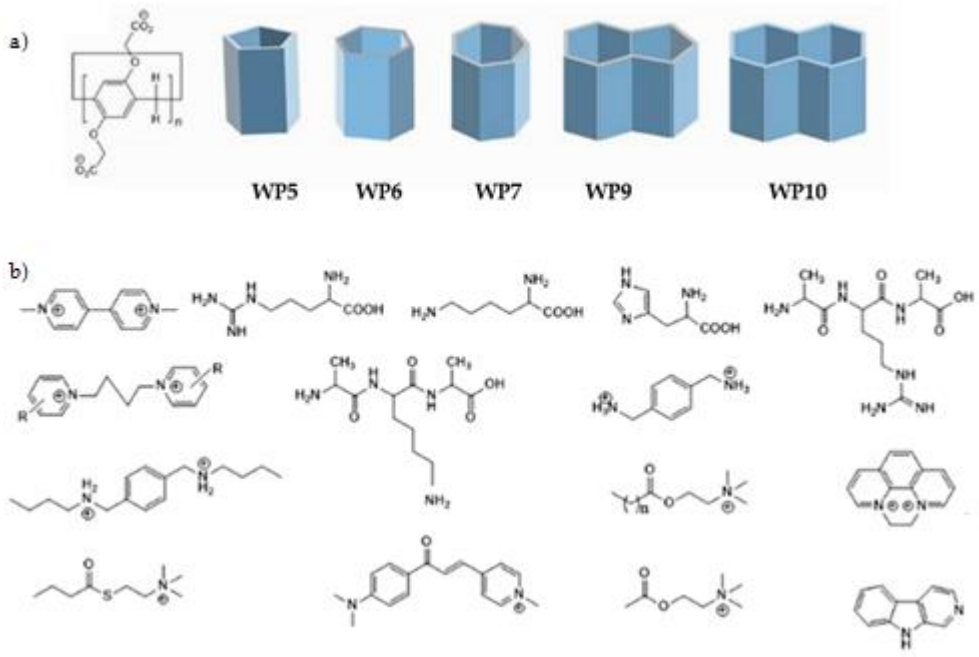

Figure 5.1.1.4. a) Molecular structure and cartoon representations of carboxylate-pillar[*n*]arene scaffolds; b) Molecular structures of guests used for binding inside the cavity of carboxylatopillar[*n*]arene. (Adapted from Ref. 15).

Water-soluble pillararenes have gained much attention as essential building blocks in the preparation of drug delivery systems.[16]

Xue *et al*.[17] reported that **WP5** can complex neutral guest such as spermine and its analogues with extremely high association constants. Huang *et al*.[18] reported on the water-soluble pillar[6]arene (**WP6**) used as a solubilising agent to enhance the solubility and bioactivity of poorly water-soluble anticancer drug tamoxifen by host–guest complexation. Another simple guest-loading system, relying solely on the cavity of

WP5, has been shown to act as a supramolecular container capable of directly encapsulate a bioactive molecule and its reversible binding and release has been controlled by pH variations.[19]

Considering that the microenvironment of an infection site is acidic because of, for instance, lactic acid accumulation,[20] we thought that pH responsive **WP5** could act as a simple drug delivery system for antibiotic drugs. Because of the good biocompatibility and low toxicity of carboxylate substituted water-soluble pillar[*n*]arene derivatives[21] and its known proclivity to bind alkylammonium guest,[22] we decided to test the affinity of **WP5** towards the drug Amikacin (**3**).

The next section will describe a potential pillararene based drug-transport system where **WP5** and the antibiotic drug amikacin interact with each other forming a stable inclusion complex in aqueous solution. Moreover, the *in vitro* delivery of amikacin by the cavity of **WP5** was achieved in a preliminary microbiological screening with a representative Gram-positive bacterial strain (*i.e.*, *Staphylococcus aureus ATCC 29213*), making this host-guest system a very promising candidate for pharmaceutical applications. In addition, preliminary host-guest interactions between **WP5** and levofloxacin (**4**), a hydrophilic broad spectrum antibiotic, were investigated by means of ^{1}H NMR in order to validate the general applicability of **WP5** as a carrier for drugs of different structures. Finally, **WP5** was employed for the preparation of layer-by-layer (LbL) thin solid films on glass surfaces loaded with the above mentioned antibiotics, with the ultimate goal of fabricating antibacterial multilayered coatings for controlled drug release.

5.2. Results and discussion

5.2.1. WP5 and Amikacin†

Amikacin is a semisynthetic antibiotic known for its activity against both Gram-positive and Gram-negative bacteria and is commonly used for a number of bacterial infections, including joint infections, intra-abdominal infections, meningitis, pneumonia, sepsis, and urinary tract infections and it is also used for the treatment of multidrug-resistant tuberculosis.[23] It needs, however, to be administered in high concentrations in order to reach the appropriate therapeutic level. Because of this high dosage Amikacin may cause serious nephrotoxicity and ototoxicity side effects.[24]

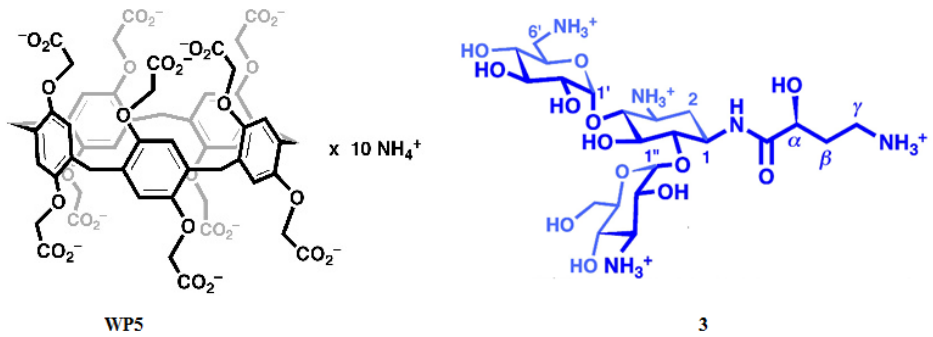

Figure 5.2.1.1. Chemical structure of carboxylatopillar[5]arene **WP5** and the drug Amikacin (**3**).

The molecular structure of this drug, possessing an α-hydroxy-γ-ammoniumbutyryl side-chain makes amikacin a good candidate for the inclusion inside the cavity of **WP5**. In addition, because of the charge

† *The experimental results reported in this section (relative to* ***WP5*** *and Amikacin) have been already published: L. Barbera et al., Org. Biomol. Chem.,* **2017**, 15, 3192.

complementarity between anionic **WP5** and cationic **3**, a combination of non-covalent interactions (electrostatic, CH-π, cation-π) was expected to synergically contribute to the pillararene-amikacin recognition process. The affinity between the two was preliminarily tested by ^{1}H NMR spectroscopy, by adding increasing amounts of **3** (0.5, 1.0 and 2.0 equiv.) to a 4.0 mM D_2O solution of **WP5**, to assess whether host-guest binding took place at all and whether this occurred in a fast or slow regime on the NMR time scale (Figure 5.2.1.2).

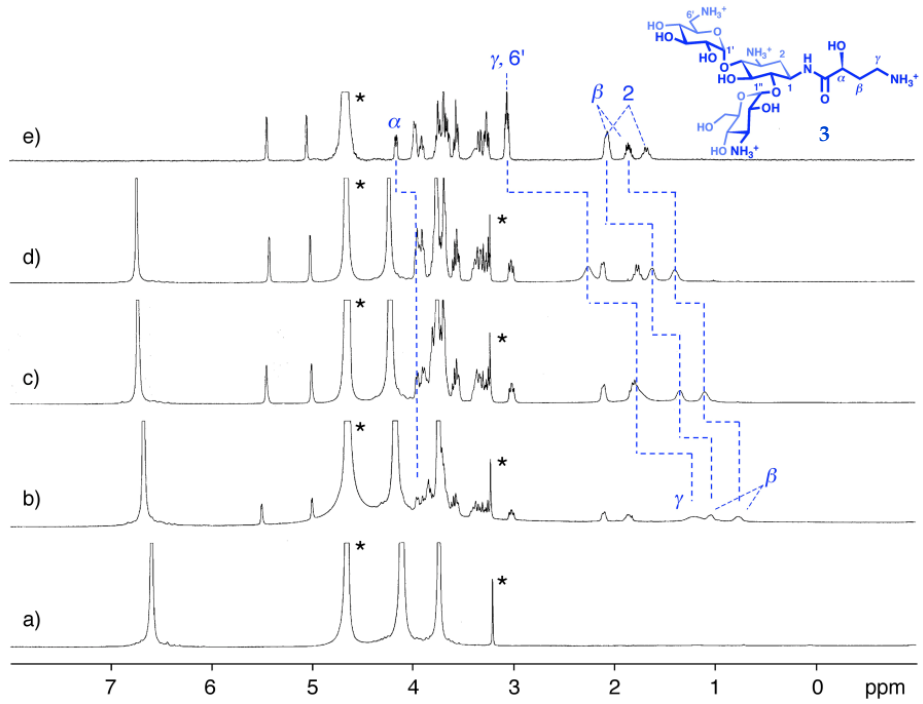

Figure 5.2.1.2 ^{1}H NMR spectra (500 MHz, D_2O, 298 K) of: a) [**WP5**] = 4.0 mM; b) [**WP5**] = 4.0 mM and [**3**] = 2.0 mM; c) [**WP5**] = [**3**] = 4.0 mM; d) [**WP5**] = 4.0 mM and [**3**] = 8.0; and e) [**3**] = 4.0 mM solutions. Asterisks indicate residual solvent peaks (HDO and CH_3OH).

Upon complexation, the hydrogen atoms of this side-chain underwent substantial upfield shifts ($\Delta\delta$= –1.85, –0.81/–0.88 and –0.23 ppm for the *γ*–*β*– and *α*-hydrogen atoms, respectively, for **WP5**:**3** = 2:1; see trace b in

Figure 5.2.1.2). The extent of these complexation-induced shifts progressively decreased as the titration went on (Figure 5.2.1.2, traces c and d). These results are in agreement with the formation of an inclusion complex undergoing fast association/dissociation, in which the α–hydroxy-γ-ammoniumbutyryl side-chain of the guest is located within the magnetic shielding region of the host cavity.

Peaks' assignments for the included alkylammonium moiety came from a COSY NMR spectrum (Figure 5.2.1.3.).

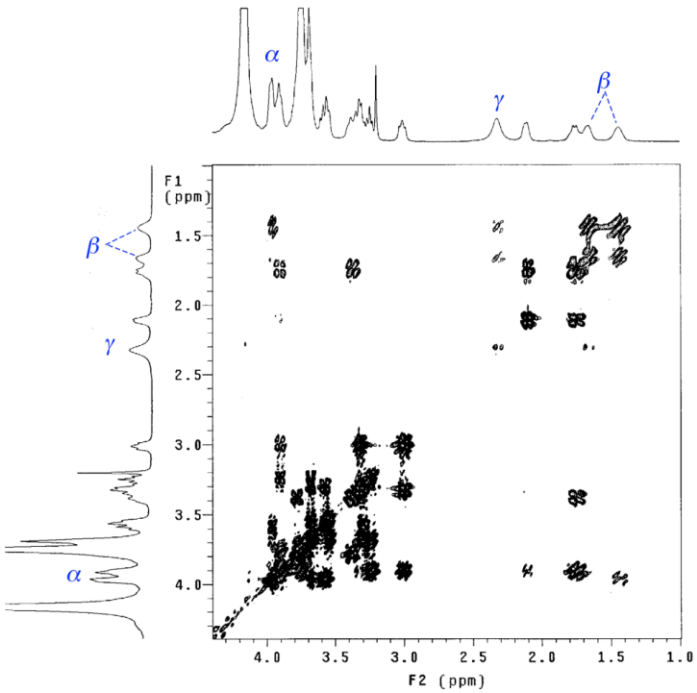

Figure 5.2.1.3. Section of the COSY spectrum (500 MHz, 298 K, D_2O) of a solution of **WP5** and **3** (15.0 mM each).

The host-guest interaction was additionally confirmed by less pronounced downfield shifts observed on specific **WP5** resonances (*e.g.*, ArH range from δ6.52 ppm to δ6.68).

2D NOESY experiment (Figure 5.2.1.4), carried out on a 2:3 host to guest solution, further confirmed the inclusion of amikacin on the basis of several intermolecular correlation peaks observed between the Ar-H and OCH_2 moieties of **WP5** and the anomeric hydrogen atoms 1' and 1" as well as the α–, β– and γ–hydrogen atoms of **3** (dashed circles in Figure 5.2.1.4).

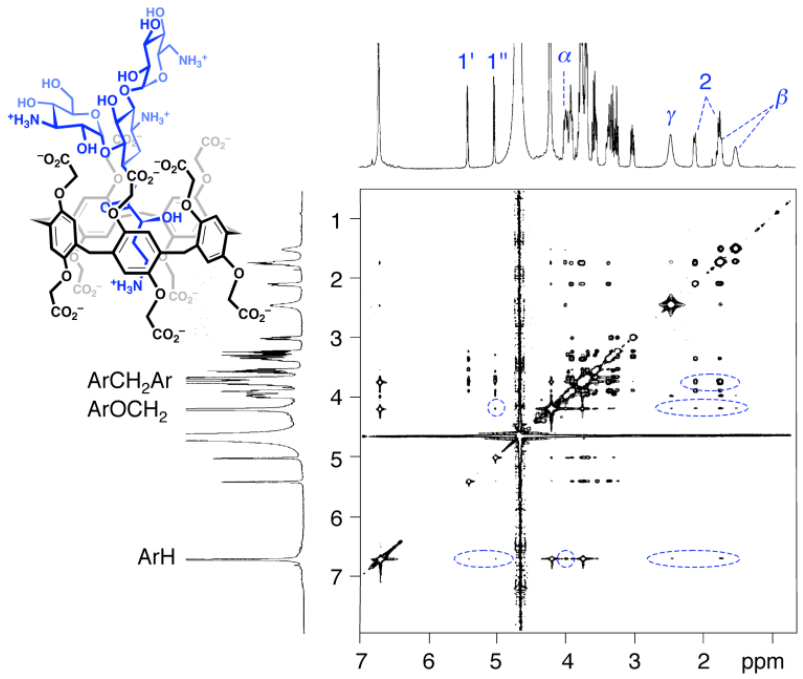

Figure 5.2.1.4. 2D NOESY spectrum (500 MHz, D_2O, 298 K) of a [**WP5**] = 15.0 mM and [**3**] = 22.5 mM solution.

Additional NOE interactions between the oxymethylene groups of **WP5** and the axial and equatorial hydrogen atoms linked to the C2 of the amikacin cyclohexyl ring were also clearly observed. According to these findings, the cooperativity of electrostatic, cation-π and CH-π interactions plays a key role in the recognition/binding process between **WP5** and **3.**

Fluorescence titration experiments were carried out in order to determine the association constant (K_{ass}) in aqueous solution. The emission spectra were recorded by adding increasing amount of amikacin to a 1.10×10^{-5} M aqueous solution of **WP5** (λ_{exc} = 280 nm). Luminescence data interpolation was carried out assuming a 1:1 complexation model. The association constant was derived from the non-linear curve-fitting[25] of the emission intensity changes of **WP5** (λ = 327 nm) upon addition of **3.** The strong value $K_{ass} = (8.48 \pm 0.17) \times 10^4$ M^{-1} confirmed the high affinity among the two (Figure 5.2.1.5.).

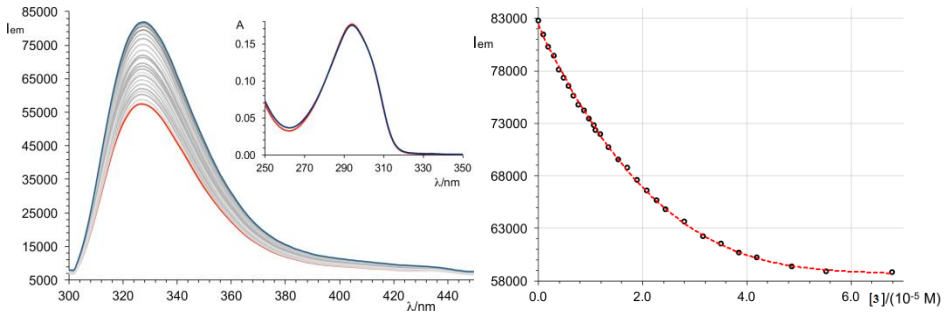

Figure 5.2.1.5. (left) Emission titration spectra (λ_{exc} = 280 nm) of **WP5** (1.10×10^{-5} M) upon addition of increasing amounts of **3** (in aqueous solution at room temperature). The inset shows the absorption spectra of **WP5** in the absence of **3** (blue curve) and at the end of titration (red curve); (right) Emission intensity changes of **WP5** (λ= 327 nm) upon addition of **3**. The dashed red line was obtained from a non-linear curve-fitting.

With a view to subsequent *in vitro/in vivo* studies and given the deleterious effect played by high salt concentrations on the association constant of a given host/guest pair (especially when electrostatic interactions are likely to be involved in the recognition process) the efficiency of the **WP5**/amikacin binding was also examined in deuterium oxide phosphate buffered solutions (PBS, 50 mM at pH 7.2), with the aim of mimicking physiological conditions more closely.

First of all, the 1:1 stoichiometry of the **WP5**-amikacin inclusion complex in a PBS was confirmed by Job's plot analysis (Figure 5.2.1.6). To this end, samples were prepared by mixing aliquots of host (2 mM) and guest (2 mM) solution in phosphate buffer (Na_2HPO_4/NaH_2PO_4 50 mM in D_2O, pH 7.2) in such a way the total concentration was kept constant ([H] + [G] = 2 mM) whereas the molar fraction of the host (χ_{WP5}) in the resulting solutions increased from 0.0 to 1.0.

NMR titration studies were therefore carried out at a fixed **WP5** concentration (1 mM) and samples were routinely prepared by dissolving solid **WP5** in a D_2O phosphate buffer solution (Na_2HPO_4/NaH_2PO_4 50 mM, pH 7.2). A stock solution of amikacin ([**3**] = 10 mM) was, in turn, prepared by using the above-mentioned 1 mM **WP5** buffered solution as a convenient solvent so as, during the titration, the host concentration did not vary upon addition of increasing aliquots of the guest. ^1H NMR titration experiments carried out in neat D_2O and in the buffer solution revealed very similar spectral patterns, thus confirming the ability of **WP5** to efficiently host the amikacin ammonium butyryl moiety within its cavity, even in a highly competitive medium

(Figure 5.2.1.7). The association constant was calculated to be (9.9 ± 1.28) × 10^3 M^{-1} by a nonlinear regression method using the WinEQNMR.[26]

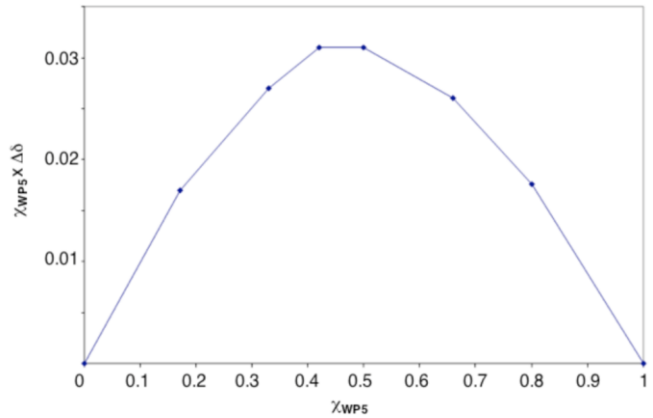

Figure 5.2.1.6. Job plot of the pillararene-amikacin host-guest complex showing the 1:1 stoichiometry between **WP5** and **3**. Complexation induced shifts ($\Delta\delta$) of the **WP5** ArH resonances are plotted against the molar fraction of **WP5**.

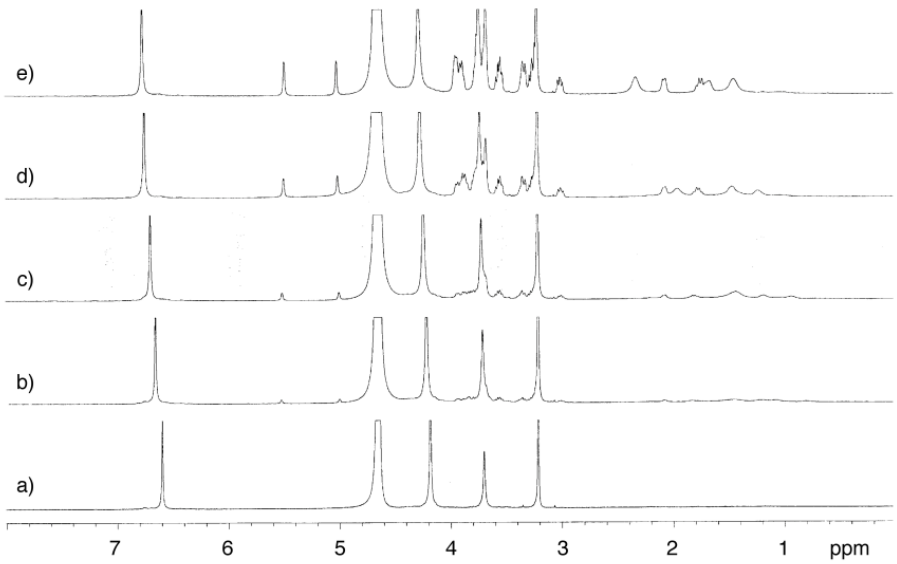

Figure 5.2.1.7. ^{1}H NMR spectra (500 MHz, 298 K, D_2O Na_2HPO_4/NaH_2PO_4 50 mM, pH 7.2) of a 1.0 mM solution of **WP5** upon titration with **3**: a) 0.0 mM; b) 0.29 mM; c) 0.57 mM; d) 1.23 mM and e) 2.06 mM.

Finally, the association constant between **WP5** and **3** in phosphate buffer solution was also determined by fluorescence studies; the obtained value (K_{ass} = (1.16 ± 0.04) × 10^4 M^{-1}) is in excellent agreement with that calculated from NMR data.

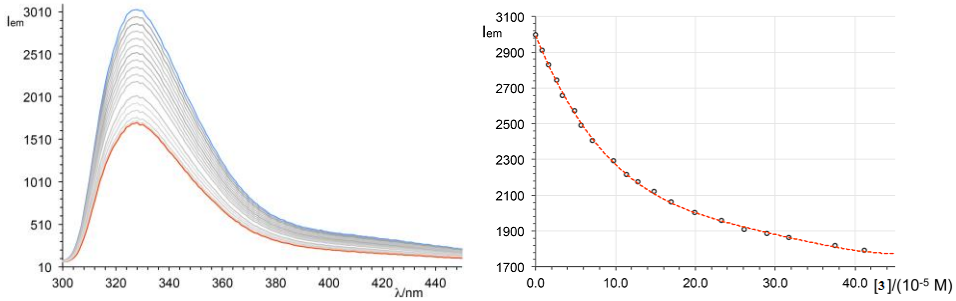

Figure 5.2.1.8. Emission titration spectra (λ_{exc} = 280 nm) of **WP5** (1.20 × 10^{-5} M) upon addition of increasing amounts of **3** in a buffered aqueous solution (Na_2HPO_4/ NaH_2PO_4 50 mM, pH 7.2). Emission intensity changes of **WP5** (λ= 327 nm) upon addition of **3**. The dashed red line was obtained from a non-linear curve-fitting.

5.2.2. WP5 and Amikacin: antimicrobial activity in vitro and release

The in vitro antimicrobial activity of this pillararene-based drug-transport system was tested against Staphylococcus aureus ATCC29213. For this purpose, the minimum inhibitory concentration (MIC) was first determined. MIC is the lowest concentration of an antimicrobial agent able to prevent the growth of a bacterial strain. In order to determine the MIC of amikacin, cultures of S. aureus ATCC 29213, at a final inoculum of approximately 10^5–10^6 bacteria per mL, were inoculated with increasing aliquots of amikacin ranging between 0.25 and 64 μg/mL. The MIC90, i.e. the lowest concentration of the drug required to prevent 90% of the microbial growth, of amikacin was found to be 4 μg/mL.

Subsequent antibacterial assays were routinely carried out at a sub-MIC concentration (2.5 μg/mL), and in the presence of increasing amounts of WP5 (0.5, 2.0 and 4.0 equiv.), to assess the efficacy of the pillararene-based guest transport system. After inoculation of the samples with a fresh culture of S. aureus (up to a final concentration of 10^6 bacteria per mL) followed by overnight incubation, bacterial growth was monitored in terms of OD_{540}, for an incubation time of 48 h.

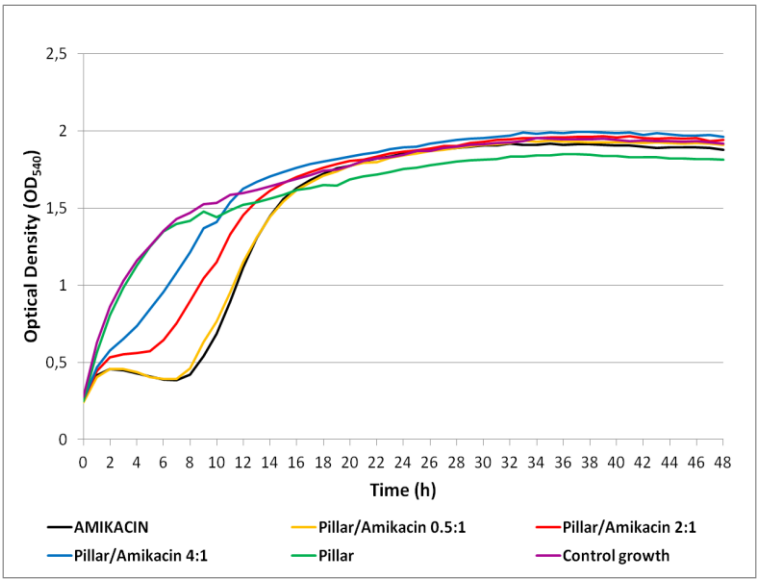

Figure 5.2.2.1. Kinetics of the growth of *S. aureus* in a MHB medium, analyzed by measuring the optical density at 540 nm (OD_{540}) for an incubation time of 48 hours, inoculated with: amikacin (2.5 μg/mL), black trace; amikacin (2.5 μg/mL) and **WP5 (**0.5 equiv., 1.6 μM), yellow trace; amikacin (2.5 μg/mL) and **WP5 (**2.0 equiv., 6.4 μM), red trace; amikacin (2.5 μg/mL) and **WP5 (**4.0 equiv., 12.8 μM), blue trace; **WP5 (**12.8 μM), green trace and control culture, purple trace.

After 2, 4 and 8 hours of incubation, the counts of viable bacteria in the treated microbial samples were estimated by a colony formation assay. As shown in Figure 5.2.2.1, the presence of **WP5** (up to 12.8 μM) showed

no toxic effects on the bacterial growth, as the OD_{540} profiles of the cultures with and without the pillararene were almost identical (Figure 5.2.2.1; green and purple traces, respectively). On the other hand, significant differences in the kinetics of growth were detected upon increasing the **WP5** concentration (Figure 5.2.2.1; yellow, red and blue traces). The number of colony-forming units (given as CFU mL^{-1}) was counted after 2, 4 and 8 hours of incubation and correlated to the concentration of **WP5** in order to determine the influence of the macrocycle on the antibacterial activity of amikacin. Over a period of 8 h, after exposure to free amikacin, the percentage of viable bacterial cells was significantly reduced (CFU ~50% with respect to the control culture) and this growth reduction remained constant over time (Figure 5.2.2.2, black bars). Conversely, with pillararene-to-amikacin ratios of up to 2:1 and 4:1, the count of viable bacteria linearly increased over time, reaching CFU values of 88 and 100% respectively after 8 hours of incubation (Figure 5.2.2.2., red and blue bars). The CFU increase observed upon increase of the **WP5** concentration, is indicative of a progressive reduction of the antimicrobial activity. This data are in agreement with an effective trapping of amikacin within the pillararene cavity, which prevent the antibiotic from efficiently inhibiting bacterial growth during the first 8 hours.

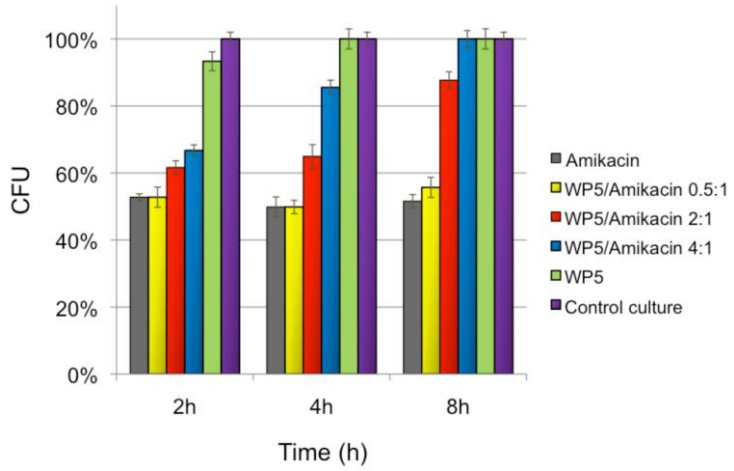

Figure 5.2.2.2. Colony-forming units (CFU) of *S. aureus* grown in a MHB after 2, 4 and 8 hours of incubation following inoculation with: amikacin (2.5 μg/mL); amikacin (2.5 μg/mL) and **WP5** (0.5 equiv., 1.6 μM); amikacin (2.5 μg/mL) and **WP5** (2.0 equiv., 6.4 μM); amikacin (2.5 μg/mL) and **WP5** (4.0 equiv., 12.8 μM); **WP5** (12.8 μM) and control culture; black, yellow, red, blue, green and purple bars, respectively.

Because the solubility of **WP5** is known to be pH-dependent,[27] we tested the release of amikacin from the cavity of **WP5** by changing the pH of the solution. After treatment of a D_2O solution of a 1:2 **WP5**-amikacin complex ([**WP5**] = 4.0 mM) with a slight excess of 6 M DCl (2 μL) the expected precipitation of the protonated form of **WP5** was observed. ^1H NMR analysis of the filtrate revealed that the amikacin resonances were shifted back to their original position (prior to pillararene addition, Figure 5.2.2.3), showing that amikacin may readily be released back into solution as a result of a pH variation. Considered the acidic microenvironment of an infection site[19], this pillar-based guest-*transport* system offers great potential in the biomedical/pharmaceutical field as an amikacin targeted-delivery system.

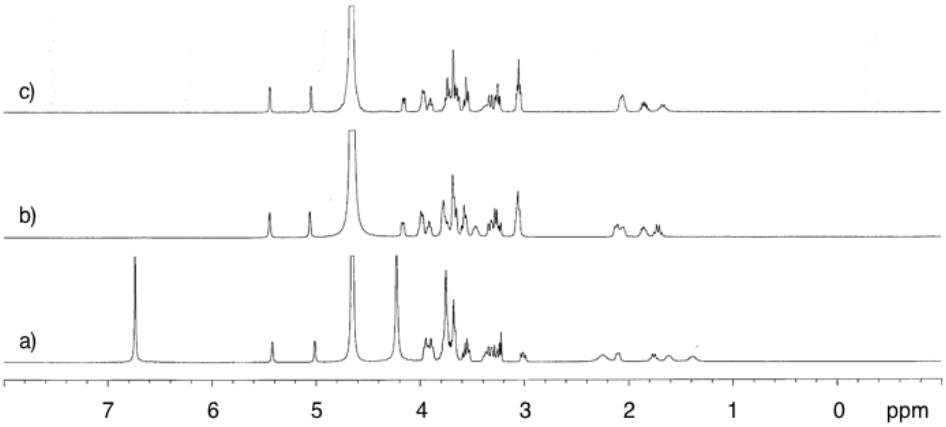

Figure 5.2.2.3. ^{1}H NMR spectra (500 MHz, 298 K) of D_2O solutions of: a) [**WP5**] = 4 and [**3**] = 8 mM; b) [**WP5**] = 4 and [**3**] = 8 mM upon addition of an aqueous solution of 6 M DCl (2 μL) and c) [**3**] = 4 mM.

5.2.3. WP5 and Levofloxacin: preliminary experimental data

Levofloxacin is a fluoroquinolone antibacterial used to treat a number of bacterial infections including acute bacterial sinusitis, pneumonia, urinary tract infections, chronic prostatitis, and some types of gastroenteritis.[28] Along with other antibiotics it may be used to treat tuberculosis, meningitis, or pelvic inflammatory disease.[29]

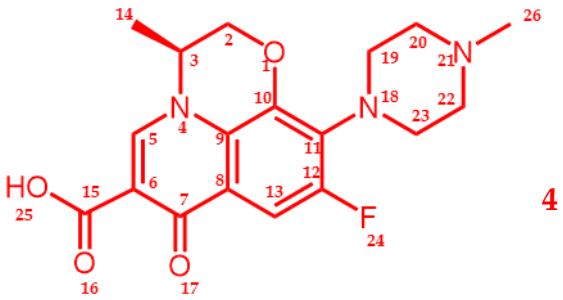

4

Figure 5.2.3.1. Chemical structure of the drug Levofloxacin **4**.

The molecular structure of this drug, makes it a good candidate for the inclusion inside the cavity of **WP5**. In order to test the affinity between this drug and **WP5**, ^{1}H NMR experiments were carried out by adding increasing amounts of **4** (0.5, 1.0 and 3.0 equiv.) to a 1.0 mM D_2O solution of **WP5.** Upon complexation, the hydrogen atoms on C20, C22 and C26 of the piperazine ring underwent substantial upfield shifts ($\Delta\delta$= -0.71 and -0.89 ppm, for the hydrogen atoms 20, 22 and 26 respectively, for **WP5**:**4** = 2:1; see trace b in Figure 5.2.3.2). Furthermore, host-guest interaction was additionally confirmed by less pronounced downfield shifts on specific **WP5** resonances (*e.g.*, ArH $\Delta\delta$ = 0.17 ppm , for **WP5**:**4** = 1:3, trace d in Figure 5.2.3.2).

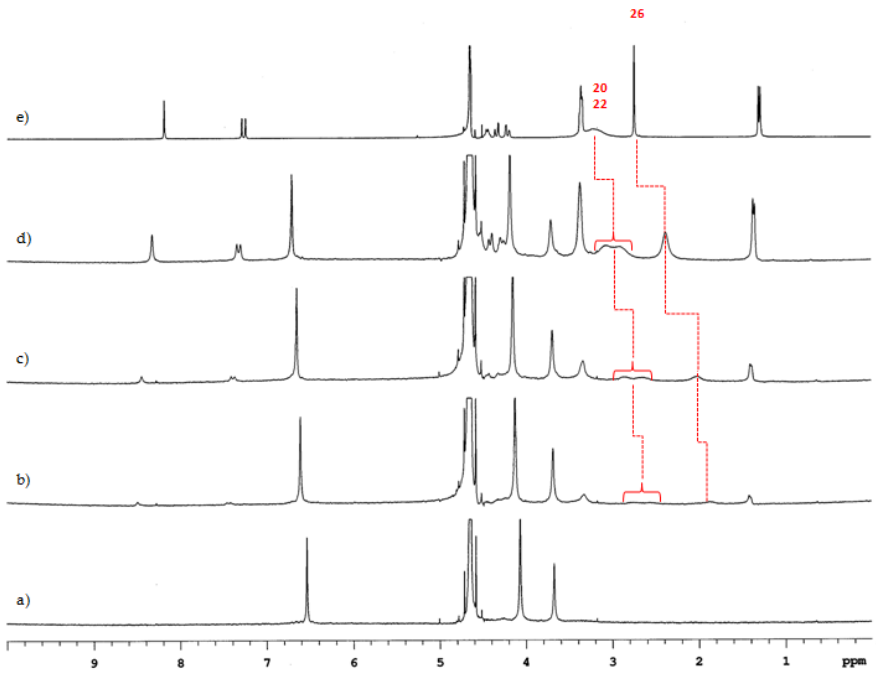

Figure 5.2.3.2. ^{1}H NMR spectra (300 MHz, D_2O, 298 K) of: a) [**WP5**] = 1.0 mM; b) [**WP5**] = 1.0 mM and [**4**] = 0.5 mM; c) [**WP5**] = [**4**] = 1mM; d) [**WP5**] = 1 mM and [**4**] = 3 mM; and e) [**4**] = 4.0 mM.

These preliminary data are in agreement with the formation of an inclusion complex undergoing fast association/dissociation, in which the piperazine ring of the guest is located within the shielding region of the host cavity.

2D NOESY experiment (Figure 5.2.3.3), carried out on a 1:1 host to guest solution (16 mM), further confirmed the inclusion of levofloxacin on the basis of intermolecular correlation peaks observed between the Ar-H and OCH_2 moieties of **WP5** and the hydrogen atoms on C19, C20, C22, C23 and C26 of **4** (dashed circles in Figure 5.2.3.3).

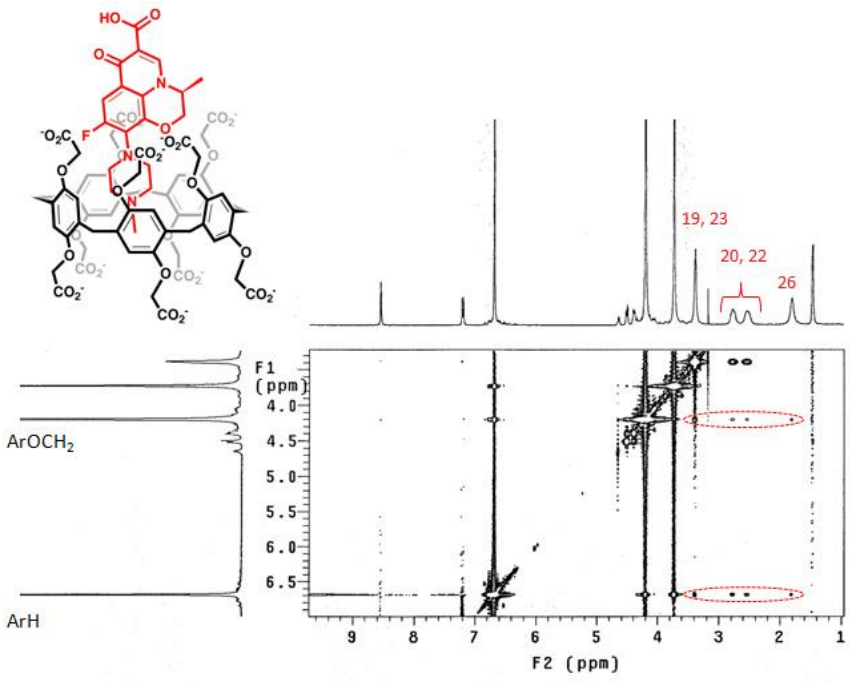

Figure 5.2.3.3. Section of the 2D NOESY spectrum (500 MHz, D_2O, 298 K) of a [**WP5**] = 16 mM and [**4**] = 16 mM solution.

NMR titration studies were also carried out in order to determine the association constant (K_{ass}) in deuterium oxide and in phosphate buffered

deuterium oxide solutions (PBS, 50 mM at pH 7.2), with the aim of mimicking physiological conditions more closely. The obtained K_{ass} values (4.0 ± 0.83) × 10^3 M^{-1} in D_2O solutions and (5.47 ± 1.16) × 10^2 M^{-1} in D_2O phosphate buffered solutions, were calculated (assuming a 1:1 stoichiometry) by a nonlinear regression method using the WinEQNMR.[26]

The results obtained with the two structurally different antibiotics amikacin (**3**) and levofloxacin (**4**), prompted us to exploit the general applicability of **WP5** in the development of multilayered films with antibiotic loading and releasing properties.

5.3. WP5 and layer-by-layer assembly

5.3.1. Introduction

Over the past few decades layer-by-layer (LbL) assembly has emerged as a powerful technology for fabricating nanostructured multilayered films and nanocomposites with tailored composition, structure, thickness and function.[30] The LbL strategy, commonly performed in water solution, represent a simple, low cost and mild method to obtain functional surface modification. LbL assemblies are formed by stepwise alternate adsorption of complementary building blocks of different nature (such as polyelectrolytes,[31] DNA, dendrimers,[32] nanoparticles (NPs),[33] polypeptides,[34] macrocycles,[35] etc.) on a substrate of almost any shape and size, occurring either via electrostatic or non-electrostatic interactions (hydrogen bonding, metal-ion coordination, host-guest interaction, covalent bonds, and so on).

LbL films have shown potential applications in the areas of nanoreactors, electrochemical devices, separation membranes, biosensors, surface modification, coatings and drug delivery. LbL-based drug delivery devices are capable of bringing together many of their advantages:[36] (i) LbL devices can be loaded with both water soluble/non-soluble substrates; (ii) they can be designed to be robust and stable within wide range of temperature, pH and ionic strength values, including in physiological conditions; (iii) drug release can be controlled by external stimuli; (iv) the release can be further controlled by assembling a variable number of layers, which act as a controllable barrier against drug diffusion; (v) multiple drug delivery is achievable by incorporating different drugs along the thickness of the films, due to the possibility of selecting the type of materials deposited along the vertical axis; (vi) multilayered films can be loaded with growth factors and stored for long periods of time as high as one year without extensive degradation or bioactivity loss; (vii) finally, the versatility of LbL allows constructing systems with the shape that is more appropriate to the desired end. However, LbL is not without disadvantages. It involves long construction times, with the assembly of a single layer taking typically a few minutes but dependent on the nature of the constituents.

Bioactive molecules such as drugs, proteins, peptides and even nucleic acids can be incorporated to LbL films following two main routes. One involves the direct inclusion of the drug as one of the building blocks during the film construction. Thus, the amount and the nature of the loaded bioactive agents can be regulated by changing the number of layers. However, in multilayered structures the building blocks may

exhibit interlayer diffusion, which may be difficult to control over their subsequent release.[37] A second route to load drugs is their immobilization by using concentrated drug solutions after the construction of the carrier. Such an approach is viable for low molecular weight drugs, which diffuse easily through the pores of the film.[38] Alternatively, both mechanisms can be used simultaneously.[39]

In the previous sections it was reported that deca-carboxylatopillar[5]arene **WP5** tightly binds amikacin and levofloxacin under physiological conditions. Thus, our next objective was to transfer the host-guest ability of **WP5** from solution to a LbL film with biocidal and anti-fouling activity to be used to prevent bacterial adhesion and proliferation on the surfaces of medical implants and devices. To this aim we have built up a LbL assembly onto glass or quartz substrates via the electrostatic interaction method, alternating layers of cationic polyallylamine hydrochloride (**PAH**) and anionic deca-carboxylatopillar[5]arene **WP5**, with the final intent to achieve anti-bacterial films after loading with model antibiotics amikacin (**3**) and levofloxacin (**4**).

5.3.2. Results and discussion

The LbL films were fabricated by alternating deposition of **WP5** and **PAH** on glass or quartz slides. First of all, to generate anionic silanol moieties on the surface of the glass, the substrates were sonicated in concentrated nitric acid (98%) for 30 minutes, washed first with distilled water and then with ethanol, and finally dried for 48 h at 60 °C. The glass surface was immersed in an aqueous solution of polyallylamine

hydrochloride **PAH** (3 mg/mL) for 15 minutes to introduce positively charged molecules onto the anionic substrate surface, washed with a large amount of water to remove the excess of unmodified positive polyelectrolyte, and dried to obtain the cationic monolayer. Then, it was immersed in an aqueous solution of **WP5** (1.3 mg/mL) for 15 minutes to introduce negatively charged molecules, washed with a large amount of water, and dried to give the bilayer with an anionic surface. Multilayered films 16L (nL, n is the number of deposited layers) were obtained by repeating the alternating immersion steps (Figure 5.3.2.1).

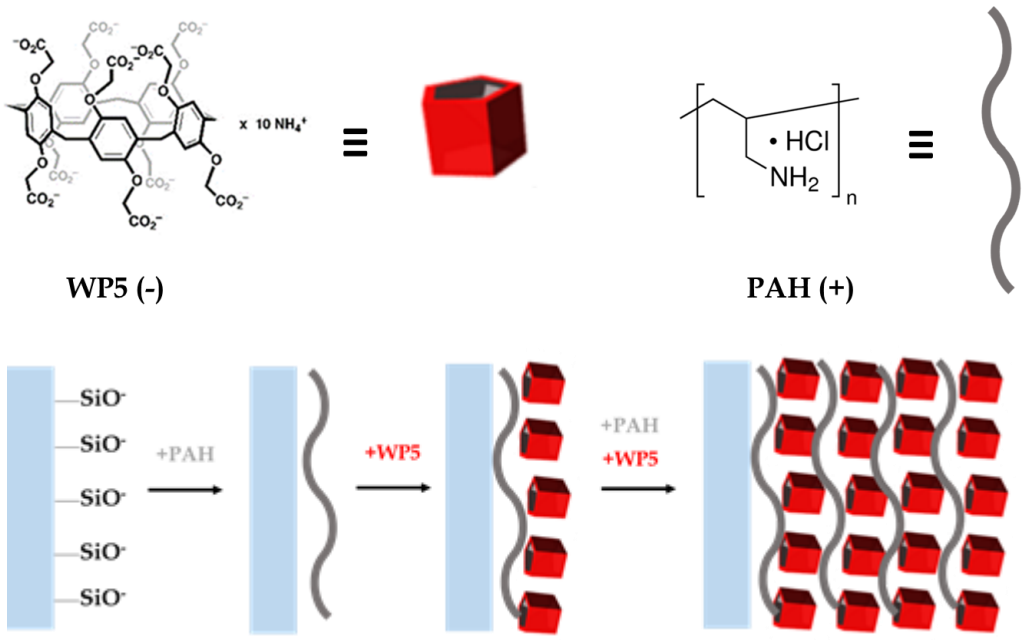

5.3.2.1. Schematic representation of the LbL-assembly

The build-up of the multilayers was monitored after each immersion step in the **WP5** solution with an UV-vis spectrometer (Figure 5.3.2.2). The absorption at λ 293 nm, which corresponds to the absorption of

aromatic moieties of the pillar[5]arene, increases with increasing number of deposited bilayers, thus confirming for the adsorption of the oppositely charged electrolytes on the surface.

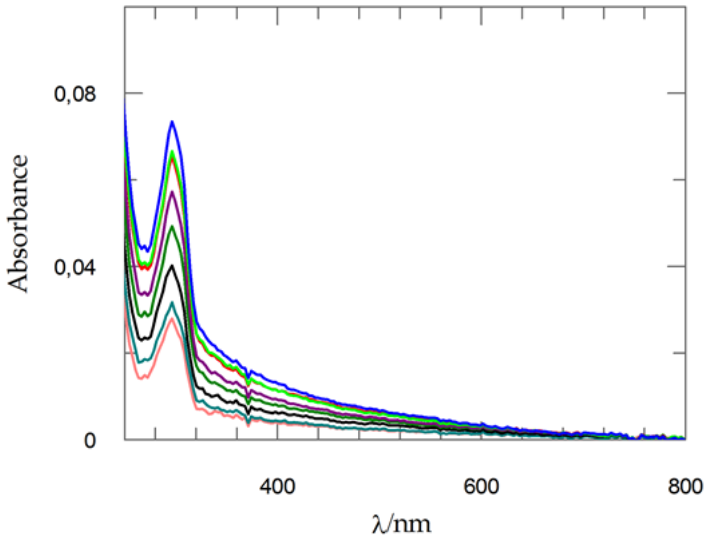

Figure 5.3.2.2. UV−vis absorption spectra of LbL-assembled multilayer films using **PAH** (+) and **WP5** (-) with layer number n = 1−16 on a quartz substrate (2L at the bottom; 16L at the top).

Finally, the 16L surface was immersed in an aqueous solution of Amikacin (8.0 mg/mL) or Levofloxacin (3.6 mg/mL) for 1 hour, washed with a large amount of water, and dried to load the drug into the multilayers by taking advantage of the high affinity between the two drugs and **WP5**. In the case of Levofloxacin UV-vis and fluorescence experiments carried out on the quartz surface confirmed the immobilization of the drug inside the multilayered films (grey lines Figure 5.3.2.3).

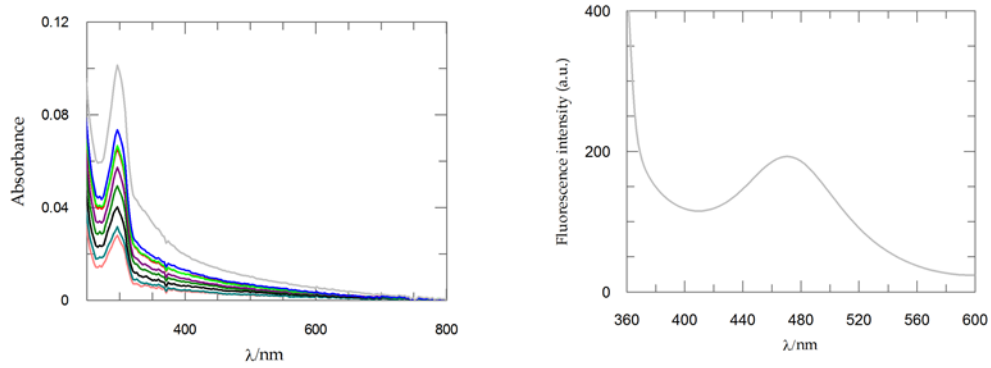

Figure 5.3.2.3. (left) UV−vis absorption spectra of LbL-assembled multilayer films first and after Levofloxacin immobilization (2L at the bottom; after loading of Levofloxacin on 16L films at the top); (right) Fluorescence spectrum of Levofloxacin loaded on 16L films (λ_{exc} 330 nm).

The antibacterial activities of the functionalized films (**WP5/PAH/drug**) were evaluated against two strains of bacteria, *P. aeuriginosa ATCC 27853* (Gram negative) and *S. aureus ATTCC 2913* (Gram Positive).

To this aim the samples and control pieces were placed into a sterile 6-well microplate, next 4 mL of the bacterial culture in MHB medium (*P. aeuriginosa* 3.5×10^4 bacteria/mL, *S. aureus* 4.5×10^4 bacteria/mL) was added to each well. For each pathogen, the microbial growth was measured at different times (2, 4, 6, 8 hours) counting the number of CFU of the bacterial suspension. Figure 5.3.2.4 shows that bacterial growth in solution was significantly reduced when bacteria were cultured in the presence of **WP5/PAH/drug** films (red and blue lines) rather than with **WP5/PAH** (green line).

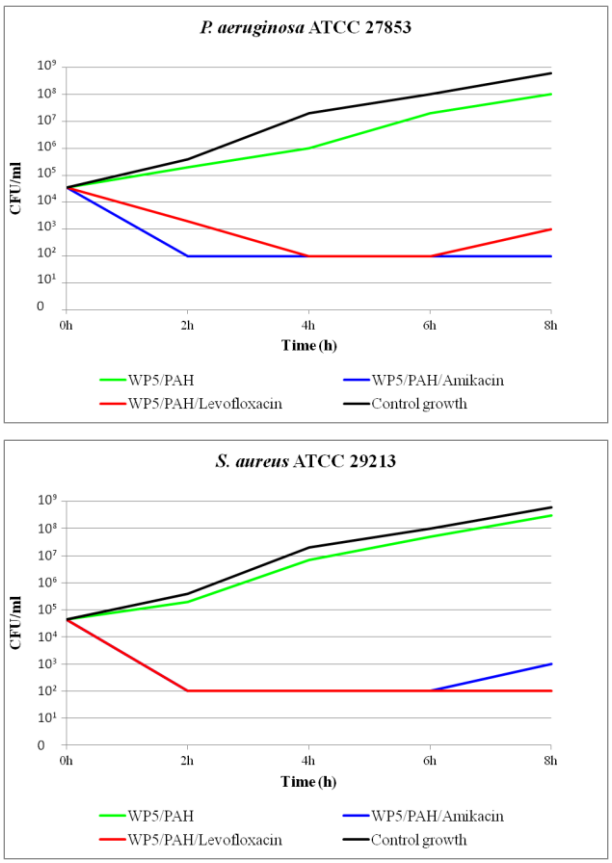

Figure 5.3.2.4. Colony-forming units (CFU) of *P. aeruginosa* and *S. aureus* grown in MHB medium after 2, 4 and 8 hours.

Conventional antimicrobial multilayered films provides two main actions for killing bacteria. Bacteria are either killed by direct contact with the surface or by the controlled release of the antimicrobial agents into the biological fluids. A standard way for quantifying the contact induced killing of bacteria on the multilayered films is the "Live and Dead" assay.[40] To this aim, after 8 hours of incubation, the adhering cells were stained by using the "Live-Dead Kit" (BacLight Bacterial Viability Kit) and fluorescence images were recorded. All bacteria on the surface

were labelled with SYTO 9 green-fluorescence dye, while only the bacteria with damaged cellular membrane were additionally stained by a red-fluorescence dye (propidium iodide).

Preliminary fluorescence images of "Live" and "Dead" on multilayered films are reported in Figures 5.3.2.5 and 5.3.2.6.

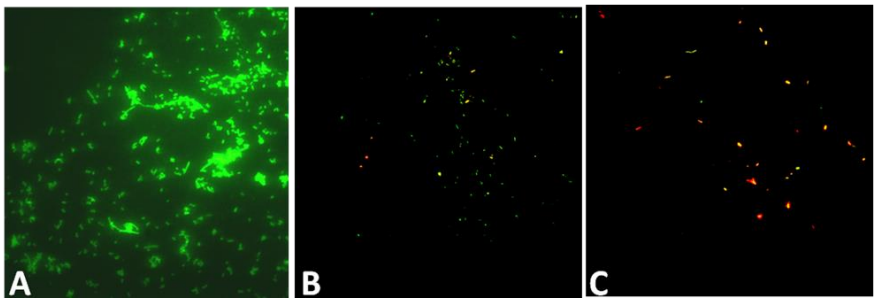

Figure 5.3.2.5. Merged image of *P. aeuriginosa* on multilayered films of: a) **WP5/PAH**; b) **WP5/PAH**/levofloxacin; c) **WP5/PAH**/amikacin.

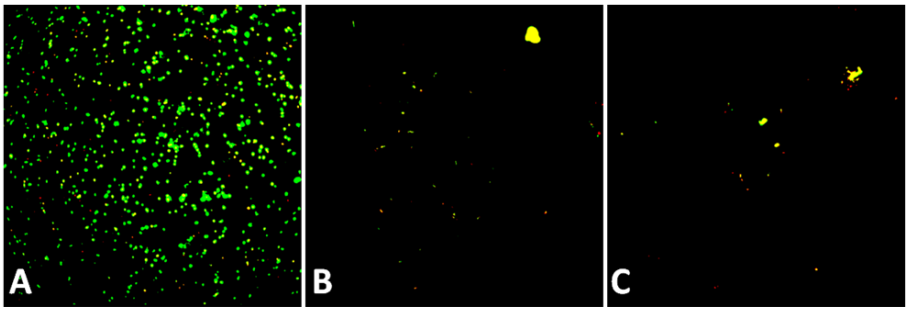

Figure 5.3.2.6. Merged image of *S. aureus* on multilayered films of: a) **WP5/PAH**; b) **WP5/PAH**/levofloxacin; c) **WP5/PAH**/amikacin.

For both bacterial strains, data show that **WP5/PAH** samples do not inhibit cell adhesion on multilayered films (Figures 5.3.2.5-A and 5.3.2.6-A), while multilayered films loaded with levofloxacin or amikacin reveal a consistent reduction of cell adhesion, for both considered strains. Furthermore, most of adhering bacteria (see Figures 5.3.2.5B,C and

5.3.2.6B,C) display a red-orange fluorescence indicating an accentuated mortality.

These preliminary experimental results show that our drug-loaded films exhibit efficient antibacterial activity, killing bacteria both by direct contact with the film surface and by the controlled release of the antimicrobial agents into the medium.

Studies are currently in progress to determine the optimal number of bilayers and the amount of antibiotic drug loaded.

5.4. Conclusions

In this Chapter I reported our successful results on the interaction of deca-carboxylatopillar[5]arene **WP5** and two model antibiotic drugs, amikacin and levofloxacin. I also described the development of **WP5/PAH/drug** multilayered films by using the layer-by-layer methodology. According to our results, the **WP5/drug** system represents a very promising candidate for the development of medical devices with antiadhesive and antibacterial properties (catheters).

5.5. Experimental section

5.5.1. Materials and Methods

Deca-carboxylatopillar[5]arene (**WP5)** was synthesised starting from pillar[5]arene[1] **1** with small modifications of the reported method.[11a] Amikacin disulfate salt **(3)** and levofloxacin (**4**) were obtained from Sigma-Aldrich. The strain of *Staphylococcus aureus* and *Pseudomonas aeuriginosa* used in the microbiological studies were purchased from the American Type Culture Collection (ATCC 29213, LGC Promochem, Milan, Italy). The other chemicals were reagent grade and were used without any further purification.

5.5.2. General Experimental Methods.

^{1}H NMR spectra were recorded at room temperature in D_2O, at 500 or 300 MHz. The solvent residual peak (δ = 4.65 ppm) was used as an internal standard for ^{1}H NMR spectra. NOESY spectra were recorded on a spectrometer equipped with a pulse-field gradient probe, using a 300 ms and 350 ms mixing time for **WP5**:**3** and **WP5**:**4** host-guest complex respectively, 16 transients for each increment (256 in total) and a relaxation time of 3 s. NMR titration studies were carried out at a fixed **WP5** concentration (1 mM) and samples were routinely prepared by dissolving solid **WP5** in a D_2O phosphate buffer solution (Na_2HPO_4/NaH_2PO_4 50 mM, pH 7.2). A stock solution of the drug ([**3**] = 10 mM; [**4**] = 5 mM) was, in turn, prepared by using the above-mentioned 1 mM **WP5** buffered solution as a convenient solvent so as, during the titration, the host concentration did not vary upon addition of

increasing aliquots of the guest. The association constants were calculated by a nonlinear regression method using the WinEQNMR program.[26]

UV/Vis absorption spectra were taken on a Jasco V-560 spectrophotometer. For steady-state luminescence measurements, a Jobin Yvon-Spex Fluoromax 2 spectrofluorimeter was used, equipped with a Hamamatsu R3896 photomultiplier. Spectra were corrected for photomultiplier response using a program purchased with the fluorimeter. The absorption and luminescence data were fitted with the SPECFIT program, [SPECFIT, Spectrum Software Associates, R. A. Binstead, Chapel Hill, 1996.].

Fluorescence images were obtained using a Leica DMRE epifluorescence microscope with Leica C Plan 63× objective, using a BP 515-560 nm excitation filter in combination with a LP 590 nm suppression filter.

5.5.3. Determination of the minimum inhibitory concentration (MIC).

MIC is the lowest concentration of an antimicrobial agent able to prevent the growth of a bacterial strain. In order to determine the MIC of amikacin, cultures of S. aureus ATCC 29213, at a final inoculum of approximately 10^5–10^6 bacteria per mL, were inoculated with increasing aliquots of amikacin ranging between 0.25 and 64 μg/mL. The MIC_{90}, i.e. the lowest concentration of the drug required to prevent 90% of the microbial growth, of amikacin was found to be 4 μg/mL. Subsequent antibacterial assays were routinely carried out at a sub-MIC concentration, namely 2.5 μg/mL, to assess the efficacy of the pillararene-based guest transport system.

5.5.4. Antibacterial activity assessment.

S. aureus ATCC 29213 was grown at 37 °C in a Mueller Hinton broth (MHB) prior to use. The microorganisms were stored in a Trypti-case Soy broth (TSB), containing 20% (v/v) glycerol, at –80 °C. Four different MHB samples containing amikacin (2.5 μg/mL) and increasing amounts of WP5 (0.0, 0.5, 2.0 and 4.0 equiv., respectively) were prepared and inoculated with a fresh culture of S. aureus up to a final concentration of 10^6 bacteria per mL. Following overnight incubation in a shaker incubator (350 rpm) operating at 37 °C, the bacterial growth was monitored by an automated turbidometry analyzer (Bioscreen C Labsystems). Ten replicates of bacterial cultures containing each of the aforementioned WP5/amikacin ratios were incubated in honeycomb plates for 48 h at 37 °C under continuous shaking. Read-outs of the bacterial culture optical density at 540 nm (OD_{540}) were periodically taken at 15 min. time intervals. Bacterial growth was monitored in terms of OD_{540}, for an incubation time of 48 h. After 2, 4 and 8 hours of incubation, the counts of viable bacteria in the treated microbial samples were estimated by a colony formation assay. The number of colony-forming units (CFU) was counted and expressed as percentage of CFU mL^{-1}.

5.5.5. Antibacterial activity of LbL systems

For each strain, the protocol was the following: (i) inoculate 50 ml of Mueller Hinton Broth (MHB) with a thawed glycerol stock, (ii) allow the culture to grow overnight at 37° C with vigorous shaking (250 rpm); (iii)

transfer bacteria in MHB fresh and incubate at 37° C with vigorous shaking (250 rpm) for three hours; (iv) dilute the bacterial culture, in exponential growth, at a final inoculum of approximately 10^4-10^5 CFU.

Then samples and control pieces were placed into a sterile 6-well microplate and next 4 mL of the bacterial culture in MHB medium (*P. aeuriginosa* 3.5×10^4 bacteria/mL, *S. aureus* 4.5×10^4 bacteria/mL) was added to each well. For each pathogen, the microbial growth was measured at different times (2, 4, 6, 8 hours) by determining the CFU of the bacterial suspension, assuming that each colony has raised from one single bacterium.

[1] Ogoshi T., Kanai S., Fujinami S., Yamagishi T., Nakamoto Y., *J. Am. Chem. Soc.,* **2008**, 130, 5022.

[2] Gutsche C.D., *Calixarenes,* The Royal Society of Chemistry, Cambridge, **1989.**

[3] (a) Ogoshi T., Kitajima K., Yamagishi T.A., Nakamoto Y., *Org. Lett.,* **2010,** 12, 636; (b) Ogoshi T., Aoki T., Kitajima K., Fujinami S., Yamagishi T.A., Nakamoto Y., *J. Org. Chem.,* **2011**, 76, 328; (c) Ogoshi T., Shiga R., Yamagishi T.A., Nakamoto Y., *J. Org. Chem.,* **2011**, 76, 618; (d) Cao D., Kou Y., Liang J., Chen Z., Wang L., Meier H., *Angew. Chem., Int. Ed.,* **2009**, 48, 9721; (e) Kou Y., Tao H., Cao D., Fu Z., Schollmeyer D., Meier H., *J. Org. Chem.,* **2010**, 75, 6464; (f) Ma Y., Zhang Z., Ji X., Han C., He J., Zeper A., Chen W., Huang F., *Eur. J. Org. Chem.*, **2011**, 27, 5331; (g) Holler M., Allenbach N., Sonet J., Nierengarten J.F., *Chem. Commun.,* **2012**, 48, 2576.

[4] (a) Strutt N.L., Forgan R.S., Spruell J.M., Botros Y.Y., Stoddart J.F., *J. Am. Chem. Soc.,* **2011**, 133, 5668; (b) Ogoshi T., DemachiK., Kitajima K., Yamagishi T., *Chem. Commun.,* **2011**, 47, 7164; (c) Ogoshi T., Kitajima K., Fujinami S., Yamagishi T., *Chem. Commun.,* **2011**, 47, 10106; (d) Zhang Z.B., Xia B.Y., Han C.Y., Yu Y.H., Huang F.H., *Org. Lett.,* **2010**, 12, 3285; (e) Ogoshi T., Yamafuji D., Kotera D., Aoki T., Fujinami S., Yamagishi T., *J. Org. Chem.,* **2012**, 77, 11146; (f) Ogoshi T., Yamagishi T., *Eur. J. Org. Chem.*, **2013**, 2961.

[5] (a) Ogoshi T., Kitajima K., Aoki T., Fujinami S., Yamagishi T., Nakamoto Y., *J. Org. Chem.,* **2010**, 75, 3268; (b) Ogoshi T., Shiga R., Yamagishi T., Nakamoto Y., *J. Org. Chem.,* **2011**, 76, 618; (c) Ogoshi T., Masaki K., Shiga R., Kitajima K., Yamagishi T., *Org. Lett.,* **2011**, 13, 1264.

[6] (a) Rekharsky M.V., Inoue Y., *Chem. Rev.,* **1998**, 98, 1875; (b) Harada A., Hashidzume A., Yamaguchi H., Takashima Y., *Chem. Rev.,* **2009**, 109, 5974; (c) Wenz G., Han B.H., Müller A., *Chem. Rev.,* **2006**, 106, 782; (d) Lee J.W., Samal S., Selvapalam N., Kim H.J., Kim K., *Acc. Chem. Res.,* **2003**, 36, 621.

[7] (a) Yao Y., Xue M., Zhang Z., Zhang M., Wang Y., Huang F., *Chem. Sci.,* **2013**, 4, 3667; (b) Yu G., Han C., Zhang Z., Chen J., Yan X., Zheng B., Liu S., Huang F., *J. Am. Chem. Soc.,* **2012**, 134, 8711; (c) Yu G., Zhou X., Zhang Z., Han C., Mao Z., Gao C., Huang F., *J.*

Am. Chem. Soc., **2012**, 134, 19489; (d) Yu G., Ma Y., Han C., Yao Y., Tang G., Mao Z., Gao C., Huang F., *J. Am. Chem. Soc.,* **2013**, 135, 10310.

[8] Li C., Zhao L., Li J., Ding X., Chen S., Zhang Q., Yu Y., Jia X., *Chem. Commun.,* **2010**, 46, 9016;

[9] Si W., Chen L., Hu X.B., Tang G., Chen Z., Hou J.L., Li Z.T., *Angew. Chem., Int. Ed.,* **2011**, 50, 12564.

[10] Zhang Z., Luo Y., Chen J., Dong S., Yu Y., Ma Z., Huang F., *Angew. Chem., Int. Ed.,* **2011**, 50, 1397.

[11] (a) Ogoshi T., Hashizume M., Yamagishi T.A., Nakamoto Y., *Chem. Commun.,* **2010**, 46, 3708; (b) Yu G., Xue M., Zhang Z., Li J., Han C., Huang F., *J. Am. Chem. Soc.,* **2012**, 134, 13248; (c) Li Z., Yang J., Yu G., He J., Abliz Z., Huang F., *Org. Lett.,* **2014**, 16, 2066; (d) Li Z., Yang J., Yu G., He J., Abliz Z., Huang F., *Chem. Commun.,* **2014**, 50, 2841; (e) Yang J., Chi X., Li Z., Yu G., He J., Abliz Z., Li N., Huang F., *Org. Chem. Front.,* **2014**, 1, 630; (f) Zhang C.F., Li S.H., Zhang C.C., Liu Y., *Org. Biomol. Chem.,* **2015**, 13, 10808.

[12] (a) Ma Y., Ji X., Xiang F., Chi X., Han C., He J., Abliz Z., Chen W., Huang F., *Chem. Commun.*, **2011**, 47, 12340; (b) Yao Y., Xue M., Chi X., Ma Y., He J., Abliz Z., Huang F., *Chem. Commun.,* **2012**, 48, 6505; (c) Wei P., Yan X., Li J., Ma Y., Huang F., *Chem. Commun.,* **2013**, 49, 1070; (d) Chen W., Zhang Y., Li J., Lou X., Yu Y., Jia X., Li C., *Chem. Commun.,* **2013**, 49, 7956; (e) Ma Y., Yang J., Li J., Chi X., Xue M., *RSC Adv.,* **2013**, 3, 23953; (f) Nierengarten I., Nothisen M., Sigwalt D., Biellmann T., Holler M., Remy J.S., Nierengarten J.F., *Chem. Eur. J.,* **2013**, 19, 17552; (g) Yu G., Zhou J., Shen J., Tang G., Huang F., *Chem. Sci.,* 2016, 7, 4073.

[13] (a) Hu X. B., Chen L., Si W., Yu Y., Hou J.L., *Chem. Commun.,* **2011**, 47, 4694; (b) Ogoshi T., Shiga R., Yamagishi T.A., *J. Am. Chem. Soc.,* **2012**, 134, 4577; (c) Ogoshi T., Kida K., Yamagishi T.A., *J. Am. Chem. Soc.,* **2012**, 134, 20146; (d) Chi X., Yu G., Ji X., Li Y., Tang G., Huang F., *ACS Macro Lett.,* **2015**, 4, 996.

[14] Guo D.S., Liu Y., *Acc. Chem. Res.,* **2014**, 47, 1925.

[15] Dasgupta S., Mukherjee P.S., *Org. Biomol. Chem.,* **2017**, 15, 762.

[16] (a) Yao Y., Xue M., Chen J., Zhang M., Huang F., *J. Am. Chem. Soc.,* **2012**, 134, 15712; (b) Duan Q., Cao Y., Li Y., Hu X., Xiao T., Lin C., Pan Y., Wang L., *J. Am. Chem. Soc.,*

2013, 135, 10542; (c) Cao Y., Hu X.Y., Li Y., Zou X., Xiong S., Lin C., Shen Y.Z., Wang L., *J. Am. Chem. Soc.,* **2014**, 136, 10762.

[17] Yao Y., Zhou Y., Dai J., Yue S., Xue M., *Chem. Commun.,* **2014**, 50, 869.

[18] Shangguan L., Chen Q., Shi B., Huang F., *Chem. Commun.,* **2017**, 53, 9749.

[19] Qi Z., Achazi K., Haag R., Dong S., Schalley C.A., *Chem. Commun.*, **2015**, 51, 10326.

[20] Torres I.M., Patankar Y.R., Shabaneh T.B., Dolben E., Hogan D.H., Leib D.A., Berwin B.L., *Infect. Immun.,* **2014**, 82, 4689.

[21] (a) Sun Y.L., Yang Y.W., Chen D.X., Wang G., Zhou Y., Wang C.Y., Stoddart J.F., *Small*, **2013**, 9, 3224; (b) Zhang H., Ma X., Nguyen K.Y., Zhao Y., *ACS Nano*, **2013**, 7, 7853; (c) WuX., Gao L., Yu X., Wang H., Wang L., *Chem. Rec.,* **2016**, 1216.

[22] Dasgupta S., Chowdhury A., Mukherjee P.S., *RSC Adv.*, **2015**, 5, 85791.

[23] (a) Sklaver A.R., Greenman R.L.,Hoffman T.A., *Arch Intern Med.,***1978**, 138, 713; (b) Cox C.E., *J Infect Dis.,***1976**, 134, 362; (c) Allen B.W.,Mitchison D.A., Chan Y.C., Yew W.W., Allan W.G., Girling D.J., *Tubercle.,* **1983**,64, 111.

[24] (a) Du M., Keeling K.M., Fan L., Liu X., Bedwell D.M., *J. Bio. Chem.,* **2009**, 284, 6885; (b) Varshosaz J., Ghaffari S., Mirshojaei S.F., Jafarian A., Atyabi F., Kobarfard F., Azarmi S., *BioMed Res. Int.*, **2013**, art. ID 136859.

[25] SPECFIT, Spectrum Software Associates, R. A. Binstead, Chapel Hill, 1996

[26] M. J. Hynes, *J. Chem. Soc., Dalton Trans.*, **1993**, 311.

[27] (a) Wang P., Li Z., Ji X., *Chem. Commun.,* **2014**, 50, 13114.

[28] (a) Poole M., Anon J., Paglia M., Xiang J., Khashab M., Kahn J., *Otolaryngol Head Neck Surg.,* **2006**, 34, 7; (b) Noreddin A.M., Elkhatib W.F., *Expert Rev Anti Infect Ther.,* **2010**, 8,14; (c) McGregor J.M., Allen G.P., Bearden D.T., Ther Clin Risk Manag., **2008**, 4, 843; (d) Schaeffer A.J., Wu S.C., Tennenberg A.M., Kahn J.B., *J Urol.,* **2005**, 174, 4; (d) Zamir D., Weiler Z., Kogan E., Ben-Valid E., Hay E., Reitblat T., Polishchuk I., *J Clin Gastroenterol.,* **2006**, 40, 90.

[29] Marra F., Marra C.A., Moadebi S., Shi P., Elwood R.K., Stark G., FitzGerald J.M., *Chest.*, **2005**, 128, 13.

[30] (a) Richardson J.J., Bjornmalm M., Caruso F., *Science*, **2015**, 348, 2491; (b) Xiao F.X., Pagliaro M., Xu Y.J., Liu B., *Chem. Soc. Rev.*, **2016**, 45, 3088.

[31] Decher G., Hong J.D., *Makromol. Chem., Macromol. Symp.* **1991**, 46, 321.

[32] Liu Z., Wang X., Wu H., Li C., J. *Colloid Interface Sci.*, **2005**, 287, 604.

[33] Srivastava S., Kotov N.A., *Acc. Chem. Res.*, **2008**, 41, 1831.

[34] Boulmedais F., Ball V., Schwinte P., Frisch B., Schaaf P., Voegel J.C., *Langmuir,* **2003**, 19, 440.

[35] Crespo-Biel O., Dordi B., Reinhoudt D.N., Huskens J., *J. Am. Chem. Soc.,* **2005**, 127, 7594.

[36] (a) Crouzier T., Sailhan F., Becquart P., Guillot R., Logeart-Avramoglou D., Picart C., *Biomaterials*, **2011**, 32, 7543; (b) Gilde F., Maniti O., Guillot R., Mano J.F., Logeart-Avramoglou D., Sailhan F., *Biomacromolecules*, **2012**, 13, 3620; (c) Guillot R., Gilde F., Becquart P., Sailhan F., Lapeyrere A., Logeart-Avramoglou D., *Biomaterials*, **2013**, 34, 5737.

[37] Wood K.C., Chuang H,F., Batten R.D., Lynn D.M., Hammond P.T., *Proc Natl Acad Sci U S A,* **2006**, 103, 10207.

[38] Sukhishvili S.A., *Curr. opin. Colloid Interface Sci*, **2005**, 10, 37.

[39] Zhang D., Zhang K., Yao Y.L., Xia X.H., Chen H.Y., *Langmuir*, **2004**, 20, 7303.

[40] He T., Chan V., *J Biomed Mater Res*, Part A, **2010**, 454.